Tampere University

Sami Lähteenmäki

EVALUATION OF CHARGE TRAPPING AND TRANSPORT PHENOMENA IN POLYMER INSULATION BY MEANS OF THERMALLY STIMULATED CURRENT MEASUREMENTS

Master of Science Thesis
Faculty of Information Technology and Communication Sciences
Examiner: Kari Lahti
Examiner: Minna Niittymäki
September 2025

ABSTRACT

Sami Lähteenmäki: Evaluation of Charge Trapping and Transport Phenomena in Polymer Insulation by Means of Thermally Stimulated Current Measurements
Maste of Science Thesis
Tampere University
Master's Degree Programme in Electrical Engineering
September 2025

The growing demand for electricity, together with increasing electrification and the expansion of distributed energy generation, is pushing electricity production further away from consumption centers into more demanding environments. Longer transmission distances increase the need to reduce losses, which in turn drives the adoption of higher operating voltages. High-voltage direct current (HVDC) technology offers a cost-effective solution for long-distance power transfer, but it also introduces new challenges, including the accumulation of space charge, which can deteriorate electrical performance of the insulation. These issues have created a need to develop new insulation materials and novel additives which can mitigate space charges while combining enhanced electrical properties with environmental sustainability.

The aim of this thesis was to provide a thorough literature review of the properties of polymeric insulations and to experimentally investigate the space charge behaviour of polypropylene (PP) blends using thermally stimulated depolarisation current (TSDC) method. Polypropylene blends are increasingly used as insulation materials in high-voltage direct current (HVDC) cables due to their favourable electrical and mechanical properties. The literature review, presented in Chapters 2–5, covers the structure and electrical properties of polymers, their ageing, degradation and breakdown mechanisms, as well as measurement techniques suitable for space charge characterisation. The experimental work focused on analysing the behaviour of polypropylene blends by varying TSDC measurement parameters, examining the influence of additives, and evaluating the resolution capability of the TSDC method.

Experimental results revealed that deep-trap filling becomes more pronounced once the poling time exceeds 50 minutes. Based on these findings, further studies on other polypropylene blends were recommended to determine whether similar behaviour occurs. The resolution of the measurement method was assessed using five identical parallel samples, complemented by a comparison with an additive-containing sample of the same PP blend. All five parallel samples followed a similar trend, and the additive was found to significantly reduce space charge accumulation. These results demonstrate that the applied TSDC method provides sufficient resolution for the objectives of the project.

Evaluating TSDC behaviour in samples of different thicknesses, it was found that the current intensity at the glass transition temperature was essentially independent of thickness. However, the current caused by space charges released from deep traps was weaker in thicker samples. According to the literature, this can be explained by increased recombination in thicker specimens. The addition of an additive, on the other hand, was observed to clearly reduce space charge accumulation regardless of the polymer composition or measurement parameters. This finding was further supported by net charge accumulation analysis and by PEA measurements conducted by the project partner, both of which showed consistent results.

Keywords: HVDC, space charge, polymer insulation, polypropylene blend, TSDC, additive, charge trapping, high-field conduction

TIIVISTELMÄ

Sami Lähteenmäki: Varausten loukkuuntumisen ja johtavuusilmiöiden arviointi polymeerieristeissä termisesti stimuloidun virtamittauksen avulla
Diplomityö
Tampereen yliopisto
Sähkötekniikan koulutusohjelma
Syyskuu 2025

Sähkönkulutuksen ja sähköistymisen kasvu sekä hajautettujen uusiutuvien energiantuotantomuotojen yleistyminen siirtävät sähkön tuotantoa kauemmas kulutuskohteista, usein vaativampiin olosuhteisiin. Pidemmät siirtoetäisyydet lisäävät tarvetta pienentää häviöitä, mikä ohjaa kohti korkeampia käyttöjännitteitä. Suurjännitetasasähköyhteydet (HVDC) tarjoavat taloudellisen ratkaisun sähkön siirtämiseen pitkiä etäisyyksiä, mutta tuo mukanaan uusia haasteita, muun muassa eristemateriaaleihin kertyvän avaruusvarauksen. Näiden haasteiden ratkaisemiseksi on syntynyt tarve kehittää uusia eristemateriaaleja ja lisäaineita, joissa yhdistyvät parantuneet sähköiset ominaisuudet ja ympäristöystävällisyys.

Tämän työn tavoitteena oli laatia kattava kirjallisuuskatsaus polymeerieristeiden ominaisuuksista sekä tutkia kokeellisesti polypropeenisekoitusten avaruusvarauskäyttäytymistä termisesti stimuloidun depolarisaatiovirta (TSDC) -menetelmän avulla. Lukuihin 2–5 jaettu kirjallisuuskatsaus käsittelee polymeerien rakennetta ja sähköisiä ominaisuuksia, niiden ikääntymis- ja läpilyöntimekanismeja sekä avaruusvarauksen mittaamiseen soveltuvia menetelmiä. Kokeellisessa osuudessa analysoitiin polypropeenisekoitusten käyttäytymistä vaihtelemalla TSDC-mittausparametreja, tutkimalla lisäaineiden vaikutusta sekä arvioimalla mittauksen erottelukyvyn toimivuutta.

Kokeellisissa mittauksissa havaittiin, että poolausajan pituus vaikuttaa syvien loukkujen täyttymiseen. Lisääntynyttä täyttymistä esiintyi, kun poolausaika ylitti 50 minuuttia. Näiden tulosten perusteella ehdotettiin jatkotutkimuksia myös muille polymeerisekoituksille, jotta voitaisiin varmistaa, onko loukkujen täyttymiskäyttäytyminen samankaltaista eri materiaalien välillä. Mittauksen erottelukykyä arvioitiin viidellä identtisellä rinnakkaisnäytteellä, ja tuloksia täydennettiin vertaamalla samaan polymeerisekoitukseen perustuvaa lisäaineellista näytettä. Kaikki viisi rinnakkaisnäytettä noudattivat samankaltaista trendiä, ja lisäaineen havaittiin selvästi vähentävän avaruusvarauksen kertymistä. Näiden tulosten perusteella käytetty TSDC-menetelmä tarjoaa riittävän erottelukyvyn projektin tavoitteiden kannalta.

Eri paksuisten näytteiden TSDC-käyttäytymistä arvioitaessa todettiin, että lasisiirtymälämpötilassa virran intensiteetti oli paksuudesta riippumaton. Sen sijaan syvistä loukuista vapautuvan avaruusvarauksen aiheuttama virta oli paksummissa näytteissä pienempi. Kirjallisuusselvityksen perusteella tämä voidaan selittää sillä, että paksummissa näytteissä rekombinaatiota tapahtuu enemmän. Lisäaineen lisääminen puolestaan pienensi selvästi avaruusvarauksen kertymistä riippumatta näytteissä käytetyistä polymeerikomponenteista tai mittausparametreista. Havaintoa tukivat myös nettovarauskertymän vertailu ja projektikumppanin tekemät PEA-mittaukset, jotka osoittivat samankaltaisia tuloksia.

Avainsanat: HVDC, avaruusvaraus, polymeerieriste, polypropeenisekoitus, TSDC, lisäaine, varausten loukkuuntuminen, korkean kentän johtavuus

USE OF AI IN THESIS

I have utilised AI tools in my thesis:

☐ No
☒ Yes

In this thesis I have used AI tools. Tools used were Copilot (GPT-4) and ChatGPT (GPT-4, GPT-5)

AI was used for translating texts between Finnish and English, improving the fluency of linguistically awkward sentence structures, and clarifying theoretical sections from source texts that were sometimes presented in a linguistically complex manner.

I acknowledge that I am fully responsible for the entire content of my thesis, including the parts generated by AI, and accept accountability for any violations of ethical standards in publications.

PREFACE

This Master of Science Thesis was done for the Electrical Engineering Unit at Tampere University as a part of the NEWGEN-project. The focus of the thesis was to measure and analyse charge transport and trapping phenomena in polymer blends.

First of all, I would like to thank Adjunct Professor and Senior Scientist Kari Lahti and Dr. Minna Niittymäki, Postdoctoral Research Fellow, for providing an interesting research topic and for their valuable advice, guidance, and support. Their contributions, including access to the necessary equipment, were essential for carrying out this thesis.

I would also like to express my gratitude to M.Sc. Eevertti Laine for the valuable discussions and support during this work. In addition, I wish to thank Lab. Engineer Mervi Koskinen and Doctoral Researcher Helmer Piirilä for their guidance and introduction to the cleanroom facilities and equipment. In addition, I would like to thank Labtech. Bengt-Olof Holmström for the smooth collaboration in providing liquid nitrogen gas.

Finally, I wish to extend my deepest gratitude to my parents, family, and godparents for their unwavering support, hospitality, and encouragement, which have been invaluable in enabling me to complete both my Master of Science degree and this thesis.

Tampere, September 30, 2025

Sami Lähteenmäki

Funded by the European Union Grant Agreement Nº 101075592. Views and opinions expressed are, however, those of the author only and do not necessarily reflect those of the European Union or CINEA. Neither the European Union nor the granting authority can be held responsible for them.

TABLE OF CONTENTS

LIST OF SYMBOLS AND ABBREVIATIONS

A	Constant
AC	Alternating current
AO1	Antioxidant
B	Constant
DC	Direct current
DP	Degree of polymerisation
FEF	Field enhancement factor
HDPE	High density polyethylene
HECO	Heterophasic polypropylene copolymer
HOMO	Highest occupied molecular orbital
HVDC	High voltage direct current
LD	Low density
LDPE	Low density polyethylene
LUMO	Lowest unoccupied molecular orbital
MIND	Mass-impregnated non draining
NaCl	Sodium chloride
OC	Open circuit
PBE	Propylene-based elastomer
PD	Partial discharge
PEA	Pulse electro acoustic
PP	Polypropylene
RACO	Homophasic polypropylene random copolymer
SC	Short-circuit
SCLC	Space charge limited conduction
TSC	Thermally stimulated current
TSDC	Thermally stimulated depolarisation current
TSPC	Thermally stimulated polarisation current
XL	Cross-linked
XLPE	Cross-linked polyethylene

C_a	Capacitance in the equivalent circuit for dielectric material
C_p	Parallel capacitance of equivalent void circuit
C_s	Series capacitance of equivalent void circuit representing dielectric material
C_v	Void capacitance of equivalent void circuit
d	Thickness, distance
ΔE_t	Energy difference between conduction band and Fermi level
E_a	Activation energy
E	Electric field strength
$\boldsymbol{E_C}$	External electric field strength
E_c	Energy level of conduction band bottom
E_f	Fermi energy level
E_{int}	Energy level of interest
E_L	Local electric field strength
$\boldsymbol{E_M}$	Electric field due to dipoles
E_{mc}	Critical electric field strength
$\boldsymbol{E_P}$	Electric field due to polarisation
E_P	Poling field
E_t	Energy level for forbidden trap states

E_v	Energy level of valence band top
$e_p(t)$	External electric field pulse
$\Delta F(z,t)$	Perturbation force acting on charges
G_a	Activation energy of conductivity
g	Kirkwood's correlation coefficient
J	Current density
k	Constant
k_b	Boltzmann constant
M_i	Molecular mass of type I
$\overline{M_n}$	Number average molar mass
$\overline{M_w}$	Weight-average molecular mass
N_A	Avogadro's constant
N_{eff}	Density of states available in the conduction band
N_i	Number of molecules of type a
N_M	Number of molecules per unit volume
N_t	Trap state volume density
n_r	Refractive index
n_c	Electron density in conduction band
n_i	Charge carrier volume density of type i
n_t	Number of occupied states per unit volume
n_0	Charges injected from electrode
n_1	Charges present in insulator
$P(E,T)$	Fermi-Dirac propability distribution
$\boldsymbol{P}$	Polarisation vector
PP-g-MAH	Polypropylene grafted maleic anhydride
$\Delta\boldsymbol{p}$	Electrical dipole moment
$\Delta p(z,t)$	Acoustic shock wave generated by the dislocation of charges
p	Pressure
$p(t)$	Total acoustic wave arriving at the transducer
$\boldsymbol{p_m}$	Dipole moment of a single molecule
p_p	Permanent dipole moment
Q	Charge per electrode unit area
q	Electric charge
q_i	Electric charge of type i carrier
R_a	Resistance in the equivalent circuit for dielectric material
R_s	Series resistance of equivalent void circuit
r	Distance
r_{max}	Maximum distance
T	Temperature
T_g	Glass transition temperature
T_m	Crystalline melting temperature
T_p	Poling temperature
Δt	Pulse duration
t_l	Statistical time lag
V_a	Applied voltage
V_{DC}	Direct current voltage
V_i	Inception voltage
V_{max}	Maximum voltage
V_{TFL}	Trap-Filled Limit voltage
V_{tr}	Threshold voltage
Δv	Volume element
v_d	Drift velocity
$v_e(t)$	Electrical signal generated by the piezoelectric transducer

w_i	Mass of a molecule of type i
$wt - \%$	Weight percent
α	Polarisability
β	Heating rate
δ	Loss angle
ε	Permittivity
ε'	Real part of complex permittivity
$\varepsilon'(\omega)$	Real part of frequency dependent permittivity
ε''	Imaginary part of complex permittivity
$\varepsilon''(\omega)$	Imaginary part of frequency dependent permittivity
ε_0	Permittivity of free space
ε_r	Relative permittivity
ε_s	Static permittivity
ε_∞	High frequency permittivity
θ_{ct}	Ratio of free charge carriers to trapped charge carriers
μ	Mobility if charge carrier
μ_i	Mobility of charge carrier of type i
μ_∞	Charge carrier mobility above critical field strength
ρ_{sp}	Space charge density
$\rho(z)$	Spatial charge density
σ	Conductivity
$\sigma(T)$	Low field electric conduction
$\sigma(T, E)$	Temperature and electric field dependent conductivity
σ_∞	High temperature reference conductivity
σ_0	Material dependent conductivity constant
τ	Relaxation time
τ_c	Transit time
τ_d	Relaxation time of the insulator material
τ_{DC}	Dielectric time constant
ω	Angular frequency
χ	Electric susceptibility
$tan\,\delta$	Dissipation factor

1 INTRODUCTION

As renewable and environmentally sustainable electricity generation, such as wind farms, large-scale photovoltaic installations, and hydropower plants are increasingly located further from population centers and areas of high electricity consumption, there is a growing need for long-distance, high-capacity transmission infrastructure. These installations are often situated in more challenging environments, for example offshore wind farms or remote solar power plants, which further increases the technical demands on transmission systems. In this context, high voltage direct current (HVDC) cable systems offer clear advantages due to their lower transmission losses, higher power density, and suitability for extended subsea and underground transmission routes, where alternating current systems would otherwise be constrained by charging current effects. Moreover, HVDC links can help prevent cascading failures and enable interconnection of asynchronous alternating current (AC) systems.[1], [2], [3]

Traditionally, HVDC cable insulation relied on mass-impregnated non-draining (MIND) paper and oil-based technologies. However, environmental concerns, more complex manufacturing and installation processes, and increasing voltage levels have encouraged a shift toward extruded polymeric insulations such as cross-linked polyethylene (XLPE) and more recently thermoplastic polypropylene (PP). [3], [4] Compared to oil-paper technologies, extruded insulations are simpler to install, and eliminate the risk of oil leakage. PP-based materials offer additional advantages, such as recyclability, higher operating temperature and transmission capacity compared to existing materials, making them particularly promising for the next generation of HVDC cables. [3], [5]

Unlike AC insulation, where polarisation effects are periodic and dissipative, direct current (DC) insulation systems are susceptible to space charge accumulation that leads to field distortion within the dielectric. Charge injection, trapping, and detrapping processes can alter the internal field distribution and contribute to premature breakdown, aging and degradation of the cable insulation, especially in the presence of temperature gradients, voltage polarity reversals and transients. [3], [5], [6]

PP has emerged as a viable alternative to XLPE for HVDC cable insulation, primarily due to its higher thermal endurance as well as its recyclability and low dielectric losses. However, pure PP is relatively stiff and brittle, especially at low temperatures. As a result, blending with elastomers or copolymers, or the addition of plasticisers or nanoparticles, is often necessary to enhance mechanical flexibility and impact resistance without compromising its electrical properties. Furthermore space charge mitigating additives are under development. [4]

The purpose of this thesis is to investigate charge trapping and transport phenomena in PP-based polymer insulation materials and additives using thermally stimulated polarisation current (TSDC) measurement technique. The thesis focuses especially on analysing the nature of space charge accumulation, its relaxation through depolarisation and analysing the results. This research is further motivated by the growing demand for HVDC cable systems capable of transmitting higher power levels, which places increasing stress on insulation materials. Consequently, space charge accumulation has emerged as a critical challenge affecting the long-term reliability and electrical performance of these systems.

Chapter 2 introduces the fundamental concepts of polymer materials, beginning with chemical bonding and molecular structure, and progressing toward their macroscopic morphology. The chapter highlights the complex, multi-scale nature of polymer structure, as each hierarchical level from atomic-scale bonding to crystallinity and morphological features, plays a significant role in determining the electrical properties of insulating polymers. Understanding these structural aspects is essential for interpreting differences between materials and for explaining their behaviour under electric stress.

The beginning of Chapter 3 discusses energy band theory, continues with different forms of conductivity and the injection and movement of charges within insulators. These mechanisms are examined in both low and high electric fields, as they determine how and under what conditions charges can move to and within a material. Next, attention is turned to the formation of space charge in dielectric materials, and finally, the key properties of dielectric materials, such as permittivity and various polarisation and relaxation mechanisms, are examined. These phenomena are essential for understanding how the electric field is distributed within the insulator and how charges interact with the structure of the material.

The long-term reliability of polymeric insulating materials is determined not only by their initial electrical and mechanical properties but also by the effects of various aging and degradation processes. These processes have a decisive influence on the dielectric strength and ultimately on the breakdown endurance of the insulation. Aging can be considered as a gradual change that may be of physical, chemical, or electrical nature. Under certain conditions, however, these processes can lead to rapid and localised damage that significantly compromises the performance of the insulation. Chapter 4 provides a general overview of such phenomena and emphasises specific features that are particularly relevant in DC applications, such as charge accumulation and its impact on electric field distribution. Furthermore, more detailed mechanisms and principles are introduced to describe how different failure phenomena evolve on different time scales, ranging from long-term aging to fast breakdown events.

The experimental part of this thesis is presented in Chapters 5 and 6. Chapter 5 discusses measurement methods suitable for studying space charge, including the TSDC method used in this work and describes how material samples were prepared. In addition, Chapter 6 presents and examines measurements made on PP compounds, additives added to them and introduces the ratios and concentrations of components and additives in PP blends, as well as the results obtained from measurements.

2 POLYMERS

2.1 Basic concepts of polymers

Polymers are long-chain molecules with high molecular weight. For this reason, polymers are sometimes referred to as macromolecules. [7] By definition, a polymer is a compound that consists of one or more species or groups of atoms, and this structure is repeated many times. As a result, the compound exhibits a set of properties that are not significantly altered by the addition of one or a few structural *repeating units* [8].

Polymers are composed of small and simple repeating units [9]. In the *polymerisation* process, *monomers* are linked together in chemical reactions to form long chains of varying lengths called polymers [10]. Monomers form a repeating structural unit, which can be made up of either identical or nonidentical monomers. For example, the different polypropylene materials studied in this thesis are formed in a polymerisation process from the monomer shown on the left in Figure 1. The n in the Figure 1 indicates the number of repeating structural units in the polymer chain, i.e. in the molecule. This is called the *degree of polymerisation* (DP). It determines the length of the polymer molecule.[11]

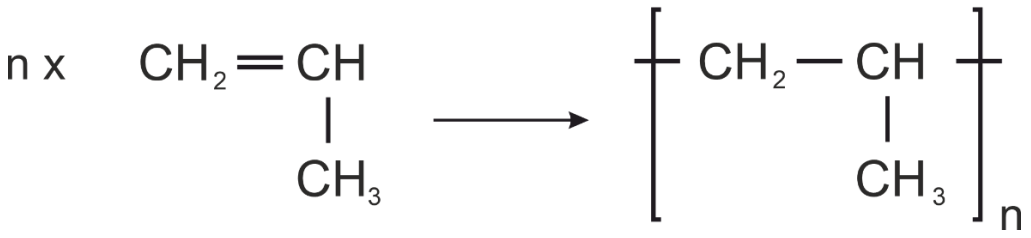

Figure 1. *General pattern of polymerisation of propylene. Monomer on the left and polymer on the right. [9]*

Oligomers are short-chain polymers whose physical properties vary depending on whether repeating units are added or removed. Polymers and oligomers are formed from monomers, but their differences can be determined by their thermal and mechanical properties for practical applications. Oligomers do not have sufficient strength to be useful in practice, whereas polymers are structurally robust enough to be used for a variety of applications requiring mechanical strength. [8], [12]

The properties of polymers are primarily based on their large molecular size, i.e. their high degree of polymerisation. According to [9], increasing the degree of polymerisation in polyethylene increases the molecular weight and the softening temperature. The further the polymer is polymerised, less its key mechanical properties change. Figure 2 a) gives an example of how the most important mechanical properties, such as tensile strength, stretch, elastic modulus and impact strength, change as the polymerisation progresses. When monomers are polymerised, a variety of polymer

molecules of different sizes are formed. [9] This is the case for at least all synthetic polymers, with the exception of a few biological polymers, which have a very well-defined molecular weight [11]. In practice each polymeric material consists of a distribution of chain lengths rather than a single uniform size. This variability is typically described using molar mass averages [9].

The two most important molar mass averages are the average molar mass $\overline{M_n}$, which indicates the average chain length of the polymer and can be expressed as follows

$$\overline{M_n} = \frac{\sum_i N_i M_i}{\sum_i N_i}, \tag{1}$$

where N_i is the number of molecules and M_i their molecular mass. The other important average, the weight-average molecular mass $\overline{M_w}$, which indicates the weight of the polymer and can be expressed according to the following formula

$$\overline{M_w} = \frac{\sum w_i M_i}{\sum w_i} = \frac{\sum_i N_i M_i^2}{\sum_i N_i M_i}, \tag{2}$$

where w_i is the weight of the molecule. Figure 2 b) shows the principle diagram of the average molecular weight of a polymer and the curve of molecular weight distributions. [7]

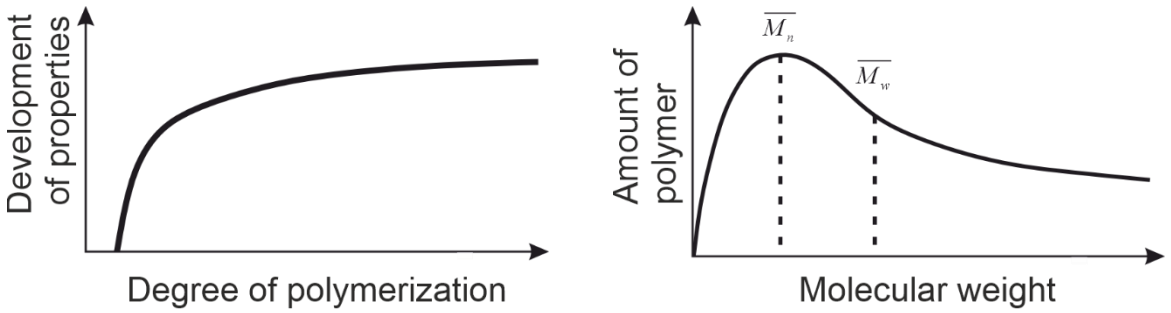

a) b)

Figure 2. *a) a principle diagram of how the most important properties develop as a function of degree of polymerisation [9] and b) a diagram of typical number and weight average molecular weights [11].*

In addition to the average of the two main molecular weight values, the ratio of the two can be compared to obtain a ratio that can explain how wide the variation in polymer chain length is. This ratio is called the *polydispersity* or *heterogeneity* index and can be expressed in the following formula

$$polydispersity = \frac{\overline{M_w}}{\overline{M_n}}. [11] \tag{3}$$

2.2 Chemical bonds

The elements tend to reach a state where their outer electron shell is filled. This occurs either by donating, accepting or sharing electrons, resulting in the formation of various chemical bonds. Bonds are divided into *primary* and *secondary bonds*, of which primary bonds are stronger, as the valence

electrons are involved in the formation of the bond. Secondary bonds, on the other hand, are weaker because they do not rely on the sharing or transfer of valence electrons between atoms. Primary bonds are divided *into ionic, covalent* and *metallic bonds*, with ionic and covalent bonds occurring in polymers. Secondary bonds are classified as *dipole-, induction-, van der Waals forces* and *hydrogen bonds.* [10]. Although secondary bonds are much weaker than primary bonds, they still have a significant influence on the properties and physical behaviour of polymers [8].

2.2.1 Primary bonds

An ionic bond is formed when two atoms transfer electrons between each other. An electronegative element accepts an electron, while an electropositive element donates one. A good example of ionic bonding is sodium chloride (NaCl), where sodium donates one electron to chlorine. In this case, sodium becomes a positive ion and chlorine a negative ion. The binding force is due to the electrostatic force between the ions. Ionic bonds are not common in polymers but are known to occur in natural resins and ionomers. [11]

Organic polymers are composed of carbon, hydrogen and often oxygen, nitrogen, sulphur or halogens, and their atoms can be bonded together by strong covalent bonds [8]. A stable electron configuration can be achieved by sharing valence electrons. The bonds formed through electron sharing are called covalent bonds. For example, in Figure 3, methane, where one carbon atom forms a bond with four hydrogen atoms, both the carbon and hydrogen atoms have their outermost electron shells filled. This is the predominant bond in polymers. Covalent bonds can be single, double or triple depending on the number of electron pairs. [11]

2.2.2 Secondary bonds

Molecules form a permanent dipole if the centres of their positive and negative charges are not at the same point. This occurs if the bonding electrons are unevenly distributed between the atoms due to the different electronegativities of the atoms. [11] An atom with a higher electronegativity attracts more electrons and becomes negatively charged, while an atom with a lower electronegativity becomes positively charged. The resulting molecules may have a dipole moment depending on their symmetry. [8]

The total dipole moment of a molecule is determined by the vector sum of the dipoles in its structure. Figure 3 shows the molecules methane, water and polyethylene, all of which have dipole moments, but their vector sum may be zero. In a methane molecule, the dipole moments are directed from the carbon atom towards the hydrogen atoms. Since methane is symmetric, the sum of all dipoles is zero, which means that it is a non-polar molecule. In a water molecule, the dipole moments point from the oxygen atom towards the hydrogen atoms. The asymmetric structure of the molecule

prevents the dipoles from cancelling each other, which results in the water molecule having a dipole moment in the direction shown in Figure 3 and is therefore polar. Polyethylene is an example of a non-polar polymer. Each carbon hydrogen bond has dipole moments, but the dipole moments of adjacent units cancel each other out. This is why polyethylene as a whole is non-polar. [8]

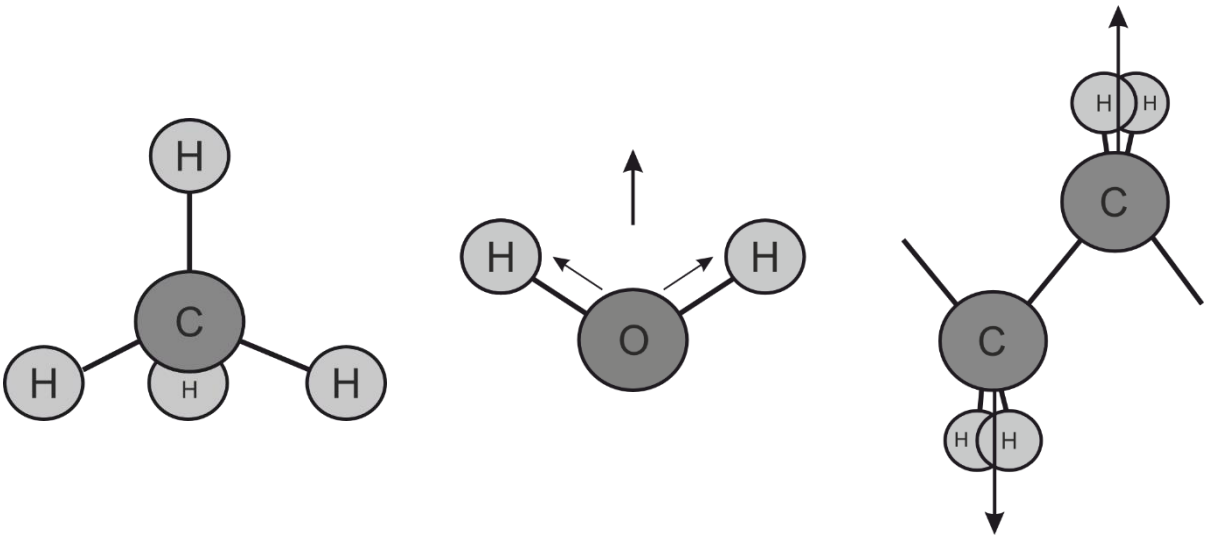

Methane Water Polyethylene

Figure 3. *Dipole moments of methane, water and polyethylene. Methane has no dipole moment when calculating the vector sum of the dipole moments of a molecule. The same is true for polyethylene, but water has a dipole moment due to its asymmetric structure and is also an example of poler molecule.*

An electric field is formed around a polar molecule, which affects the nuclei and electrons of surrounding molecules or atoms. As a result, the surrounding molecules become polarised, creating induced dipoles. The interactions between stationary and induced dipoles are called induction forces. [8], [11]

Non-polar molecules can also experience momentary dipoles, although their average positive and negative charge centres are at the same point. This is because the electrons are constantly moving around in the molecule, and an imbalance of charge centres, or dipole, momentarily forms in the molecule. When two adjacent molecules are exposed to each other's momentary dipoles, attractive forces are created between them. This interaction is called the van der Waals force. Van der Waals forces are weak interactions and occur in all types of molecules, including non-polar ones. Although these forces are weak, they have a significant effect on the physical properties and behaviour of polymers. [11]

Hydrogen bonding is a special form of dipole interaction in which a positively charged hydrogen atom bonds strongly to an electronegative atom, such as fluorine, oxygen or nitrogen. Hydrogen bonds are relatively strong compared to other dipole bonds because the small size of hydrogen allows the

atoms to interact closely. In the structure of polymers, hydrogen bonds occur particularly between functional groups and have a significant influence on the material properties and behaviour. [11]

2.3 Polymers structure

2.3.1 Classification and chemical variations of polymers

Polymers can be classified in many ways according to their origin, structure, formation method, atomic bonding, thermal behaviour, intended use and polymerisation technique, including bulk polymerisation, solution polymerisation, suspension polymerisation and emulsion polymerisation. In addition, polymers are further classified into condensation polymers and addition polymers based on the polymerisation reaction. [11]

Polymers can be either *natural* or *synthetic*. Natural polymers include proteins, which are biological polymers, and natural rubber from plants. Synthetic polymers, on the other hand, cover a wide range of materials that can be classified into different categories, such as *fibres*, *elastomers* and *adhesives*. [11]

Polymers can be classified according to their structure into linear, branched and cross-linked polymers. As stated at the beginning of this chapter, polymers are composed of a large number of structural units, which are linked together by covalent bonds under suitable conditions. The formation of these bonds is described by the concept of *functionality*, which expresses the ability of a molecule to form bonds under specific polymerisation conditions. [11]

A molecule can be *monofunctional*, *bifunctional* or *polyfunctional*, depending on whether it has one, two or more reactive units that allow it to attach to other molecules. For example, in the polymerisation of propylene, as shown in Figure 1, the double bond between the carbons opens, allowing the structural units to join through new bonds. In this case, the functionality of propylene is 2 because it can form two new bonds. However, depending on the circumstances, the functionality can be different than two. The formation of a polymer requires at least bifunctionality. When bifunctional monomers are used in a polymerisation reaction, the result is always linear polymers. In contrast, polyfunctional reactions may result in non-linear structures, such as branched chains or cross-linked structures. Branched structures are formed when the growth of a side branch of a polymer stops before a new bond is formed. A cross-linked structure is formed when the growing polymer chains are linked together. [11] The structures are illustrated in Figure 4.

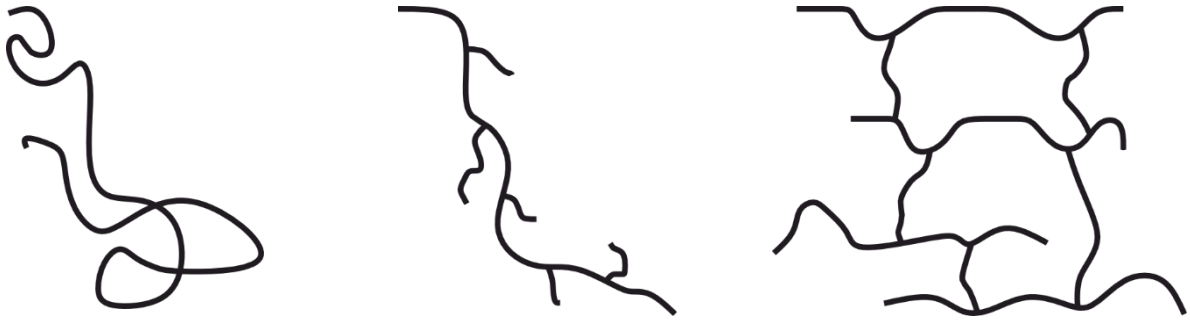

Figure 4. *Principle of linear, branched and cross-linked polymers.*

Polymers can also be classified according to their secondary, weaker bonds. The structure of the molecule affects how closely they can be arranged in proximity to each other. Molecules with a regular structure can fit very close together, strengthening intermolecular bonds. Such polymers are called fibres, typically linear and symmetrical polymers with strong intermolecular interactions often arising from polar groups. On the other hand, asymmetric molecules form weaker intermolecular bonds, leading to flexible polymer chains. Such polymers are called elastomers. Their chain segments can move locally, but the movement of the entire polymer chains is limited by individual cross-linkages that give the material its elasticity. Between fibres and elastomers, there are plastics. It is sometimes difficult to distinguish between fibres and plastics, even if they are chemically different. For example, the polypropylene discussed in this thesis can be classified as either a fibre or a plastic, depending on the processing technology used. [11]

Polymers consist of repeating structural units, which in turn can be made up of either one or more different monomers. If all structural units come from the same monomer, the polymer is called a *homopolymer*. On the other hand, if the structural units are formed from two or more different monomers, the polymer is a *copolymer*. Copolymers can be further divided into four subcategories, *random*, *alternating*, *block* and *graft* copolymers. In a random copolymer, the structural units are scattered in the chain in no particular order. In an alternating copolymer, the structural units alternate regularly. In a block copolymer, the polymer chain consists of longer sequences of segments alternately connected to each other. In a graft copolymer, on the other hand, the backbone chain of one structural unit is joined by branch chains of another structural unit. Figure 5 shows four different types of copolymers. [11]

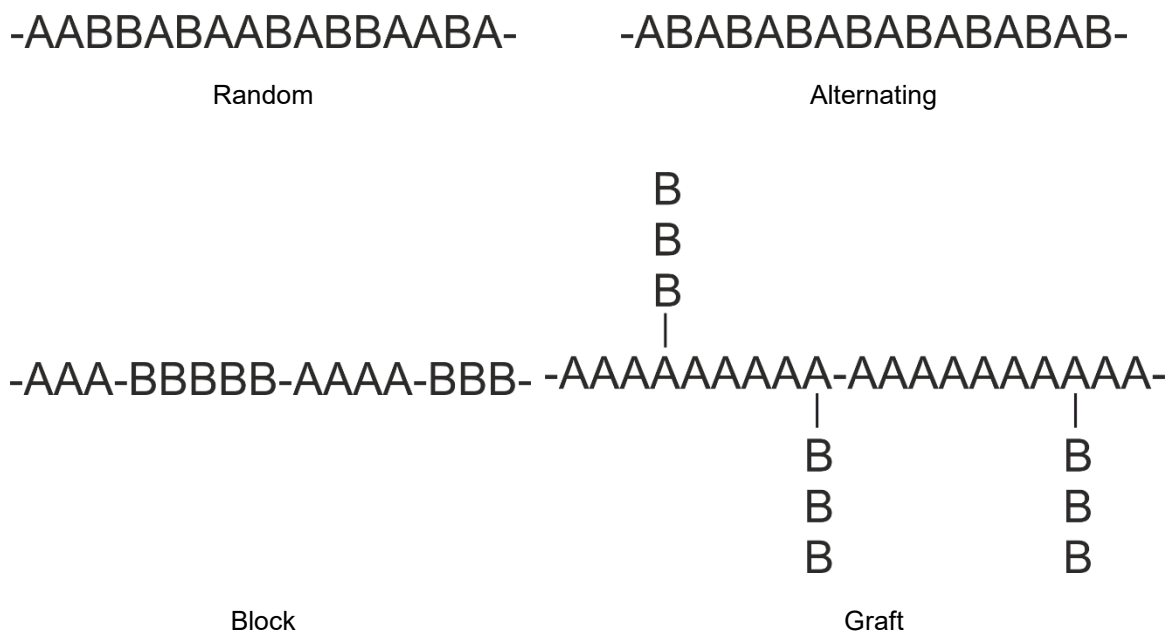

Figure 5. *Basic concept of the different types of copolymers: random, alternating, block and graft copolymer.*

Based on thermoplasticity, polymers can be classified into *thermoplastics* and *thermosets* [9]. Thermoplastics soften when heated and harden when cooled. These processes are therefore reversible and can be repeated. At the molecular level, secondary forces holding the chains together weaken and allow more movement of the chains. When a thermoplastic polymer is overheated, it loses its ability to be reshaped. Thermoplastic polymers are generally quite soft. Most linear polymers or polymer chains with only a few branched flexible side chains are thermoplastic [13], while thermosets form a network polymer skeleton that does not soften when heated [7]. The adjacent molecular chains are cross-linked with covalent bonds. When heated, these bonds resist thermal vibration and chain rotation and thus thermosets do not soften when heated. About 10-50 % of the repeating structural units of thermosets are cross-linked. When the thermoset is heated to a high enough temperature, these intermolecular bonds are broken, leading to degradation of the polymer. [13]

2.3.2 Conformation and configuration

The structural regularity of a polymer chain is considered in terms of *recurrence regularity* and *stereoregularity*. Recurrence regularity describes how uniformly the repeating units occur in the chain and stereoregularity describes how the three-dimensional order of the repeating units in the chain is arranged. By repeatability, for example, the polypropylene in Figure 1 could be arranged in three different ways, from *head-to-tail*, *head-to-head* or *tail-to-tail*. Figure 6 shows how the structural units of polypropylene could be arranged. In reality, in known polymers, only the first head-to-tail

configuration is found in measurable quantities. [11] Although the molecular formula of the different configurations may be the same, their structure is different and potentially affects the properties of the molecule [14].

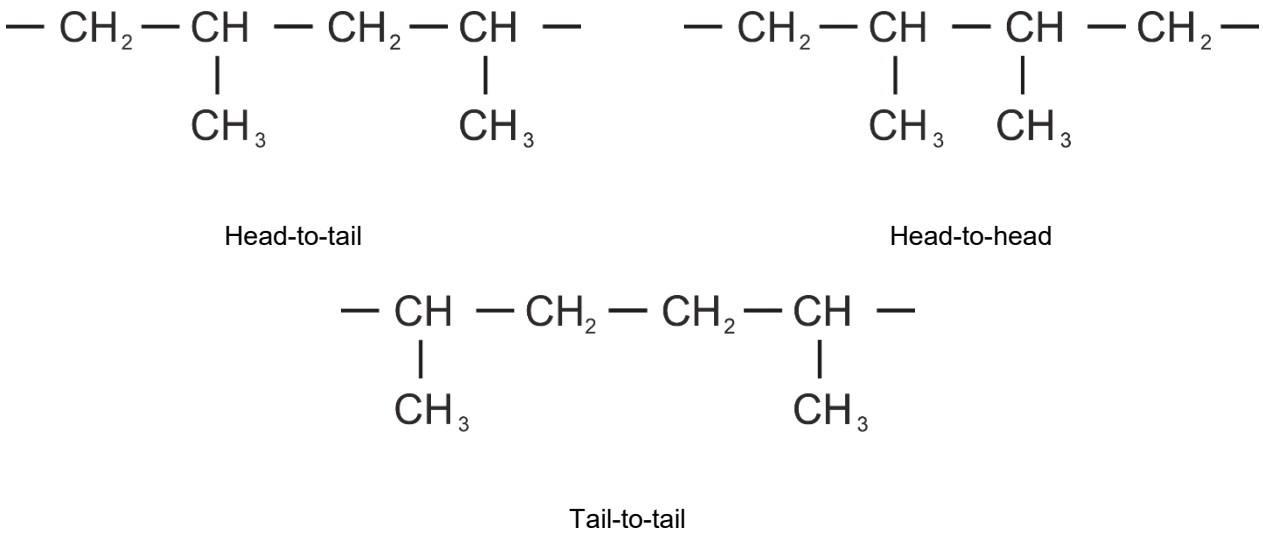

Figure 6. *Three different options for recurrence regularity of polypropylene. The last two forms are not found in measurable quantities.*

There can be geometric differences, which occur in molecules with a double bond. An example of such geometric differences represented in Figure 7 is but-2-ene, whose cis and trans forms illustrate how the structure of the molecule can also affect its polarity. [8] The cis structure often has a higher dipole moment because the polar groups are closer together. The transformation, on the other hand, is usually more symmetrical and less polar. In the case of polymers, this isomerism can significantly affect the mechanical and elastic properties of the material. [13]

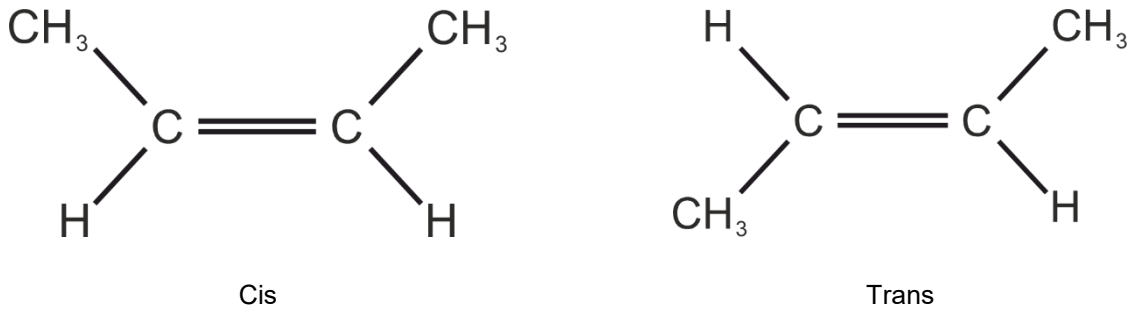

Figure 7. *As an example of cis and transforms illustrated with But-2-ene.*

Tacticity describes how the spatial order of the basic units of a polymer chain is distributed in the main chain. In an *isotactic* polymer, the X-group is regularly arranged so that all units are either in d- or l-form, i.e. either to the right or to the left of the spine of the chain as viewed from the end of the chain. In a *syndiotactic* polymer, the configuration alternates regularly, with the X-group repeating in the order d-l-d-l-d-l. In an *atactic* polymer, the X group is distributed irregularly with respect to the carbon backbone, i.e. their structure is disordered. [10] Figure 8 shows the isotactic, syndiotactic

and atactic forms of the molecules, which in the case of polypropylene show the regular or irregular arrangement of the $-CH_3-$ group.

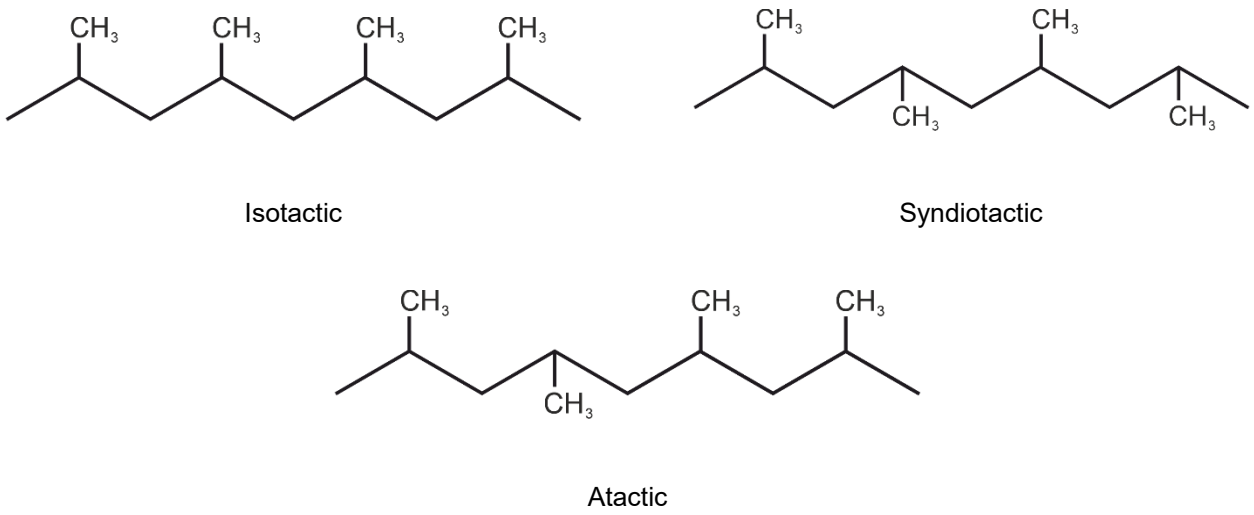

Figure 8. *Iso-, syndio- and atactic forms of polypropylene.*

In a polymer molecule the carbon-carbon single bond can be twisted, allowing the chain to take different conformations. In an extremely ordered form, all the carbon atoms in the molecular chain are aligned in the same plane, forming a zigzag pattern. Such a structure is typical of crystalline and highly ordered polymers such as polyethylene. At the other extreme, the molecular chain is completely randomly ordered, which is characteristic of amorphous polymers and polymers in melt or solution [11].

2.4 Polymer morphology

2.4.1 Morphology and factors affecting it

The structure of a polymer and the interactions between molecules determine whether the material is essentially crystalline or amorphous. In a crystalline polymer, the chains are regularly arranged, whereas in an amorphous polymer the chains are randomly entangled and twirled. [11]

Polymer crystallisation is influenced by intermolecular forces, primarily van der Waals forces, which are secondary bonds. Crystallisation requires regular and tight chain arrangement [15], and factors such as chain mobility, strong interchain bonds, and structural regularity play a key role [11]. For example, isotactic polypropylene crystallises, whereas atactic polypropylene does not due to differences in molecular packing [8]. In general, iso- and syndiotactic polymers crystallise more easily than atactic ones. Flexible molecular chains are more affected by thermal motion, making crystallisation more difficult. Certain functional groups influence flexibility by either increasing or decreasing chain mobility, while polar groups can also affect crystallinity. Hydrogen and dipole bonds

strengthen intermolecular forces, promoting crystallisation, whereas bulky side groups may obstruct it. [11]

Polymer crystallisation is influenced by surrounding conditions, particularly *nucleation*, the initial stage where crystal structures begin to form. Nucleation can occur spontaneously, due to impurities, or through nucleation-promoting additives. [15] Crystallisation begins via *homogeneous* or *heterogeneous* nucleation. In homogeneous nucleation, crystals form randomly as molecules organise themselves or align with existing crystals. In heterogeneous nucleation, crystals grow around impurities, catalyst residues, pigments, or surface irregularities. [13] This process can be controlled by nucleating agents, which influence nucleation density and rate. Polymer crystallisation is influenced by cooling rate. Rapid cooling prevents polymer chains from organizing into a regular structure, increasing the amorphous fraction and specific volume. Slow cooling allows greater crystallinity as chains have more time to align. The effect of temperature on polymer structure is reflected in specific volume changes. In crystalline polymers, specific volume drops sharply at the melting point as molecules pack more tightly. In amorphous polymers, volume decreases linearly with temperature until reaching the glass transition temperature T_g, without an abrupt change. [15]

During the manufacturing process, when producing thin films, the flow of the polymer during cooling from the molten state into a sheet-like thin film may affect the orientation of polymer chains and thus its morphology [11]. In particular, the chains may extend rather than adopt their typical helical structure [15].

Polymer crystals grow from lamellae, which are thin sheet-like structures made up of folded molecular chains. The lamellae are typically about 10-20 nm thick, 1 μm long and 0.1-1 μm wide [15]. Since molecular chains in polymers are generally longer than lamellae, the formation of lamella requires that the molecular chain is folded. The ends of the chains can either fold back from the edges of the lamella, extend outside the lamella and fold back into the lamella, or end inside the crystal, creating a defect in the crystal. [11] Figure 9 illustrates a simplified model of the lamellar structure, demonstrating how molecular chain folding and termination can lead to various imperfections within the crystalline regions of a polymer.

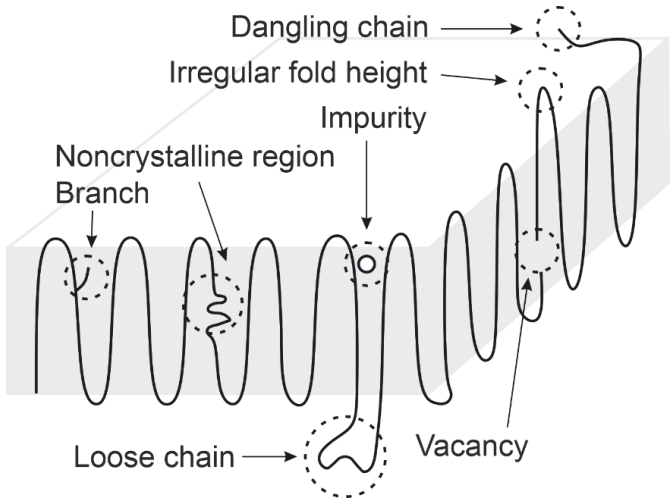

Figure 9. *Schematic representation of a crystalline polymer's lamellar structure, highlighting common irregularities and defects such as dangling chains, vacancies, impurities, and non-crystalline regions.*

During polymer crystallisation from the melt, crystalline and amorphous regions are formed. As crystallisation progresses, spherulites develop, expanding at the expense of amorphous material, which consists of uncrystallised residues [11]. The polymer melt contains molecules with varying molecular weight, branching, and tacticity. Higher molecular weight, less branched molecules crystallise first, pushing shorter, atactic, and highly branched molecules to the edges of growing spherulites. [15] As spherulites expand, their growth fronts meet, binding them together. Though primarily crystalline, spherulites contain chain ends, dislocations, and impurities, influencing their size and perfection. Crystallisation rate significantly affects final crystallinity, fast crystallisation increases amorphous content, while slow crystallisation promotes a more complete crystal structure. As a result, polymer crystallinity can vary widely. [11] In Figure 10 spherulite growing from nucleation centre is represented.

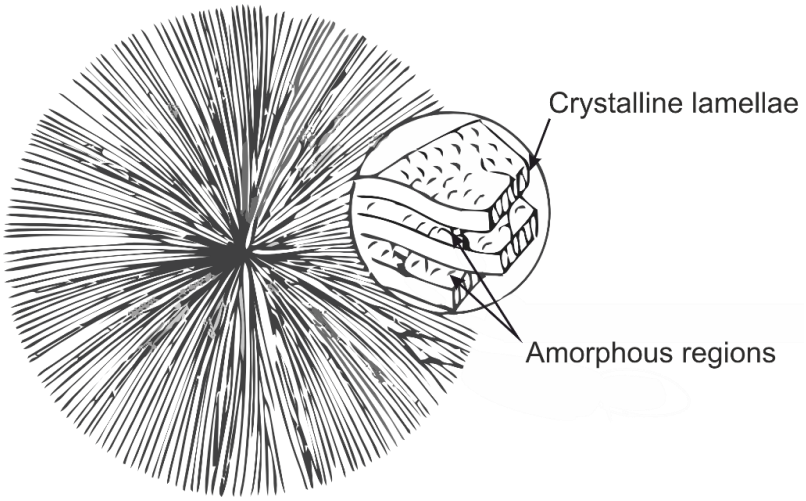

Figure 10. *Spherulite structure consisting of crystalline lamellae growing from a nucleation point and separated by amorphous regions. The schematic enlargement illustrates how alternating crystalline and amorphous phases organise within the spherulite. [15]*

Cross-linking a linear polymer before crystallisation can prevent the crystallisation of a normally semi-crystalline polymer. Usually, crosslinking is done with a heat-activated catalyst, which often requires a temperature higher than the melting point of the polymer. In this case, cross-linking can start before crystals are formed, which prevents molecular rearrangement and crystallisation. However, there are also cross-linking methods that do not require such high temperatures, allowing the material to retain its crystalline structure. Examples of such methods are silane cross-linking and cross-linking by radiation. [15]

Defects may occur in the polymer structure itself. Defects reduce the packing efficiency of polymer chains within the crystalline lamellae, which increases the specific volume of the crystalline regions and consequently lowers the melting point of the polymer. [11] Voids and hollow structures are also always present in polymers, which can occur during the manufacturing process, for example as a result of cross-linking, impurities and additives. The movement of molecules also means that space is likely to be created and lost continuously, leading to fluctuations in thermal density. [15]

Polymers are rarely found as such, but often have various substances added to them to change their structure and properties. These added substances can be classified as *auxiliaries*, *additives* and *compounding agents*. Auxiliaries are compounds that are almost entirely consumed during the manufacturing process, leaving only small residues. For example, catalysts used in cross-linking are included in the category of auxiliaries, although they may remain in the insulating material after manufacture. Additives do not significantly change the chemical structure of the polymer, but they do affect its properties during use. They are typically added in concentrations of less than 10%. Additives include lubricants and parting agents, stabilisers, flame retardants, pigments, plasticisers,

antimicrobials and antistatic agents. Blending agents are used in higher concentrations of 10-70% and alter the properties of the polymer both during the manufacturing process and after use. [15]

2.4.2 Thermal transition

Polymers are made up of molecular chains of different lengths, which means that their change of state occurs over a range of temperatures, rather than at exactly one temperature. The polydispersity of a polymer, i.e. the extent to which it contains molecular chains of different lengths, affects the temperature range over which state changes occur. [13] Polymers can be divided into *glassy*, *rubbery* and *melt* states, the presence of each depending on temperature. Thermal energy promotes molecular motion, while intermolecular bonds resist it. Therefore, the state changes in polymers depend on their structure. Polymers have two main state transition temperatures, the *glass transition temperature* T_g and the *crystalline melting point* T_m. [11] These transition temperatures are important in determining the applications of the material [13]. Depending on the source, the glass transition temperature of polypropylene which is studied in this thesis is reported to be around -15° to -10°C and the melting temperature is around +165° to +175°C [11], [13].

With amorphous polymers, below the glass transition temperature, the material is hard, brittle and glassy. When the glass transition temperature is reached, the polymer becomes more flexible and enters a rubbery state. This change occurs over a relatively narrow temperature range called the glass transition temperature. In semi-crystalline polymers, the same change only applies to the amorphous regions, as the crystalline structures remain rigid and unchanged. Only at the melting point, the crystals melt and the polymer becomes a viscous liquid. [11]

The different states of polymers can be studied by examining their specific volume as a function of temperature as shown in Figure 11. In amorphous polymers, the volume increases steadily with increasing temperature. When the temperature exceeds the glass transition temperature, the coefficient of thermal expansion increases, resulting in a faster increase in volume. Below the glass transition temperature, the amorphous polymer is in the glassy state, where it is hard and brittle, while above it becomes softer and rubbery, i.e. it enters the rubbery state. As the temperature rises further, the polymer reaches its melting point and turns into a liquid. Semicrystalline polymers behave in the same way, but the changes in the glass transition temperature are less pronounced because the crystalline regions remain rigid and solid. Only at the melting point the crystals melt, resulting in the polymer becoming liquid, with a larger increase in intrinsic volume than with an amorphous polymer. [13]

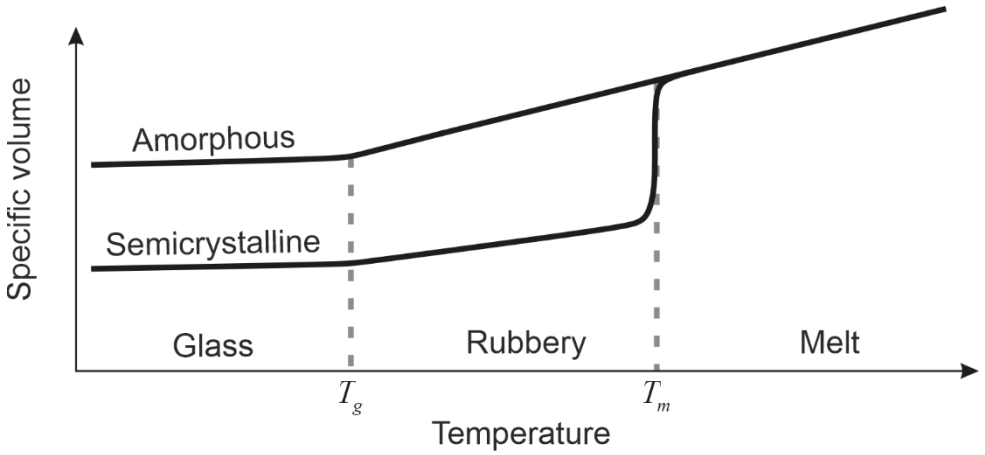

Figure 11. *Specific volume of amorphous and semicrystalline polymers as a function of temperature.*

At the molecular level, in an amorphous polymer below T_g, the molecular chains are solidified and only atoms or small side chains can vibrate. As the temperature increases, the amplitude of the vibrations increases, weakening the strength of the secondary bonds. As heating continues, the molecules become more mobile and require more free space, resulting in an increase in intrinsic volume. The glass transition temperature is affected by many structural and external factors, such as chain flexibility and stiffness, polarity, chain interactions, the influence of geometric factors, copolymerisation, molecular weight, cross-linking, crystallinity, pressure and plasticisers. [11] For example, the polypropylene samples measured in this work have a higher melting temperature than polyethylene because the methyl side group in polypropylene is larger than the hydrogen atom alone in polyethylene. The larger side group is more effective it is in preventing molecular rotation, which has the effect of raising the melting point. [13]

3 ELECTRICAL PROPERTIES OF POLYMERS

3.1 Energy band theory

Electrical properties of materials are fundamentally determined by their atomic structure and the interaction between atoms. To understand electrical conduction in dielectrics, it is useful to begin by examining the energy levels of individual atoms and how they change as the atoms are brought closer together. Energy band theory provides insight into how electrons occupy different energy states and how these states influence electrical conductivity, charge injection, and trapping. This theory can be adapted to understand how more complex and disordered materials like polymers behave.

According to Bohr's atomic model, electrons in single, isolated atoms can only be located at certain discrete energy levels [16], but in solids the situation can be imagined slightly differently. Atoms form bonds with each other, so that the energy values of individual atoms start to diverge [10]. Pauli's exclusion principle states that an atom can have two electrons in one energy level if they have opposite spins [16]. When atoms arrange themselves into a crystalline structure or form molecules, for example, the interaction of electrons with similar initial energies leads to a slight divergence in energy levels. [15] When a large number of atoms form a molecule, the energy levels are densely packed together, forming what are known as *energy bands* [10], [17]. In these bands, electrons can move relatively freely to an adjacent energy level within the band, provided that the space is not already occupied. [15]

In crystals bound by covalent bonds at absolute zero temperature, all electrons are located at the lowest possible energy level on the *valence band*. As the temperature rises, some of the electrons in the valence band may gain enough energy to cross the forbidden *band gap* between the bands to move to the *conduction band*. The distribution of electrons at different energy levels is described by the Fermi-Dirac distribution function. It gives the probability that a given energy level is occupied by an electron. The distribution can be represented as follows:

$$P(E,T) = \frac{1}{1 + \exp\frac{E_{int} - E_f}{k_b T}}, \tag{4}$$

where E_{int} is the energy level of interest, E_f is the fermi energy, k is the Boltzmann constant and T is the temperature. Figure 12 a) and b) shows the Fermi-Dirac distribution together with the valence and conduction bands, illustrating how an electron can gain sufficient energy to transition from the valence band to the conduction band leaving behind a hole. In the Figure 12 b) on the right-hand side, it is shown how an increase in temperature increases the probability that a given energy level is occupied. The higher the temperature, the more likely that higher energy levels are also occupied.

This can be observed in the probability graph as a flattening of the slopes of the curves. If the energy level is exactly at the *Fermi energy level*, the probability of occupation is exactly 50%. The Figure 12 a) also reveals the so-called forbidden band gap between the valence and the conduction bands. [15] At the molecular level, the corresponding concepts are the *highest occupied molecular orbital* (HOMO) and the *lowest unoccupied molecular orbital* (LUMO) [18].

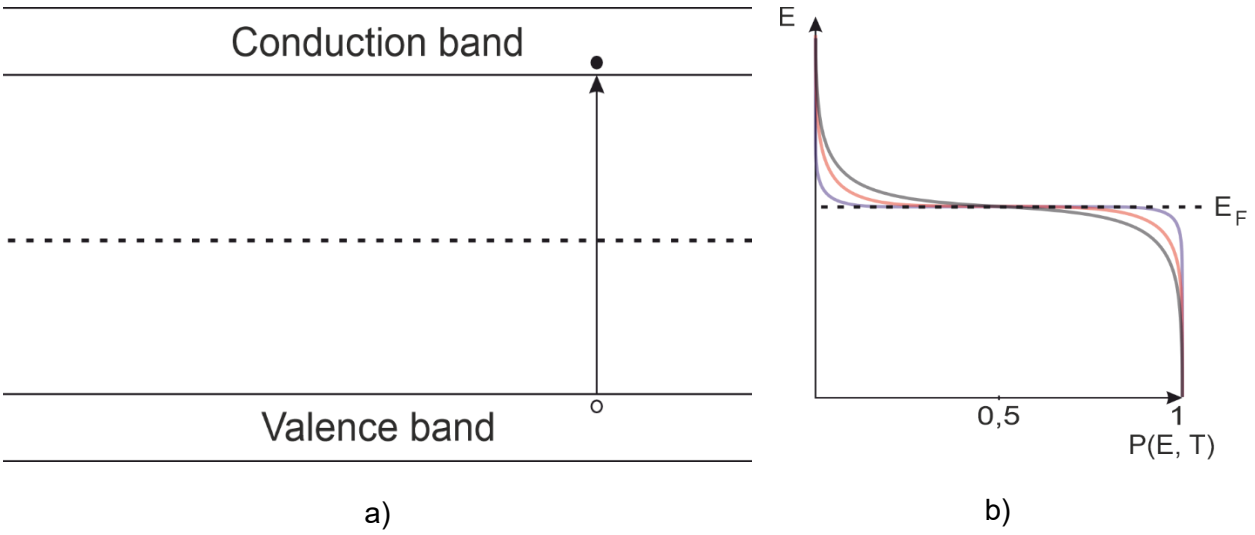

Figure 12. *Energy band diagram of a covalently bonded crystal on a) and on b) the graph of Fermi-Dirac distribution showing the probability of occupying energy level E as a function of temperature.*

With minor modifications, the properties of polymers can be studied using energy band theory. Traditional theory assumes that a material is a completely periodic crystal with a three-dimensionally regular atomic order. However, polymers are composed of long molecular chains of approximately 10^3-10^5 monomers, in which the atoms are strongly bonded to each other by covalent bonds. [15] As the length of the polymer chain increases, so does the number of atomic orbitals. The interaction of these orbitals results in a rearrangement of the molecular orbitals, leading to a distribution of energy levels in densely packed energy bands. [19] This distribution of energy levels is illustrated in Figure 13. The larger the molecule, the more densely packed the energy levels are in close proximity to each other, which allows them to be treated as continuous energy bands. However, such a continuous band is an idealised representation and represents a large set of very close, but still discrete, energy levels [20]

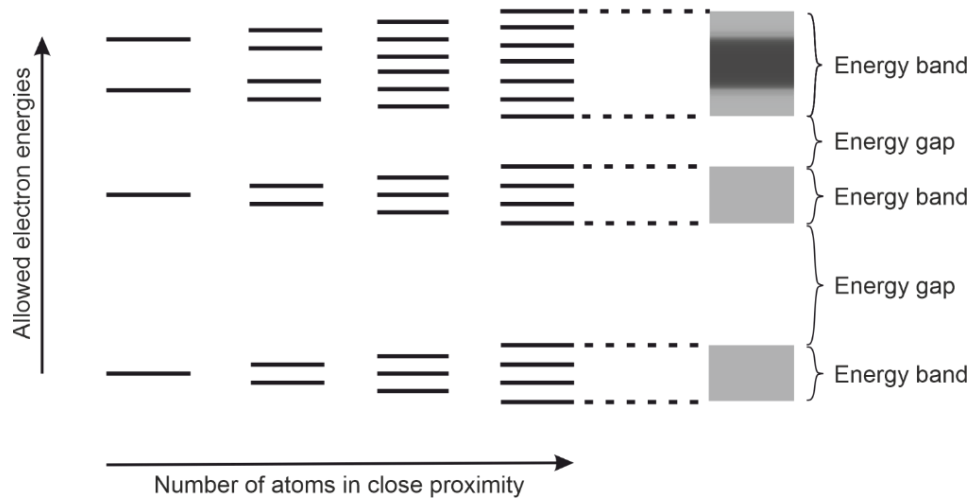

Figure 13. *Schematic representation of formation of energy bands for molecules. Discrete individual states are so close together that they can be considered to form energy bands.*

Polymers are subject to structural disorder. In most cases, polymer chains, whether in the amorphous or crystalline state, contain irregularities. This disorder of periodicity prevents the formation of the ideal bands that would be formed by periodic crystal structures. [15] Structural disorder causes *localised energy states* that extend into the forbidden band gap. In addition to physical disorder, such as conformation, configuration rotation and so on, molecules also contain chemical disorder, such as antioxidants, impurities, cross-linking residues and oxidation products. Chemical disorder also affects the physical structure, as impurity atoms bound to the backbone of the polymer may differ in size and position from the original ones, adding new energy levels to the forbidden band gap. Chemical disorder often dominates the space charge, and are usually thought to be responsible of deep traps. [21]

Local energy states within the forbidden band gap are called *traps* and can act as either hole or electron trap. Traps for holes are typically located above the valence band, while electron traps are located below the conduction band. When a charge carrier, such as a hole or electron, enters such a trap, it can distort the local electric field around it, creating a potential well from which it is difficult to escape. The time spent in the trap state depends on the depth of the trap, i.e. the energy required to remove the charge carrier from the trap. The deeper the trap, the longer the charge carrier remains in the trap. Charge carriers that become trapped due to the electric field distortion they themselves create can be considered a form of *space charge*. [15]

Traps can be divided into shallow and deep traps. Shallow traps are often associated with structural disorder, such as misalignment of molecular chains or deviations from equilibrium positions, which affect the local polarisation energy. For example, dynamic disorder, i.e. time-varying disorder caused by thermal motion, can lead to temporary localised energy states at the edges of the energy bands and form shallow traps. It has been shown that such temporary disorder can form even within an ideal crystal structure and specifically lead to shallow traps. [18]

The density of local energy states between the valence and conduction bands can be quite high, which can make it difficult to clearly separate individual energy bands within the forbidden band gap. However, it is still possible to roughly determine where the mobility of charge carriers change significantly [15]. Figure 14 shows the principle of how local states can be distributed in valence and conduction bands and the band gap between them. The Figure 14 shows that the *density of states* is highest within and in the immediate vicinity of the valence and conduction bands. The density of states decreases towards the middle of the band gap. The closer the adjacent states are to each other, the more likely it is that charge carriers can move to next state.

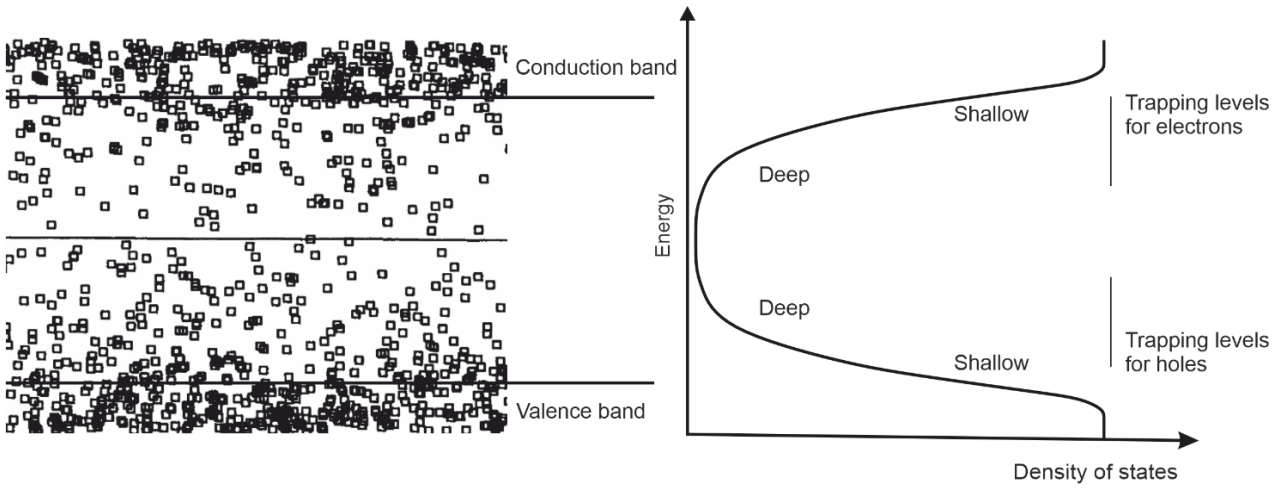

Figure 14. *Schematic representation of localised states on the left and the density of states on the right.*

3.2 Conductivity

When considering charge carriers, in this case electrons in a situation where no electric field is applied to the material, the electrons move in the material, but their net motion is zero, i.e. the charges move randomly in all directions, but over time they can be assumed to be at the same positions as at the start. Charge carriers can also be holes or ions. [15], [22]

Under the influence of electric field electrons in the material experience a force $F = qE$ and begin to move against the direction of the electric field. The movement of the electrons is slowed down by collisions in the crystal structure. Despite the collision resisting the motion, the electrons have a net motion called the drift velocity v_d. This motion creates current I in the material. The electric current per cross-sectional area is expressed as current density.

The current density is thus dependent on both the electric field strength E and the properties of the material. With certain simplifications, it can be said that the current density is almost directly proportional to the electric field strength. This relationship is called Ohm's law. Ohm's law, like many other laws, holds under certain conditions. Current density J can be expressed in terms of conductivity σ and electric field E as follows

$$J = \sigma E. \quad (5)$$

Conductivity can be expressed in general terms in the presence of several charge carriers as follows

$$\sigma = \sum_{i=1}^{N_c} |q_i n_i \mu_i|, \quad (6)$$

where N_c is the amount charge carrier species, q_i is electric charge of *i*-th type charge carrier, n_i is volume density and μ_i is mobility. The above formulas are often derived for conductors and semiconductors and are often valid with sufficient accuracy. However, as such, this does not apply to insulating materials, as charge carriers are unlikely to be free to move, and those electrons with sufficient energy to be in the conduction band in polymer molecules are likely to decay very quickly and become trapped again. [15], [16], [22]

In addition, an increase in temperature should reduce the conductivity of the material. This is due to the vibrations of the crystal lattice under the effect of temperature rise. Therefore, charge carriers collide more frequently within the structure, resulting in shorter time between collisions and lower charge carrier velocity. [15], [22]

3.3 Injection and movement of charge

Conduction mechanisms are often divided into low and high field phenomena. Low-field conduction mechanisms include ohmic and ionic conduction. High field conduction is divided into electrode and bulk-controlled mechanisms, each with its own sub-mechanisms. [15], [22], [23]

At high electric field strengths *electrode-controlled conduction* is determined by the electrical properties of the electrode-insulator interface. One essential element is the height of the *potential barrier* at the interface, which is influenced, for example, by the material of the electrode. This is related to the electrode's work function, the amount of energy required to remove an electron from the material. In *bulk-controlled conduction*, the electrical properties of the insulator itself are crucial. Such properties include the energy, spacing and density of the trap states, the mobility of charge carriers, the relaxation time of the dielectric material and the density of states in the conduction band [24].

Electrons in dielectric materials are strongly bound, which makes their electrical conductivity very low. At absolute zero, all energy states below the Fermi energy level are occupied, and the upper states are unoccupied. In this case, the conduction band is empty and has no electrons for conduction. As the temperature rises, some of the electrons gain enough energy to move to the conduction band, allowing them to contribute to carrying the current. At the same time, holes are also created which act as positive charge carriers and contribute to current generation. At normal electric field strengths range, the current in dielectric materials remains very low, because their conductivity is on the order of 10^{-20}-10^{-8} $\Omega^{-1}cm^{-1}$. [24]

At low electric field strengths, the relationship between current and voltage obeys Ohm's law. In *Ohmic conduction*, charge carriers, electrons and holes reach an average velocity that is directly proportional to the field strength. This model describes conductivity reasonably well in conductors and semiconductors, but for more detailed analysis, especially in non-ideal materials, more sophisticated models are needed that take into account, for example, the effect of trap states. [15], [22]

In *ionic conduction* ions move through a substance enabling electrical conductivity. In an ideal crystalline structure, ions are regularly and tightly organised, which limits their mobility. In practice, however, crystal structures contain defects that allow the ions to move. Two types of defects are essential for ionic conduction, Schottky and Frenkel defects. In Schottky defects, a pair of ions, positive and negative ions, leaves the crystal structure, leaving behind two vacancies. In a Frenkel defect, a single ion moves away from its original position and settles in another, normally empty, spot in the crystal structure. In both cases, empty spaces are created in the structure that can be filled by other ions, allowing ions to move around and thus increase electrical conductivity. [16]

At high electric field strengths, conduction is governed by mechanisms beyond Ohmic behaviour. A potential barrier forms at the electrode–insulator interface, which charge carriers must overcome to enter the insulator. If the electric field provides sufficient energy for the charge carrier to surmount this barrier, the process is referred to as Schottky injection. If the field is strong enough to narrow the potential barrier so that charge carriers can tunnel through it, the phenomenon is known as Fowler–Nordheim injection. In such cases, the current–voltage relationship becomes non-linear, and the current may vary proportionally to the square of the applied voltage. High-field conduction is typically classified into electrode-controlled and bulk-controlled mechanisms. [15], [22], [24] The bulk-controlled mechanisms discussed in this thesis include space-charge-limited conduction (SCLC), Poole–Frenkel emission, hopping conduction, and the field-limiting space charge model. These conduction processes will be examined in more detail in the following sections.

3.3.1 Low-field conduction mechanisms

In ohmic conduction, the charge carriers are the electrons on the conduction band and the holes in the valence band. The current density of the ohmic conduction mechanism has a linear relationship with the electric field, and the current density due to this mechanism can be observed at low field strengths. Although the energy gap between the conduction and valence bands in insulators is large and the number of free charge carriers is very small, it is never exactly zero. [15]

To analyse conductivity in more detail in insulators, the concept of trap-free conduction presented in the section, 3.2 Conductivity, needs to be further developed and the concept of trap-limited conduction needs to be introduced. The local energy states that are potential states for charge

carriers are located in the forbidden band gap between the conduction and valence bands. The charge carriers can move between the states, sometimes becoming trapped, thus limiting the effective mobility of the charge carriers. In Figure 15 a simplification that all forbidden trap states are located at the same distance from both the bottom of the conduction band E_C and the Fermi energy level E_f at energy level E_t has been made. There are N_t such states per unit volume. Let ΔE_t denote the difference between the bottom of the conduction band and the Fermi energy level.

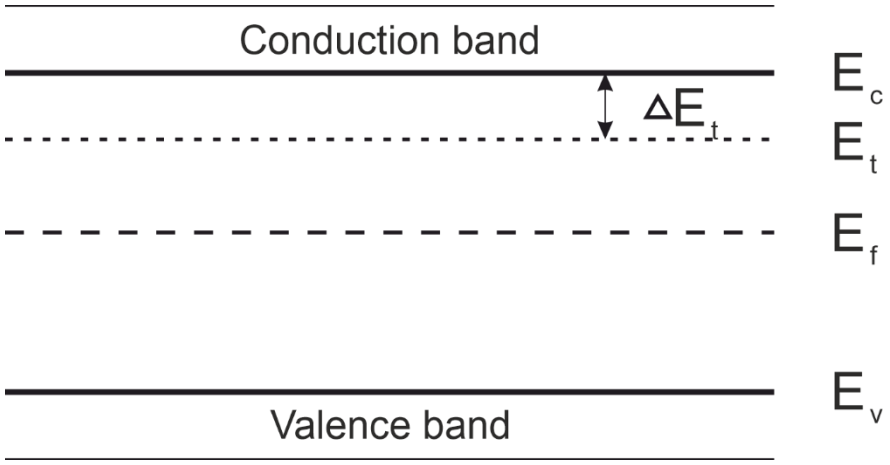

Figure 15. *Energy diagram of a dielectric. The energies of the trap states are presented in one plane to easy mathematical analysis.*

Using the Fermi-Dirac distribution and the assumption that $E_C - E_f \gg k_b T$, the number of electrons per unit volume in the conduction band n_c and the number of occupied states per unit volume n_t can be presented

$$n_c \approx N_{eff} \exp\left(-\frac{E_C - E_f}{k_b T}\right) \tag{7}$$

$$n_t \approx N_t \exp\left(-\frac{E_t - E_f}{k_b T}\right), \tag{8}$$

where N_{eff} is the density of states available in the conduction band. Dividing equation 7 with equation 8 gives the ratio of free and trapped charge carriers

$$\theta_{ct} = \frac{n_c}{n_t} = \frac{N_{eff}}{N_t} \exp\left(-\frac{\Delta E_t}{k_b T}\right). \tag{9}$$

The coefficient θ_{ct} considers the number of charge carriers available in the insulator, reducing the number of charge carriers that can be conducting by $n\theta_{ct}$ instead of just number of charge carrier, n. It can thus be concluded that traps limit the mobility of charge carriers by a factor θ_{ct}, i.e., in the presence of traps, the time spent by charge carriers on the same distance is increased due to traps, without reducing the number of charge carriers per unit volume. [22], [23]

Ionic conduction is the result of the movement of ions under the influence of an electric field. Polymeric materials may contain small concentrations of ions, which are formed as a result of chemical reactions or oxidation of the material. Ions may also be formed by the decomposition of

contaminants or absorbed water under the influence of an electric field. In addition, ionic species can form on electrode surfaces and diffuse into the insulation. An ion with a charge q polarises its environment. As a result of polarisation, atoms and molecules rearrange themselves to provide protection for the ion. The polarisation of the environment reduces the electrostatic energy of the ion, creating a potential barrier or potential well. The ion must gain energy to get out of this potential well. [15], [21], [25]

In ionic crystals, conduction is mainly internal conduction, because temperature-induced vacancies in the crystal structure allow ions to move. Two well-known such defects in the structure are the *Schottky* and *Frenkel defects*. In a Frenkel defect, an ion moves from its original position to another one in the crystal structure. This creates two imperfections in the crystal structure, an empty space in the crystal structure and an ion misplaced within the structure. A Schottky defect occurs when oppositely charged ions leave the crystal structure, leaving vacant sites behind. Schottky defects always occur in pairs. Both defects create an empty spot in the crystal structure, which can be filled by a nearby ion. This again creates a vacancy in the place of the ion that filled the previous vacancy. The resulting chain reaction can cause ions to move through the solid and increase the conductivity of the material. [16], [25] Ionic conduction follows an Arrhenius-like relationship as follows

$$\sigma(T) = \sigma_{\infty} \exp\left(-\frac{\mathrm{G_a}}{k_b T}\right), \tag{10}$$

where σ_{∞} is the reference value for conductivity at very high temperatures ($T \to \infty$) and G_a is the activation energy of conductivity at very high temperatures [22], [23].

Vacancies in the crystal structure that are not occupied by host ions can act as charge carriers in ionic conduction. This phenomenon occurs only in ionic crystal structures. In non-ionic materials, conduction is primarily determined by the nature and concentration of impurities. Although insulating materials such as polymers are not inherently ionic, they can still contain ions. [23] In insulating polymers, it is reasonable to assume that ions originate from polymerisation catalysts, degradation products, absorbed moisture, and other impurities introduced during the manufacturing process [22], [25]. Figure 16 a) shows schematic representation of cubic crystal structure containing anions marked as black and cations marked as white, b) Schottky and c) Frenkel defects.

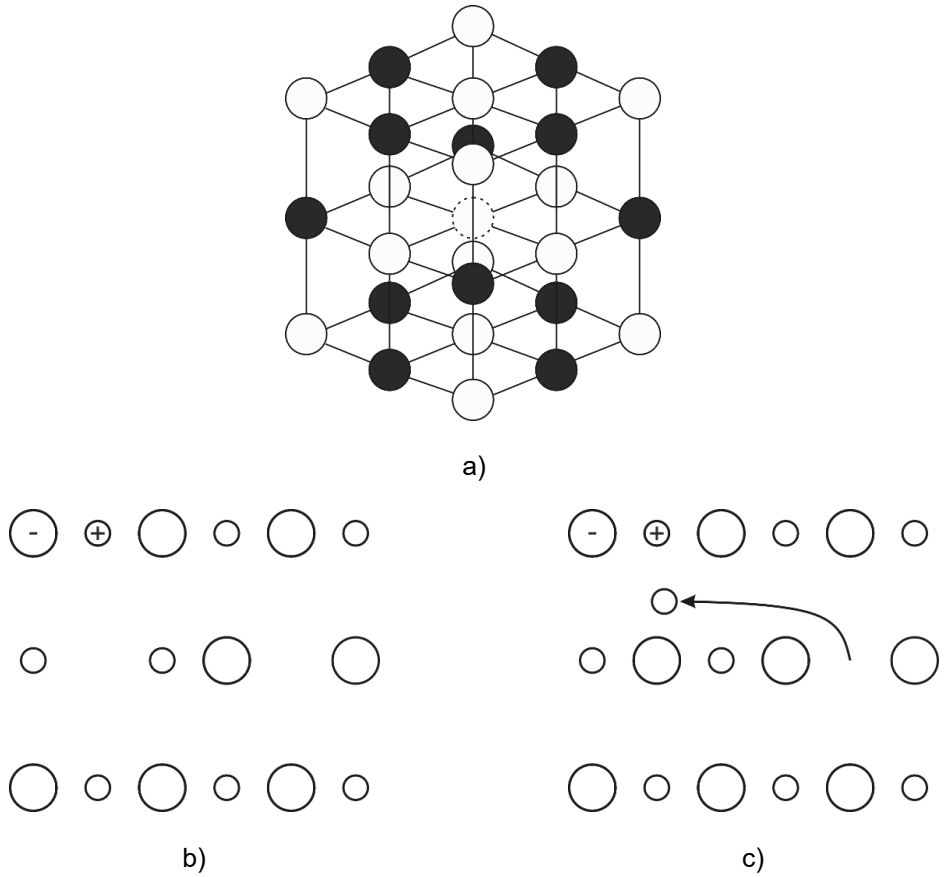

Figure 16. *Schematic representation of a) a vacancy in the crystal lattice that allows ionic conduction, positive cations in black and negative anions in white. b) Schottky and c) Frenkel defects.*

The behaviour of charge carriers at electrode interfaces depends on their type. Ions have difficulty in moving to an electrode as a mass, and as a result they often are blocked at one electrode and remain near the insulator interface. This leads to the formation of a *heterocharge*, which in turn changes the electric field distribution in the material. Ions trapped at the interface can react with opposite charge carriers, such as injected electrons, allowing them to be electrically neutralised. Electronic charge carriers such as electrons and holes, on the other hand, can pass through the insulator and exit through the opposite electrode. This exit may occur unhindered or it may require additional energy if there is a potential difference at the interface that provides resistance to the exit of the carriers. [15], [21], [22], [25]

3.3.2 High-field conduction mechanisms

This section provides a more detailed overview of high-field conduction mechanisms. Electrode-controlled processes include Schottky and Fowler–Nordheim injection, as well as their combined mechanisms. Bulk-controlled conduction mechanisms covered here are hopping conduction, space-charge-limited conduction (SCLC), Poole–Frenkel emission, and the field-limiting space charge model

Often the Coulombic potential between the electrode and the insulator limits the transport of charge carriers crossing the interface. Under the influence of a high electric field, this potential barrier can be reduced in both height and width. Lowering the barrier increases the probability that charge carriers have sufficient energy to cross it. In *Schottky injection*, also referred to as thermionic emission in the literature, charge carriers gain the necessary energy from thermal excitation and the applied electric field to overcome the potential barrier at the metal–insulator interface. [22], [24]

The charge carrier, which should not have sufficient energy to cross the potential barrier, may still be located on the other side of it. This mechanism is referred to *as Fowler-Nordheim injection* and is based on the fact that a high electric field reduces the potential barrier width and increasing the probability of the charge carrier tunnelling through the barrier. This phenomenon cannot be explained by classical physics, since a charge carrier with insufficient energy would be reflected back. However, according to quantum mechanics, the charge carrier has a non-zero probability of being on the other side of the barrier [17], [22], [24]

If the electric field is not strong enough to reduce the width of the potential barrier, the charge carrier encounters the full height and width of the barrier, and if the charge carrier still tunnels its way through the barrier the mechanism is then called *direct tunnelling*. A form of conduction that combines Schottky injection and tunnelling is called *thermionic field emission* in which the charge carrier receives part of its energy from thermal motion and then tunnels through the thinned potential barrier. [24]

All the above conduction mechanisms can be represented by simplified energy band diagrams. The theoretical basis of the diagrams is the injection of electrons from a metal rod into a vacuum. In this way, the work function of the metal is equal to the potential barrier. The magnitude of the potential barrier at the interface can vary depending on the conditions, it is influenced by impurities, structural imperfections, materials used for example. [21], [22] The schematic diagrams presented in Figure 20 are simplifications, and more detailed and advanced descriptions are also available in the literature, for example in [22] and [17]. However, the representation used is sufficient to provide a basic conceptual understanding.

The conduction mechanisms within an insulator depend on its electrical properties [24]. Although the number of charge carriers in an insulator is usually very small, in a thin film and with good electrode contacts, charges can be injected into the insulator under the influence of a sufficiently large electric field [22]. In this case, the current flow can be governed by several different mechanisms which are categorised as bulk-controlled conduction mechanisms.

Space charge limited conduction (SCLC) can be explained by energy band theory, which takes into account the traps in the material. The theory is presented in two parts, the first part consisting of an

insulator free of traps and the second part consisting of an insulator containing traps. In the theoretical treatment, electrons are assumed to be the charge carriers [15], [22]

In a trap free insulation, the charge density n can be considered to consist of two parts. The charges already in the insulator n_0 and injected from the electrode n_1. Hence, the current density can also be thought of as consisting of two parts, the Ohmic and the space charge limited part

$$J = \frac{n_0 q \mu V}{d} + \frac{9\varepsilon_0 \varepsilon_r V^2}{8d^3}, \tag{11}$$

of which the first part after the equivalence sign is the Ohmic part and the second is the space charge limited part. In the equation, d is the thickness of the insulator, q is the charge, μ is the mobility of the charge carriers, ε_0 is the vacuum permittivity, and ε_r is the relative permittivity. From the equation, it is useful to note the different dependence of the two mechanisms on voltage. By experimentally plotting the current density as a function of voltage and both represented on a logarithmic scale, one can determine from Figure 17 a threshold voltage point V_{tr} where the space charge limited term begins to dominate the current density equation. [22]

In an insulator with traps, all charges injected into the insulator affect the space charge distribution, but only a small fraction affects the current. With the coefficient θ_{ct} that takes into account free and trapped charge and especially the charge carriers available to conduction. This part affecting the current has a large influence on the space charge limited part of equation 11. Therefore, the current density can be expressed in terms of the traps as follows

$$J = \theta_{ct} \frac{9\varepsilon_0 \varepsilon_r V^2}{8d^3}. \tag{12}$$

The equation holds for shallow traps, i.e. when the difference between the trap and Fermi level energies is significantly larger than the charge carrier thermal energy $E_t - E_f \gg k_b T$. [22]

In the Figure 17 $J - V$ curve follows Ohm's law at voltages lower than threshold voltage $V < V_{tr}$, which means that the density of thermally generated free charges n_0 inside the insulator is higher than the density of injected charges n_1. It follows that the injected charge carriers tend to redistribute in the insulator such that the electric charge in the insulator remains neutral. [24]

When the threshold voltage V_{tr} is reached, more charges are injected into the insulator and their *transit time* τ_c becomes equal to the *relaxation time* τ_d of the insulator material. The density of injected charge carriers n_1 increases to equal the density of thermally generated free charges n_0 in the insulator. At higher voltages, the current density follows the equation 12. This implies a transition from ohmic conduction to space charge-limited conduction, in the mechanism the charge carriers start to become trapped, and the conduction no longer follows Ohm's law, but becomes space charge-limited. When operating in a region where the voltage is $V_{tr} < V < V_{TFL}$ the traps begin to fill,

and a space charge is generated. Injected excess carriers dominate thermally generated carriers because the transit time of injected carriers is too short. [24]

An increase in voltage can increase the density of injected free charge carriers so much that the Fermi energy level E_f rises above the electron trap level E_t. *Trap-Filled Limit,* V_{TFL} , determines the transition from trap-limited $J - V$ behavior to trap-free $J - V$ behavior. When all traps are filled, excess injected charges are free to move in the insulation material. This means that at V_{TFL}, the electric current increases abruptly from a low trap-limited value to a high trap-free space charge-limited current. V_{TFL} is defined as the voltage required to fill the traps. In other words, the voltage at which the Fermi energy level exceeds the trap level. [15] Figure 17 shows how the current density in the SCLC changes with increasing voltage on a logarithmic scale. Figure 17 shows four different conduction regions, which can be divided as follows:

1. Ohmic region $0 < V < V_{tr}$ $J \propto V$
2. Space charge limited conduction $V_{tr} < V < V_{TFL}$, $J \propto V^2$
3. Trap filled region $V = V_{TFL}$, $slope = \infty$
4. Trap free SCLC $V > V_{TFL}$, $J \propto V^2$

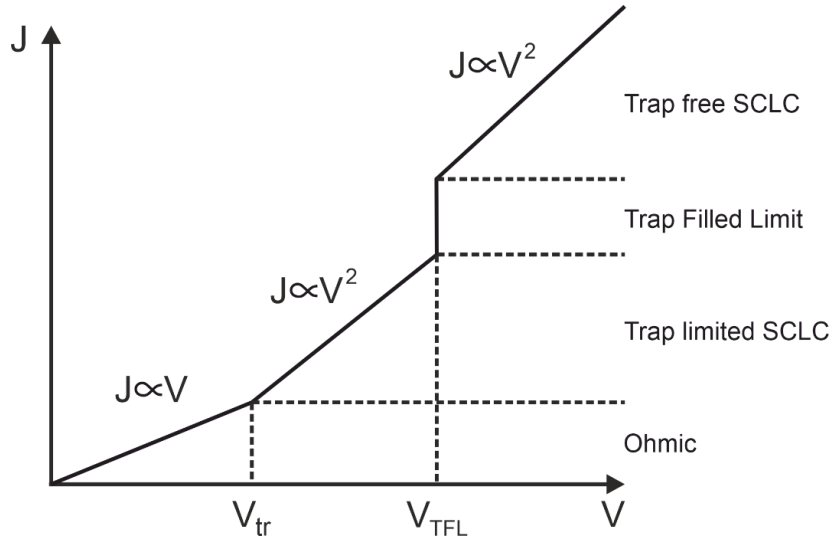

Figure 17. *Schematic current density-voltage relationship in SCLC. Current density and voltage plotted on a logarithmic scale. In ohmic conduction region current density follows linear relationship to voltage. In trap limited SCLC and trap free SCLC regions relationship follows square ratio.*

In reality, the energy levels of the traps are not at the same level, as assumed to facilitate theoretical analysis, but are more widely distributed. Due to this the transitions between regions 2 and 3, as well as between regions 3 and 4 in Figure 17, are more gradual rather than abrupt. This occurs because as the voltage is increased the Fermi energy level rises, and more trap levels are filled. To conclude, it can be noted that often the breakdown occurs before reaching the last region and that space-charge limited conduction holds for thin insulating films. [15], [22]

Figure 18 presents a process of how the distribution of charge carriers in the SCLC is shaped under different voltage conditions. At first state a), the voltage V is below the threshold voltage V_{tr}, where charge injection into the insulator is negligible and the charge carriers within the insulator dominate conductivity. At state b) dielectric relaxation is observed, allowing charges to be distributed uniformly in the insulator and maintaining a relatively uniform field distribution. At state c), the voltage reaches the limiting value V_{tr}, allowing as much charge to be injected as is generated within the insulator by the field strength. At state d) the voltage V has exceeded the threshold voltage V_{tr} and more injected charges are present than are generated in the insulator, but there are still many free traps in the insulator. At state e) the voltage is in between threshold voltage and trap filled limit $V_{tr} < V < V_{TFL}$, at which point the injected charges begin to fill the traps and a space charge is generated in the insulator. In state f), the voltage V has already exceeded the trap filled limit voltage V_{TFL} and the traps are filled, at which point the current density in the trap free region starts to follow the quadratic relationship with the voltage again. However, in practice breakdown has already occurred at this point, as pointed out in [22].

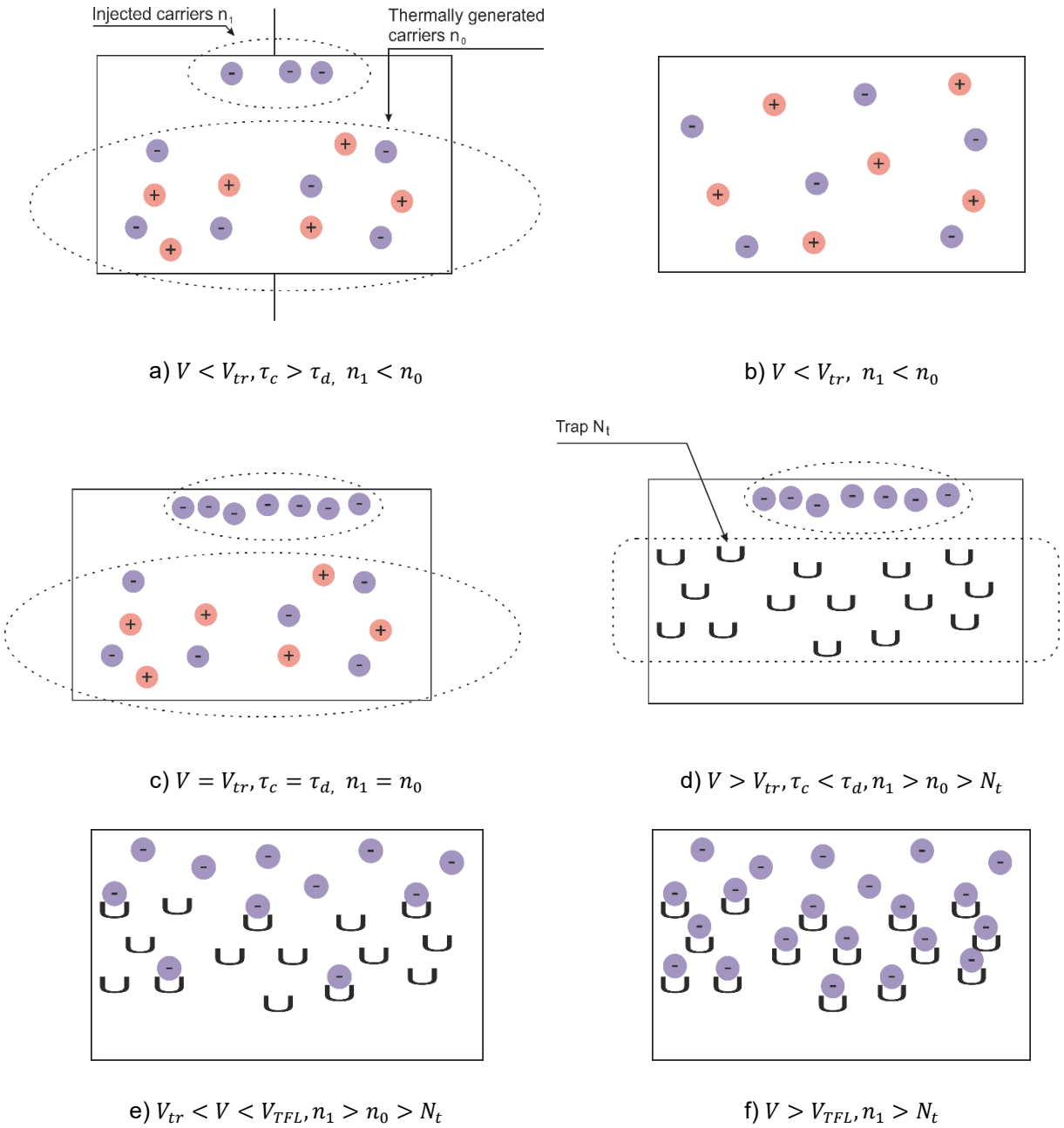

Figure 18. *Carrier distribution in dielectric film under weak carrier injection from electrode in a), b) and c). In d), e) and f) carrier distribution in dielectric thin film under strong carrier injection from electrode.*

Charges can be transferred from one state to another in an insulator by crossing the potential barrier with energy from heat, by direct tunnelling or by heat-assisted tunnelling [15]. *Hopping conduction* corresponds to the situation where a trapped electron by thermal activation has gained energy to be at the same level as the adjacent empty state, without crossing the potential wall, after which it can move from state to state by tunnelling [21]. In comparison to Poole-Frenkel conduction, where the potential barrier is crossed by thermal activation in hopping the potential barrier is never surpassed but the charge carrier tunnels from one state to another [24]. Often in literature the term hopping is

used, which is somewhat misleading, since this conduction mechanism is more precisely a thermally assisted tunnelling [15].

Mathematically, the probability of the charge carrier transferring from one state to another can be represented as the product of the tunnelling and thermal activation probabilities. As the distance between spaces increases, the probability of thermal activation increases, but the probability of tunnelling decreases exponentially. Because of these opposing effects, the transition is most likely to occur at a given optimal distance. In [15], this distance and the associated maximum probability are derived. Here, we will settle for the result that conductivity in hopping conduction can be written as

$$\sigma = A * \exp\left(-\frac{B}{T^n}\right), \tag{13}$$

where A and B are constants found in the literature and n is between 0.25 and 0.5, depending on the source. Detailed formulas and related quantities for the determination of constants A and B are given in more detail in references. [15], [26]

The theory suggests that at high electric fields, the potential barrier of a trapped charge carrier, thereby increasing the likelihood that thermal energy is sufficient to overcome the barrier and release the carrier. This phenomenon is known as the *Poole–Frenkel mechanism*, which is considered to be the internal material counterpart of Schottky injection at the electrode-insulator interface. [27] In the Poole-Frenkel mechanism, the electric field reduces the potential barrier at trap states within the insulator, while in Schottky injection, a similar lowering of the barrier occurs at the electrode-insulator interface. In both cases, the energy needed to overcome the potential barrier is provided by thermal energy. [22], [24]

For the Poole-Frenkel mechanism to occur, the insulator must have a wide band gap and the material must contain charge carriers, either holes or electrons [27]. The mechanism is sensitive to the concentration of defects and donor centres, as defects such as traps can reduce the amount of free charge carriers and thus reduce conductivity [15], [24]. The Poole-Frenkel effect typically occurs at high electric field strengths and temperatures [24]. Figure 19 presents how the electric field lowers the height of the potential barrier in the field direction and thus reduces the energy required for thermal activation to overcome the potential barrier. V_{max} is the difference between the potentials at the highest point of the potential barrier without and with the electric field, r_{max} is the distance of the potential barrier from the bottom of the trap after adding the field.

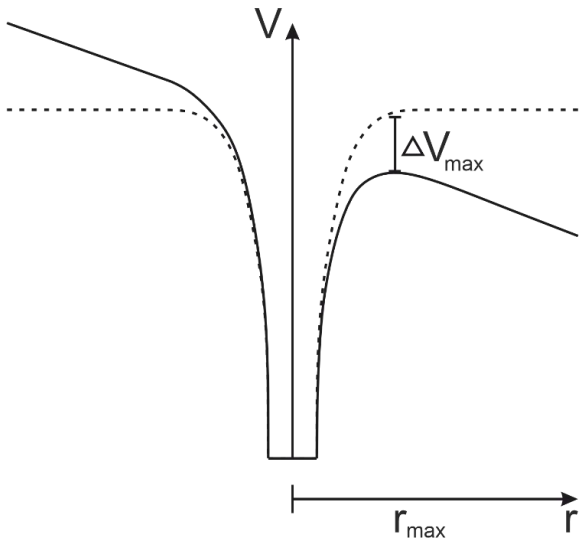

Figure 19. *A schematic illustration of how electric field reduces the height of the potential barrier in field direction in the Poole Frenkel mechanism.*

It has been understood for a long time that if charge is injected from the electrode into the insulator, a space charge may form in the vicinity of the electrodes, causing a local reduction in field strength. At a certain critical field strength E_{mc}, the mobility of charge carriers in polymers increases strongly, several times that of normal. This has been suggested to be due to the electrons gaining so much kinetic energy that they stay in the conduction band. For this reason, the *field-limiting space charge model* assumes that charge carrier mobility is

$$\mu = 0, \qquad when\ E < E_{mc} \tag{14}$$

and

$$\mu = \mu_{\infty}, \qquad when\ E > E_{mc}. \tag{15}$$

The mobility μ_{∞} refers to the charge carrier mobility when the electric field exceeds the critical field strength. This increase in mobility is analogous to space charge-limited conduction at the trap-filled limit, where the current rises sharply as the voltage increases. [15] When the field strength surpasses the critical value E_{mc}, charges are injected from the electrode into the insulator, forming homocharge. These charges migrate to regions within the insulator where the field remains below the critical level. The accumulated homocharge then reduces the field strength near the electrodes. Consequently, charge injection from the electrode ceases once the electric field throughout the insulator falls below the critical threshold, provided that the localised charges remain stationary. [24] However, in polymeric materials, the situation is further complicated by structural heterogeneity. Electrical conductivity differs between the amorphous and crystalline regions, and the material may exhibit anisotropic behaviour, meaning that conductivity can vary with direction. Furthermore, the critical field strength may in some cases exceed the dielectric breakdown strength of the material, causing electrical breakdown before the critical field is even reached. [22]

Figure 20 provides a simplified illustration of high-field conduction mechanisms at the metal–insulator interface, a) - d), as well as some those occurring within the insulator, e) and f), summarising the principles of conduction mechanism.

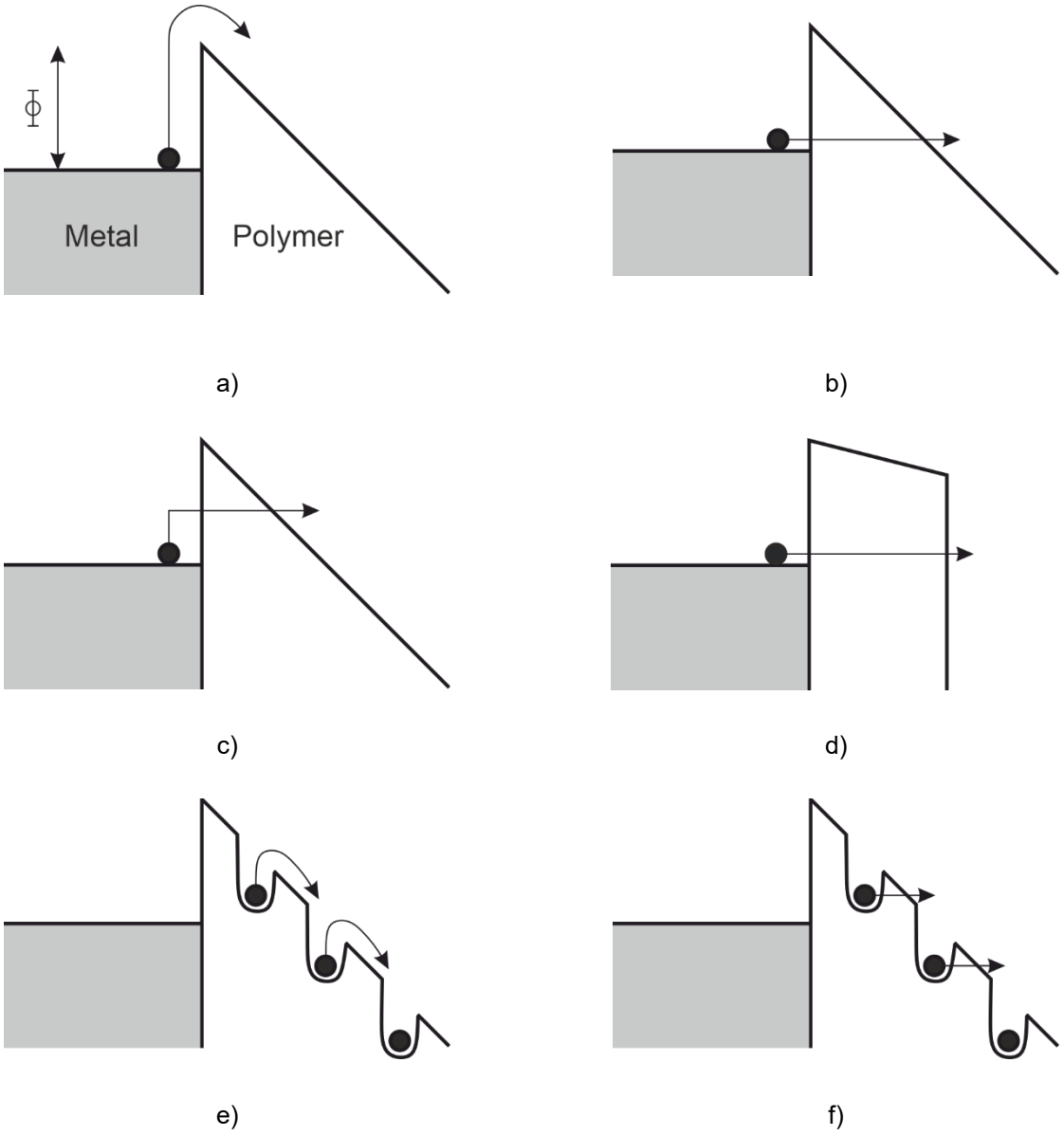

Figure 20. *Schematic representation of coulombic potential barrier at metal-polymer interface and mechanisms how charge carrier overcomes the barrier in electrode-controlled conduction. a) Schottky injection, b) Fowler-Nordheim injection, c) thermionic field emission and d) direct tunnelling. In e) Poole-Frenkel mechanism and in f) hopping conduction which are bulk controlled mechanisms.*

3.4 Space charge accumulation

This section discusses the formation of space charge and the trapping of charges in insulation and presents a few mechanisms by which charge accumulates and becomes trapped in insulation, such as electronic charge injection, field assisted thermal ionisation of impurities, spatially

inhomogeneous electric polarisation, steady DC current coupled with spatially varying ratio of permittivity to conductivity and physical- and chemical defects. The term space charge was originally used to describe the accumulation of electric charge between electrodes as a result of electron injection in a vacuum diode. Space charge can also accumulate in a solid insulator, distorting the electric field distribution within the insulator. If the density of space charge is relatively high, it can cause failure and breakdown of the insulation structure. [28]

The formation of space charge in insulating materials under a DC electric field has been demonstrated in numerous studies. This phenomenon arises from changes in the material's conductivity, which depends on both temperature and electric field strength. In polymers, conductivity has been extensively investigated using various research methods, and it has been established that space charge formation is closely linked to conduction mechanisms, charge transport, and the trapping and release of charges within the material. Space charge can originate either from charges injected at the electrode–insulator interface or from charge carriers inherently present in the material's structure. [29]

In general, homocharge is caused by the injection of charges into the insulator and heterocharge is caused by processes in the insulating material or by the movement of charge carriers being blocked at the opposite electrode. The difference between homo- and heterocharge is illustrated in Figure 21. The formation of an accumulated space charge in a material can be a complex process that depends on many factors, such as the experimental conditions, the geometry of the sample, the type and material of the electrode, the nature and properties of the electrode-polymer interface, and the polymer material itself, its chemical composition, degree of crystallinity, morphology, manufacturing history and the content of impurities or additives. [29]

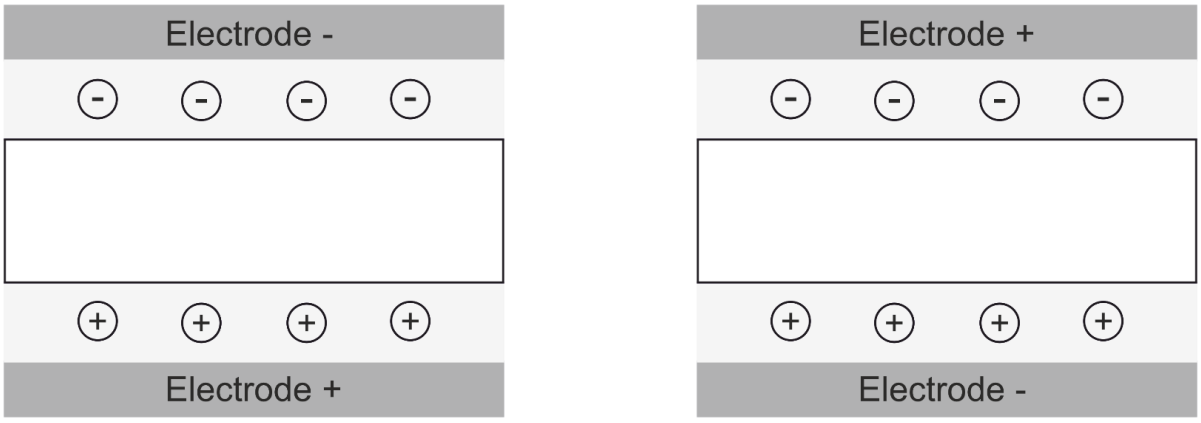

Figure 21. *Illustration of space charge formation, a) homocharge, where charges of the same polarity accumulate near the electrode, and b) heterocharge, where charges of opposite polarity accumulate near the electrode.*

3.4.1 Charge generation

As discussed in section 3.3.2 High-field conduction mechanisms, charge injection from the metal–insulator interface can occur under certain conditions. However, it is worth emphasizing that charge carrier injection from the electrode–insulator interface almost always occurs to some extent, especially at high electric field strengths. This mechanism leads to the formation of *homocharge* near the electrodes, which means that the charge accumulated in the vicinity of the electrode has the same polarity. As a result, the electric field strength is reduced in the immediate proximity of the interface but enhanced in the central region. In contrast to the above, if charge transport within the bulk of the insulator dominates over interfacial charge injection, the accumulation of *heterocharge* may occur. In this case, the charge of opposite polarity to the electrode accumulates near the interface, thus reinforcing the local electric field near the electrodes but reduces it in the central region. The space charge density has been found to depend on temperature, with charge accumulation tending to be stronger at lower temperatures. This behaviour is attributed to the reduced mobility of charge carriers at low temperatures, which hinders their transport and favours trapping within the insulating material. [22], [28]

Field assisted thermal ionisation of impurities in the insulator can result in the separation of an electron and a positive ion. Often the electrons recombine very quickly after this, but those electrons that do not and are unable to leave the other electrode form a space charge in the insulator. Assuming that no more charge carriers are injected from the electrodes into the insulator. The electrons create a current that disappears over time. The remaining positive ions are assumed to be weakly mobile and form a net charge that is fairly evenly distributed in the insulator. When a field strength of opposite polarity is applied to the sample, similar charge accumulation has been observed as *a mirror image*, assuming identical electrodes and a homogeneous sample. [28]

Ionisation of impurities is likely to be observed in almost all polymers, but it is unlikely to be the dominant or only mechanism that accumulates space charge. It is worth noting that even at very low moisture concentrations, the ionisation of impurities and cross-linking by-products increases. [28] As an example of this, an article [30] studied low density (LD), cross-linked (XL) and high density polyethylene (HDPE) and found that in low density polyethylene (LDPE), moisture promotes ionisation of contaminants, in XLPE, by-products are more strongly and easily ionised, and in HDPE, contaminants act as traps due to moisture.

Molecules with a permanent dipole moment can be distributed unevenly within the insulation material, or their dipole orientation may only partially align with the external electric field. Due to this non-uniform distribution, a *spatially inhomogeneous electric polarisation* can develop inside the material. Such dipolar molecules can form during the manufacturing of the insulation, for example during crosslinking. If these molecules are mobile under the influence of an electric field, they tend to drift toward the edges of the material near the electrodes. At the electrodes, surface charges neutralise the field generated by these dipoles, but they may still influence the local electric field distribution. [4] When the direction of the external electric field is reversed, the dipolar molecules attempt to reorient along the new field direction. In this process, the direction of their polarisation vector changes, while its magnitude remains constant. This phenomenon is believed to be at least partially responsible for the mirror image effect. The mirror image effect refers to the phenomenon where the reversal of the electric field direction causes the internal charge distribution in the sample to also change in a mirror-symmetric manner. [22]

Electrons injected from electrodes into the insulator affect the behaviour of molecules with a permanent dipole moment by changing the electric field distribution and thus the orientation of the molecules. The injected electrons form a homocharge in the vicinity of the electrodes, which weakens the field strength in the vicinity of the electrode and thus affects the orientation of the dipoles. If the external electric field is not strong enough, the dipoles will not be perfectly aligned in the direction of the field and may remain partially oriented. As the field strength increases, the orientation of the dipoles intensifies until it reaches a saturation point where the dipoles are fully aligned with the field. This occurs at a sufficiently high field. [28]

According to the electromagnetic theory, space charge accumulates in a bulk sample under the influence of direct current as follows

$$\rho_{sp} = J \cdot \nabla\left(\frac{\varepsilon_0 \varepsilon_r}{\sigma}\right). \tag{16}$$

In polymer insulators, the conductivity σ is a function of both temperature T and field strength E. [29] In a sample with DC current flowing through it, where the ratio of permittivity ε and conductivity σ varies locally, a space charge may be generated. In polymer insulators, the temperature dependence of permittivity is usually negligible, but the variation of conductivity as a function of temperature can

be significant, leading to the formation of a space charge. This phenomenon arises from the spatial variation in the ratio of permittivity to conductivity under steady DC current conditions. Since conductivity is dependent on both temperature and electric field strength, it can be expressed as a function of these parameters as follows

$$\sigma(T,E) = \sigma_0 \exp\left(-\frac{\frac{G_a}{k_b T}\sinh(cE)}{E}\right), \tag{17}$$

where σ_0 is the material constant, G_a is the thermal activation energy and $sinh(cE)/E$ is the dependence of conductivity on field strength. [28] Depending on the temperature conditions of the insulation, the field strength may be higher at the inner edge of the insulation or at the outer edge of the insulation [31].

From Figure 22, it can be observed that in a DC cable, as the temperature gradient across the insulation increases, the electric field distribution becomes increasingly distorted. Curve B represents a cable with a small temperature gradient, where the electric field is still relatively uniform. As the thermal gradient increases (C), the field starts to redistribute, and in the case of a high temperature gradient (D), the electric field near the outer radius of the insulation becomes significantly stronger than near the conductor. The thermal gradient results from Joule heating of the conductor, the cooling effect of the environment and the thermal resistivity of the insulation material, i.e. how good the thermal conductivity of the insulation is [29], [32]. This phenomenon, where the electric field strength increases toward the outer edge of the insulation, is known as *stress inversion*. In contrast, the electric field distribution in an AC cable (curve A) follows the typical inverse radial dependence, with the highest field at the inner conductor. The temperature gradients associated with the DC cable curves in Figure 22 follow the relation where $\Delta T(B) < \Delta T(C) < \Delta T(D)$.

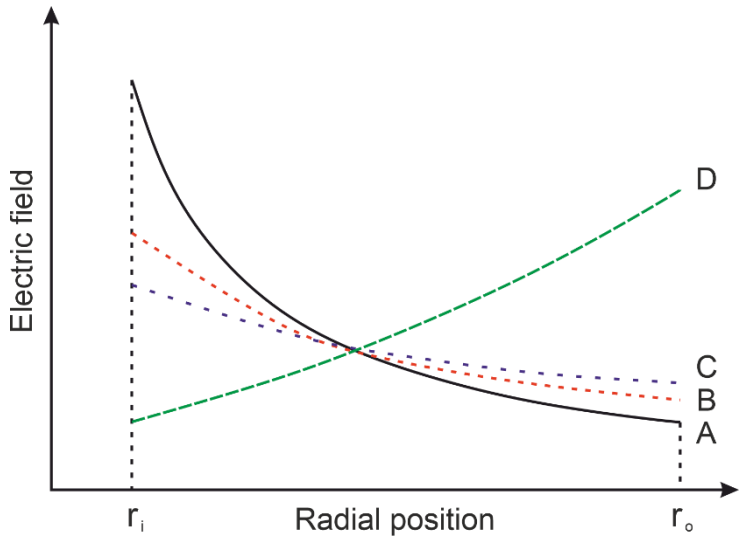

Figure 22. *Schematic illustration of stress inversion due to temperature gradient. Curve A shows a typical electric field distribution in an AC cable. Curves B-D illustrates the electric field distribution in a DC cable with different temperature gradients. The temperature gradients are in the following order* $\Delta T(B) < \Delta T(C) < \Delta T(D)$.

In switching conditions or other transient conditions, it takes time to reach a state of steady state of the electric field distribution in the DC cable. For example, as soon as the DC voltage is switched on, the electric field is distributed capacitively in the insulator, i.e. in the same way as in an AC cable, as shown in Figure 22, curve A. Over time, the field evolves towards a resistive distribution, starting to resemble the curves B-D in Figure 22, depending on the magnitude of the temperature gradient. The rate of settling of the field distribution is determined by the dielectric time constant defined by the equation $\tau_{DC} = \varepsilon/\sigma$, where ε is the permittivity and σ the conductivity. Since conductivity is strongly temperature dependent, the time constant and hence the evolution of the field distribution is also temperature dependent. [22]

3.4.2 Charge trapping

Energy band structures derived from semiconductor physics are a good starting point for understanding the properties of polymer insulators. The theory does not fully explain the conductivity or trapping properties of insulators due to their complex nature [22], but it helps to better understand the concept as a whole. Many studies and publications have focused on polyethylene because many insulation materials are similar to PE and have a relatively simple chemical structure according to [21].

Many insulating materials possess a wide band gap, where charge carriers should not be located. Calculated and experimental measurements have shown this to be around 8.8 eV for polyethylene, which would result in very low conductivity in the material. Such conductivity values, in theory 10^{-45}

S/m, have not been encountered in real measurements because the energy band structure is much more complex than the idealised model often presented in the literature. [15], [22]

Molecular simulations can be used to study the properties and behaviour of individual atoms and molecules. The aim of these simulations is to understand how the macroscopic properties of matter arise when atoms and molecules interact with each other. In the case of polymers, the properties of a single chain can be studied by looking at its repeating structural units. In contrast, understanding the properties of crystalline or amorphous regions requires consideration of the interactions between multiple chains. Such an approach has been used, for example, to investigate how microscopic structural defects affect the formation of spatial charge in polymer materials. Accurate modelling of polymeric materials requires considering not only individual chains but also various structural defects. These include physical anomalies, such as molecular weight variations and free volume, and chemical irregularities, such as chain branching and additives. [21]

Molecules can have different conformations, meaning that parts of the chain can twist around bonds. The simplest and lowest energy conformation is the *all-trans* structure, where the carbon chain is perfectly straight. Deviations from this conformation cause a structural disorder of the molecular chains, which can be called *physical disorder*. This disorder affects the band structure of the molecule, creating localised energy states between the valence and conduction bands, in the forbidden band. These states are called traps and charge carriers can become trapped in them for different lengths of time. [21] Earlier in Figure 14 schematic illustration of these localised states were presented. Localised states can enhance the transfer of charge carriers within the insulation material in the ways already described in sections 3.3.1 and 3.3.2.

In addition to structural defects in materials, *chemical defects* can also occur. Chemical defects can be divided into two groups, the first consisting of defects in the polymer chain and the second group consisting of cross-linking by-products and antioxidant by-products used in cable insulation. [33] Such chemical disorder often also causes physical disorder, because the size and position of the foreign atoms and molecules differ from those of the polymer itself. In addition, foreign atoms and molecules may have different electrical properties, resulting in the creation of energy states in the forbidden band. These energy states are typically located at a deeper energy level and form so-called deep traps. Deep traps are thought to have a particular impact on the formation of space charge [21]. Studies on polyethylene [33] and [34] analysed the depths of physical and chemical traps, and the results suggest that shallow traps are more often associated with physical imperfections, while deeper traps are typically the result of chemical defects. However, it is important to note that there is an overlap in the depths of physical and chemical defects, and they cannot be explicitly classified as shallow or deep traps based on their mechanism of origin.

What physical and chemical defects have in common is that both cause structural disorder, which affects the energy band structure of the material and creates localised energy states between the conduction and valence bands, forming traps. Physical defects are primarily related to conformational variations in molecular chains, such as chain rotation, while chemical defects are caused by contaminants such as impurities, additives or reaction products. Physical defects often result in shallow traps that facilitate charge transport, while chemical defects typically result in deep traps that trap charge carriers for longer periods of time, particularly affecting space charge formation.

3.5 Fundamentals of dielectrics

The aim of this chapter is to examine how macroscopic properties of a material, such as relative permittivity ε_r or external field strength E, relate to microscopic properties such as polarisability α or local field strength E_L and introduce the mechanisms of polarisation. For example, polarisation and permittivity affect the local electric field distribution, charge trapping and charge mobility in the material, all of which are relevant to understanding the measurements and results considered in this thesis. In addition to this, the chapter presents the complex permittivity, its frequency dependence and relationship to losses, and the relationship of permittivity to various relaxation mechanisms.

Polarisation mechanisms and dielectric properties play a central role in how electric field is distributed within the dielectric material. Inhomogeneities such as interfaces, defects or structural discontinuities can lead to local charge accumulation, altering the internal field distribution and creating potential trapping sites. The different polarisation mechanisms ranging from rapid electronic and atomic responses to slower dipolar and interfacial processes contribute differently to the material's overall polarisation and electric behaviour. These phenomena influence how charges move through or become immobilised within the dielectric.

3.5.1 Polarisation

Many literature references have shown how a material can respond to an applied electric field using a plate capacitor arrangement as an example and the fundamental formulas for this phenomenon can be found in references such as [10], [16], [25], [26], [35]. When a dielectric material is placed between the plates of a plane capacitor, the system shown in Figure 23 is subjected to an external electric field which induces charges on the material, which are distributed on its surface in the same way as on the plates of the capacitor. The charge formed on the dielectric surface is opposite to the charge on the adjacent capacitor plate. This phenomenon is called polarisation. [10]

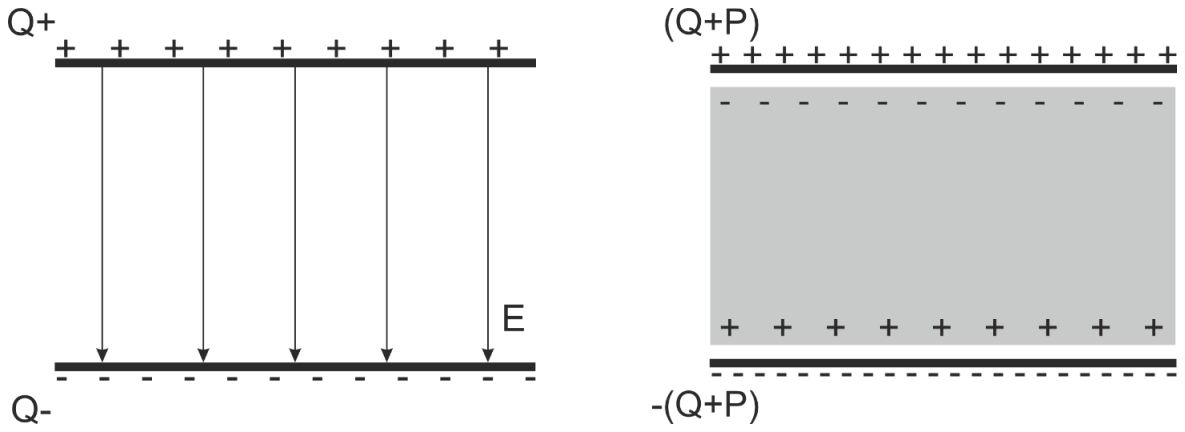

Figure 23. *Parallel plate capacitor without dielectric a) and dielectric b) in between the plates.*

The electric field causes positive and negative charges in a dielectric material to move in slightly different directions, resulting in a dipole moment $\boldsymbol{\Delta p}$ for a given volume Δv. In this case, polarisation can be defined as the dipole moment per unit volume

$$\boldsymbol{P} = \frac{\Delta \boldsymbol{p}}{\Delta v}. \tag{18}$$

Since each volume element contains several molecules, the total polarisation P is obtained by calculating the sum of all individual dipole moments p_m

$$\boldsymbol{P} = \frac{1}{\Delta v}\sum_{m} \boldsymbol{p_m}. \tag{19}$$

The total polarisation is shown as an additional charge on the electrodes of the capacitor. These bound charges are the result of the polarisation of the material under the influence of an external electric field. [5] Figure 24 shows a polarised piece of material and its associated polarisation vector $\boldsymbol{P}$. Each volume element Δv is represented as a dipole with charges $+q$ and $-q$. This illustrates how polarisation is formed as the sum of the individual dipoles in the whole material.

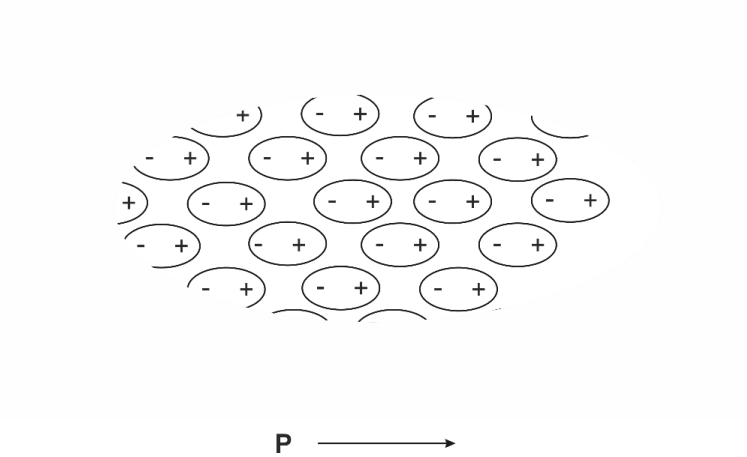

Figure 24. *Polarisation vector $\boldsymbol{P}$ represented in a sheet of dielectric material.*

The polarisation of the material in the electric field causes the accumulation of bound charges on the electrodes, which increases the capacitance compared to a vacuum. This is described by the relative permittivity ε_r which is a material-specific quantity and normally independent of the electric field strength. The permittivity indicates how efficiently the material stores electrical energy by polarisation. The polarisation $\boldsymbol{P}$ due to the electric field is related to the permittivity as follows

$$\boldsymbol{P} = (\varepsilon_r - 1)\varepsilon_0 \boldsymbol{E} = \chi \varepsilon_0 \boldsymbol{E}, \tag{20}$$

where ε_0 is the permittivity of the vacuum and χ is the electrical susceptibility. [10]

At the molecular level, polarisation arises from the dipole moments of individual molecules, which are proportional to the local field $\boldsymbol{E_L}$ and the polarisability α. The total polarisation is the sum of these moments

$$\boldsymbol{P} = N_M \alpha \boldsymbol{E_L}, \tag{21}$$

where N_M is the number of molecules per unit volume [10], [36].

Polarisation can be broken down into different mechanisms, with total polarisation being the sum of all of them. According to [37], the polarisation mechanisms can be divided into the following categories..

1. Electronic polarisation
2. Atomic or ionic polarisation
3. Dipole polarisation
4. Space charge polarisation

Electronic polarisation can be modelled by considering an atom with a positive nucleus in the centre surrounded by a spherical electron cloud. When an external electric field acts on the atom, the electron cloud moves slightly away from its equilibrium position with respect to the nucleus, creating an internal dipole moment in the atom. The small mass of electrons allows a very fast response to changes in the electric field, which is why electron polarisation can occur at very high frequencies. It

is the fastest of the polarisation mechanisms and does not depend on temperature, but is directly proportional to the electric field strength. [37]

In *atomic polarisation*, positively or negatively charged atoms and ions move slightly relative to each other under the influence of an external electric field. This polarisation mechanism is slower than electron polarisation because the mass of the atoms or ions is much greater than that of the electrons, so their movement under the influence of the field is slower. Atomic polarisation occurs in all molecules, whether they are polar or non-polar. However, the phenomenon is more intense in molecules where the bonds between atoms are weak. Bond displacement involves structural changes, such as changes in bond lengths and angles, and rotation and bending of polar groups with respect to each other. [10] The effect of atomic polarisation on the overall polarisation is often relatively small compared to electron polarisation, but exceptions do occur. Particularly in ionic compounds, atomic polarisation can be a significant or even dominant mechanism. Like electron polarisation, atomic polarisation is temperature independent. However, its magnitude is influenced in particular by the bond energies of the molecule and crystal structure, which determine how easily atoms can move under the influence of the field. [36]

Dipole polarisation, or *orientation polarisation* occurs in materials whose molecules have a permanent dipole moment. When such a material is subjected to an external electric field, the permanent dipoles tend to orient themselves in the direction of the field. In this way they contribute to the overall polarisation of material. However, the orientation of the dipoles is not instantaneous, but slower than the motion of, for example, electrons or atomic nuclei, making orientation polarisation a much slower mechanism than electron or atomic polarisation. [36] Furthermore, orientation polarisation is temperature dependent. As the temperature increases, the thermal motion of the molecules intensifies, which tends to randomise the orientation of the dipoles and weaken the field-induced order. Thus, high temperature reduces the effect of orientation polarisation on the total polarisation. [37]

Space charge polarisation, also known in the literature as *interfacial polarisation*, occurs when charges accumulate locally within material or at interfaces because of charge movement under the influence of an electric field. This mechanism differs from those discussed earlier, i.e. the displacement of electrons or ions bound to atoms and molecules by an electric field, whereas in space charge polarisation the field is distorted on a larger scale. Such charge accumulation often occurs in the bulk of the material or at surfaces, especially in regions where conductivity changes occur, such as at crystal-amorphous interfaces, material defects and cracks. Moisture also increases conductivity and cause charge build-up. Space charge or interfacial polarisation is the slowest of all polarisation mechanisms. [26] In Figure 25, all the aforementioned mechanisms are described and illustrated in principle.

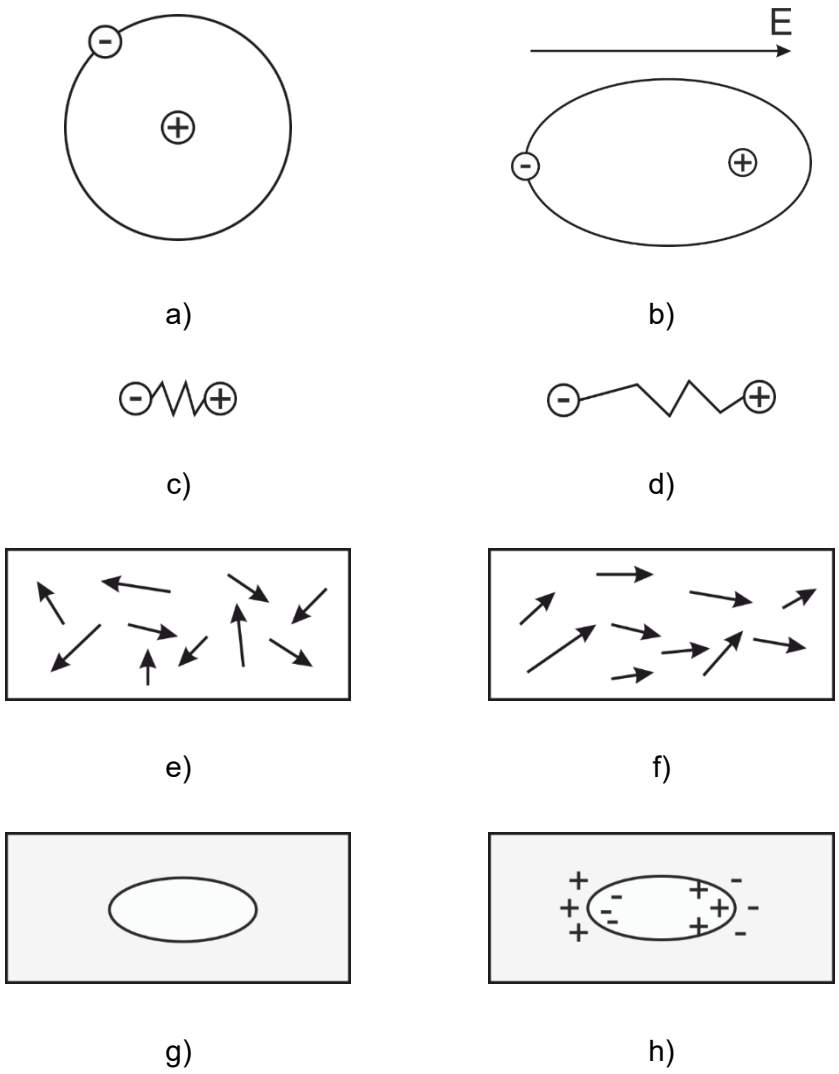

Figure 25. *Polarisation mechanisms in dielectrics. a), c), e) and g) before applying an electric field and b), d), f) and h) after applying an electric field. b) electronic d) ionic, f), dipolar or orientational polarisation, and h) space charge polarisation.*

The concept of *local electric field* E_L is central to understanding the behaviour of dielectric materials at the molecular level. Although the external electric field appears uniform at the macroscopic scale, inside the material the field is distorted by local charges and dipoles. To determine the local electric field, the Lorenz model takes into account three factors, external field E_C, electric field E_P due to the polarisation of the surrounding material, and the field E_M due to dipoles inside the region of interest. [25]

$$\boldsymbol{E_L = E_C + E_P + E_M} = \frac{\varepsilon_r + 2}{3}\boldsymbol{E}. \tag{22}$$

From this, further deriving and combining the knowledge that the electric field induces a dipole moment in the molecules, Clausius-Mosotti equation can be derived, which combines the relative permittivity ε_r at the macroscopic level and the polarisability α at the molecular level as follows

$$\frac{\varepsilon_r - 1}{\varepsilon_r + 2} = \frac{N_M\,\alpha}{3\varepsilon_0}. \tag{23}$$

The Clausius-Mosotti equation does not take into account, for example, the existence of permanent dipoles, the relative orientation between molecules and the temperature dependence. These shortcomings have been corrected in later theories to include the effect of permanent dipole moments, the refractive index n_r and Kirkwood's correlation coefficient g, which describes the mutual orientation of molecules. As a result, Fröhlich arrived at a more accurate equation describing molar polarisation

$$\frac{(\varepsilon_r - n^2)(2\varepsilon_r + n^2)}{\varepsilon_r(n^2+2)^2}\frac{M_w}{p_p} = \frac{N_A g p_0^2}{9\varepsilon_0 k_b T}, \tag{24}$$

where M_w is the molar mass of the material, p_p the permanent dipole moment and N_A the Avogadro constant. This equation takes into account the behaviour of polar molecules and temperature dependence. [10]

3.5.2 Complex permittivity

Dielectric materials are never completely ideal but always have some electrical conductivity. For this reason, some electrical energy is converted into thermal energy, i.e. losses. At DC, losses are mainly due to conductivity, whereas at AC, losses are also due to molecular friction. The combined effect of these results in dielectric losses, which in real materials are unavoidable. A lossy dielectric medium can be modelled by the parallel coupling of resistance R_a and capacitance C_a as shown in Figure 26.

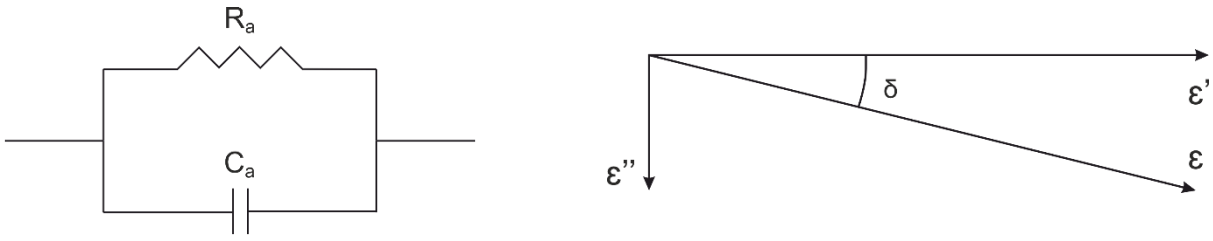

Figure 26. *Equivalent circuit used to model lossy dielectric structure represented in a) and complex permittivity in b).*

The permittivity of a dielectric material is complex as shown in Figure 26 and can be expressed as follows

$$\varepsilon^* = \varepsilon' - j\varepsilon'' = \varepsilon\angle - \delta, \tag{25}$$

Where ε' is the real part of the complex permittivity, which is related to the energy stored in the medium and corresponds to the capacitance C_a in the equivalent circuit. The imaginary part ε'' describes energy consumption, i.e. the losses in the medium, and is also called the *dielectric loss*

factor. This component is related to the resistor R_a in the equivalent circuit. The loss angle δ of a dielectric material is used to describe how much the material deviates from the ideal. The loss angle can also be expressed as

$$\tan\delta = \frac{\varepsilon''}{\varepsilon'} \approx \frac{\varepsilon''}{\varepsilon}. \quad (26)$$

Since the conductivity of many dielectric materials used as insulators is very small, $\tan\delta$ also called the *dissipation factor* can be approximated by the latter part of equation 29. [37]

3.5.3 Relaxation

Dielectric relaxation describes the delay with which the polarisation and hence the permittivity of a material follows a changing electric field. For example, the polarisation of molecules does not have time to follow a fast enough changing field but instead lags it. As a result of the delay, some of the energy is converted into heat. [37] Since polarisation mechanisms are activated in different frequency bands and relaxation times vary, permittivity and dielectric losses are also frequency dependent [10]. Debye's dispersion equations can be used to describe frequency dependent complex permittivity using the following equations

$$\varepsilon'(\omega) = \varepsilon_\infty + \frac{\varepsilon_s - \varepsilon_\infty}{1 + \omega^2\tau^2} \quad (27)$$

$$\varepsilon''(\omega) = \frac{(\varepsilon_s - \varepsilon_\infty)}{1 + \omega^2\tau^2}\omega\tau, \quad (28)$$

where ε_s is the static permittivity when frequency $\omega \to 0$, ε_∞ is the high-frequency limit when frequency $\omega \to \infty$, and τ is the relaxation time. [36] Figure 27 shows the dielectric dispersion curves of Debye, where the maximum losses can be observed at ω_{max}. At the same point, experimental results can also be used to determine the time constant τ to express the relaxation time. Also, it can be noticed that with low frequencies $\varepsilon' \to \varepsilon_s$ and ε' becomes small. On the other hand, when operating at high frequencies $\varepsilon' \to \varepsilon_\infty$ and ε'' becomes small again.

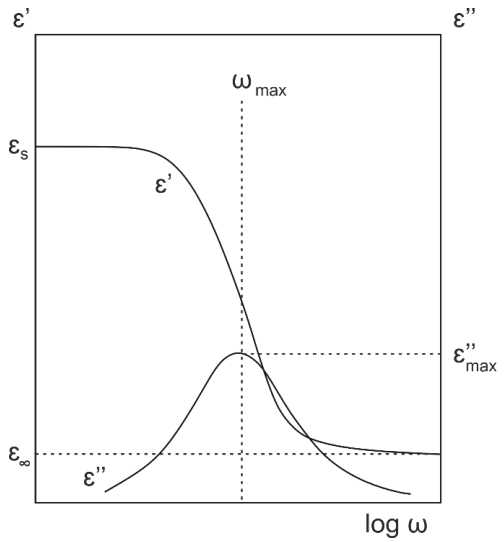

Figure 27. *Debye dispersion curves for dielectric.*

Debye's theory is based on a single relaxation time but has been extended by models that take into account the effect of multiple relaxation times. These, of which more can be found in [10], [38], [39] [3], [8], [9], provide more accurate dispersion curves and more accurate information on the dielectric behaviour of the material. Debye's assumption of spherical, independent dipoles does not hold, for example, in long-chain polymers where molecules interact with each other. This leads to variable relaxation times and a wider dispersion frequency range. [10]

In polymers, relaxation processes can be roughly divided into relaxation of amorphous and crystalline regions. In crystalline polymers, relaxation can take place either inside the crystal or at its edges. In amorphous regions, relaxation occurs before reaching the glass transition temperature as local movements associated with the main or side branches of the molecular chain, or near the glass transition temperature as a cooperative movement of the whole main chain.

The temperature dependence of the relaxation time is exponential and can be described by Arrhenius' law as follows

$$\ln \tau = \frac{E_a}{k_b T} + constant, \tag{29}$$

where E_a is the energy required to move from one molecular state to another. When plotted, the graph $ln\tau - 1/\tau$ should be a linear straight line, but when considering dielectric relaxation of polymers, it is often found that the dependence between the time constant τ of relaxation and the temperature inverse $1/T$ does not follow a linear Arrhenius law, but the graph is curved, especially in the vicinity of the glass transition temperature T_g. This suggests that the amount of energy E_a required for the transition from one molecular state to another in polymers is not constant, but that the transition from one state to another becomes easier as the temperature increases. This phenomenon is related to the so-called *cooperative relaxation*, where several polymer chain

segments must move simultaneously to allow structural rearrangement or dipole relaxation. Therefore, the Arrhenius model does not quite apply as such to the description of the relaxation behaviour of polymers near the glass transition temperature. [10]

The glass transition temperature is associated with a significant change in the mobility of the polymer chains. Above T_g, the segments are sufficiently mobile to be affected by the change in temperature of the polymer chain rearrangement. Below T_g, the segments are frozen in place and there is little movement. [10] Molecular motion requires empty spaces, the so-called free volume [38]. Figure 11 in Chapter 2.4.2 showed how the volume of a polymer increases as a function of temperature. From Figure 11, it can be concluded that above a certain critical free volume, molecular segments have sufficient space to orientate. [10]

In solid polymers, there are usually several different relaxation processes. This diversity is most easily seen in a scan of dielectric loss at constant frequency as a function of temperature. Figure 28 shows a basic plot of the dielectric loss curve. In the graph, relaxation peaks occur, named starting at the highest temperature α, β, γ..., of which the α relaxation peak is called the primary relaxation and other peaks visible in the graph are called secondary relaxations. [10]

The significant increase in molecular segment mobility occurring at the glass transition temperature T_g gives rise to the α-relaxation, which is the primary and most prominent relaxation peak. Below T_g, large-scale chain motion is restricted, so any observed relaxation peaks originate from other, more localised motions. In amorphous polymers, the development of β-relaxation is mainly attributed to the rotation of side groups around C–C bonds, conformational flips of cyclic units, and localised motions of main chain segments. [10] In semi-crystalline polymers, relaxation behaviour is generally more complex due to the presence of both amorphous and crystalline phases. Molecular motion can occur in either phase, which may cause the β-relaxation to split into two distinct components. Furthermore, additional relaxation modes are often observed above T_g, typically associated with molecular motions constrained by the crystalline regions. [38] In non-polar polymers, relaxation peaks can be very weak, even though the same underlying mechanisms as in amorphous materials are still present [10].

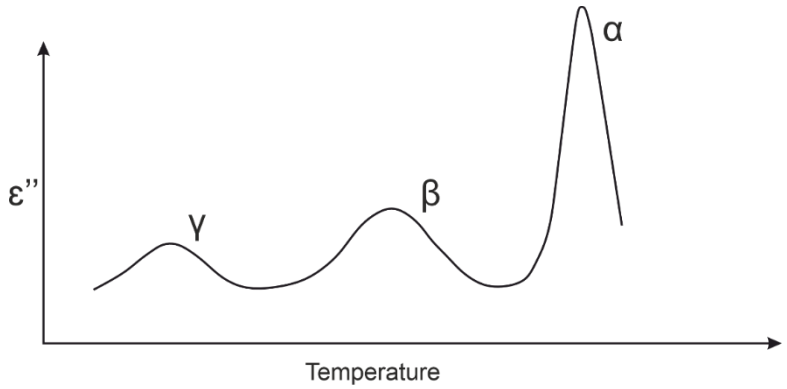

Figure 28. *Schematic illustration of a dielectric loss curve, showing the different relaxation processes.*

In crystalline polymers, molecular chains are arranged in a regular zigzag pattern. If a chain contains a polar group and an electric field is applied to it, a torque is generated which tends to rotate the chain around its axis. However, this motion is limited by the interaction of the surrounding chains in the crystalline structure. If the chain does not fold back into the crystal immediately at the edge of the crystal, but only afterwards, the twisting or folding of the chain beyond the crystal region is no longer limited by the crystal structure. Furthermore, in the case of long chains, it should be noted that they no longer behave as rigid bars but may also twist. Another relevant aspect of the dielectric relaxation process is the presence of chain strands outside the main chain and cross-linking bonds that prevent certain molecular movements. [10]

The electrical behaviour of dielectric materials can be significantly affected by various structural discontinuities and impurities in the material. The resulting variations in properties can be referred to as the *Maxwell-Wagner effect*. [10], [40] The phenomenon occurs when a material has regions of different permittivity ε and conductivity σ, i.e. $\varepsilon_1\sigma_2 \neq \varepsilon_2\sigma_1$, when two materials are stacked on top of each other in a planar capacitor, as already discussed. In this case, charges accumulate at the interfaces of the materials under the influence of the electric field, leading to an uneven distribution of the electric field and local polarisation. [37], [40] Typical discontinuities include cracks, gaseous cavities or different material phases such as the boundaries of amorphous and crystalline regions. Electrically conducting impurities, such as metal particles or moisture, can also cause local conductivity differences and contribute to charge accumulation at interfaces. [10]

In these cases, the electric field is unevenly distributed, which increases charge accumulation and affects the dielectric response of the material. For such systems, Wagner derived a mathematical model of complex permittivity where its real and imaginary parts, ε' and ε'', and constant k are represented as follows

$$\varepsilon' = \varepsilon'_\infty \left(1 + \frac{k}{1+\omega^2\tau^2}\right) \tag{30}$$

$$\varepsilon'' = \frac{\varepsilon'_\infty k\omega\tau}{1+\omega^2\tau^2} \tag{31}$$

$$k = \frac{9f\varepsilon_1'}{2\varepsilon_1' + \varepsilon_2'}. \quad (32)$$

The significance of the equations is that they show how differences in permittivity and conductivity in a dielectric material caused by impurities can give rise to a phenomenon similar to relaxation due to dipole orientation. In such cases, the relaxation time changes and the maximum of the loss tangent shifts to a different frequency range in the dispersion plots. This makes the phenomenon easily mistaken for other relaxation mechanisms, although it is due to charge accumulation at interfaces rather than dipole relaxation related to the molecular structure. [10]

4 POLYMER AGING, DEGRADATION AND BREAKDOWN

The most important properties of solid insulators are sufficient electrical and mechanical strength. Electrical strength is not usually a problem if there is enough space available for the insulator, but mechanical strength is equally important in many applications. Insulation often must function at high temperatures, which is why heat resistance is often the most important selection criterion. Over time and with use, insulation materials age and degrade, and their properties deteriorate due to various mechanical, thermal, and electrical stresses. [37]

Breakdown occurs when a thermally or electrically activated mechanism causes the number of charge carriers to increase to such an extent that the material loses its insulating capacity. Aging, degradation, and breakdown describe three different phenomena that damage insulation on different time scales, although some of the mechanisms that promote them may belong to more than one of these groups. The following Figure 29 shows aging, degradation, and breakdown, as well as some mechanisms that cause them, on a theoretical timeline which can be used to observe their development over time and their differences. Aging and degradation can be seen as slow processes that, over time, may lead to insulation failure as a result of breakdown. [37], [41]

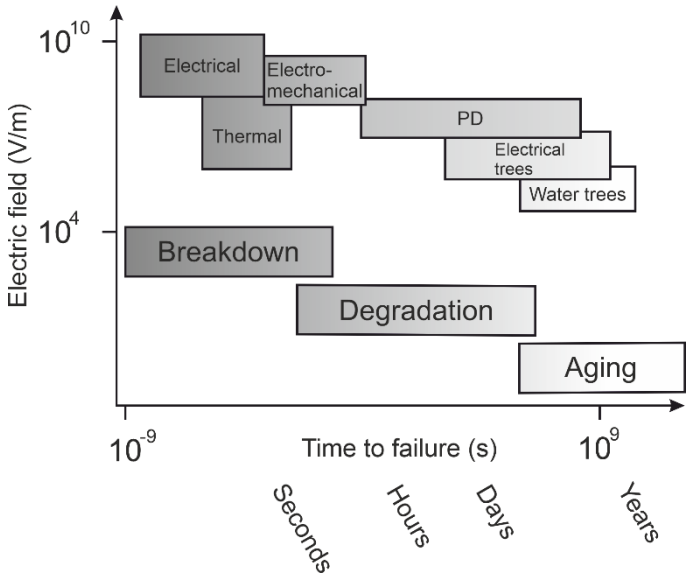

Figure 29. *Failure mechanisms of dielectric materials as a function of electric field strength and time to failure, illustrating the transition from rapid breakdown at high fields to long-term processes at lower fields.*

4.1 Physical aging

Physical aging is essentially a process in which the movement of polymer chain segments in amorphous regions decreases. The closer the polymer is cooled to its glass transition temperature, the slower its recovery from mechanical or electrical stresses become. When a polymer is cooled from the melt below its glass transition temperature, its macromolecular chains remain in a metastable state. This means that the polymer has higher enthalpy, entropy, and specific volume than a material in equilibrium represented in Figure 30. Most amorphous and semi-crystalline polymers that have undergone such heat treatment remain in a state of thermal imbalance. Since the polymer has not yet reached thermodynamic equilibrium, it continues to undergo slow conformational changes, known as physical aging or *structural relaxation*. These spontaneous relaxations reduce the enthalpy of the polymer as the chain segments rearrange themselves toward a lower energy level. [42], [43]

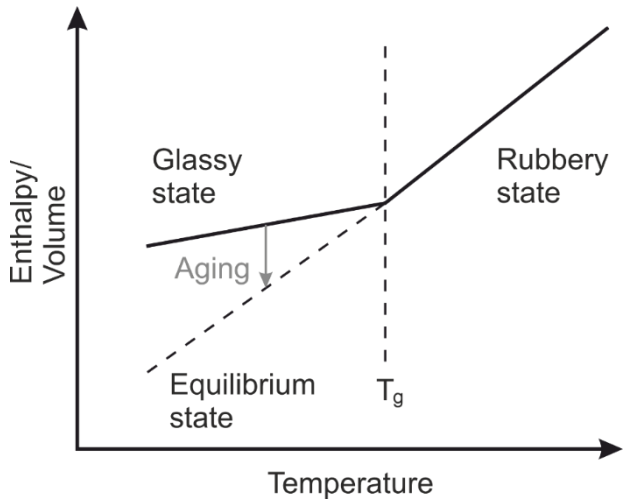

Figure 30. *Schematic representation of specific volume or enthalpy as a function of temperature, illustrating the glassy and rubbery states, the glass transition temperature and the effect of physical aging.*

Physical aging leads to changes in the properties of the polymer, for example, the glass transition temperature is observed to be higher than its apparent glass transition temperature would be expected to be, and gas permeability, tensile modulus, and brittleness increase [42]. Aging is also associated with a decrease in free volume. As the free space decreases, segment motion slows down, reaching a new equilibrium state after stress changes becomes increasingly slower. Physical aging is a self-slowing process, as the segment motion required for chain rearrangement slows down as the free volume decreases. [15]

Physical aging occurs significantly only below the glass transition temperature T_g, as the segmental movement of the chains is sufficiently slow there. A few degrees below T_g, the metastable state can persist for months or even years, depending on the material. Further below T_g, the movement of the

chains is practically stopped, and no significant aging occurs. [15] However, in semi-crystalline polymers, the chains in amorphous regions near crystals may have limited mobility, in which case the local T_g of these regions may be higher than the bulk T_g of the polymer. For this reason, physical aging can occur in semi-crystalline polymers above the bulk T_g, especially at the interfaces between amorphous regions and crystalline lamellae. [44] A similar phenomenon can also occur in materials reinforced with fillers, where the filler particles restrict local chain movement [15].

However, the physical aging of semi-crystalline polymers is not limited to a reduction in free volume and a slowing down of segmental movements. During aging, significant changes occur in the phase composition, crystallinity increases as a result of secondary crystallisation, and an intermediate, amorphous-like phase increases. This intermediate phase increases mechanical properties such as elastic modulus and yield strength. [45]

Both mechanical and electrical stress can affect the segmental movements of polymer chains. In semi-crystalline polymers, mechanical stress can increase the size and number of small cavities. Mechanical stress also causes slow crystallisation in amorphous areas, leading to an increase in density in these areas. Since the total volume of polymers is constant at a given temperature, the increase in density in one area is compensated by the formation of micro voids and discontinuities in another area. In addition, the number of interfaces between amorphous and crystalline areas may increase, which increases the density of defects and trap sites and local space charges. Such physical aging increases the vulnerability of dielectric materials to other electrical breakdown phenomena, such as partial discharges, electric trees, and water trees. [15]

At high operating temperatures, the small and imperfect lamellae of semi-crystalline polymers might melt and recrystallise into thicker lamellae when they cool down. Similarly, the formation of micro voids intensifies at high temperatures due to mechanical stress, which further weakens the insulating properties. [5] Physical aging leads to time-dependent performance characteristics because it has a modifying effect on the properties of the material. [45]

4.2 Chemical aging

Free radicals and ions are the most common causes of *chemical aging* in polymers. They are highly reactive and can initiate chain reactions that lead to either the breakage or cross-linking of molecular chains. Chain scission can occur randomly at different points, resulting in large molecular fragments, or as an unzipping like reaction, in which volatile monomers and side groups are released. Chain reactions can be triggered, for example, by heat, oxygen, UV or ionizing radiation, mechanical stress, or chemical impurities. Oxidation can also be accelerated by by-products left from the manufacturing process, especially if they contain metal ions that catalyse the reaction. [15]

Ionizing radiation and high-energy electrons can accelerate degradation by creating small fragments that easily break down through unzipping mechanism. In polymers with high polymerisation temperatures, the same process can also be used to achieve cross-linking, which can improve mechanical and thermal properties. [15]

At high temperatures, aging is mainly caused by chemical reactions accelerated by the temperature. For example, the combination of oxygen and heat can accelerate chain scission, promote oxygen diffusion into the polymer, and produce by-products or free radicals. Moisture, on the other hand, weakens the structure and aging resistance of most polymers, often through hydrogen bonding and hydrolysis, and its effect can be enhanced in combination with high temperatures. [46]

Cross-linking, especially when triggered by radiation, can continue slowly for years. This increases the crystallinity of the polymer and causes microstresses that cause the material to become more brittle. In addition, antioxidants added to dielectrics do not always remain permanently in the polymer, they can migrate out of the material or accumulate into large clusters. This not only reduces the effectiveness of antioxidant protection and exposes the material to oxidation but can also cause stress cracks and thus accelerate electrical breakdown. In the long term, the combined effects of oxidation, moisture, and radiation can form a complex, continuously propagating chain reaction in which free radicals are generated and consume the material at an accelerating rate. [15]

4.3 Electrical aging

The aforementioned chemical and physical polymer aging processes can occur without the influence of an electric field and are often slow processes that alter the properties of the polymer from its original state [9]. However, an electric field can accelerate or interact with these mechanisms and thus further age the insulation. Electrical aging can be said to occur when the strength of the electric field effects the aging of the dielectric material. Electric field, especially DC field, can cause the decomposition and movement of ionised and ionisable by-products. This leads to a deterioration in insulation capacity due to increased losses and local stress peaks, even though no visible damage is yet apparent. Electrical aging and degradation processes include, for example, water and electrical trees and partial discharges (PD). [15]

4.3.1 Water tree

Water trees are microscopic, tree-like, and often branched structures that form in electrical insulation materials due to the combined effects of an electric field and moisture. They develop from structural imperfections in the insulation, such as scratches, impurities, pores, or water-filled micro voids. The internal structure of water trees consists mainly of small, spherical micro voids, rather than continuous channels or cracks. Water trees are generally classified into two categories, bow-tie

trees, which grow from water-filled voids, and vented trees, which grow from the semiconductive layer. [2]

The growth of vented trees can typically be divided into three main stages, an inception stage, rapid but gradually decelerating propagation stage, and a stage in which growth slows down significantly or almost completely stops. In contrast, the growth of bow-tie trees usually saturates. [15] Water tree propagation is driven by the intensification of the electric field at the tree tip, which directs the access of water and ions into the polymer and promotes the formation of water-filled microcavities. The growth rate and extent of propagation are essentially influenced by the tree type, the magnitude and duration of the electric field, and the characteristics of the growth site, such as local defects, interfaces, and the dielectric permittivity of the material. The higher and longer the electric field is applied, and the more favourable the environment is for water transport, the further and faster a water tree can develop over time. [47] Water treeing is primarily a long-term aging or degradation mechanism, typically progressing over months or even years [15]. Although water trees are more common under AC fields, they can also occur under DC. In particular, harmonic components superimposed on a DC voltage can accelerate water tree growth. [44]

The space charge present in the surroundings of a water tree can either enhance or reduce the local electric field. Charge density, type of space charge and polarity of the voltage applied to the cable also have an effect on electric field changes and impact on water tree propagation. These factors can either promote or inhibit the ionisation processes that drive tree growth. [48] Water tree development is also affected by several other factors, such as temperature, the nature of the electrolyte, and the morphology of the insulation material. While modern cable insulation can withstand water treeing for long periods without sudden failures, water trees can still significantly shorten service life and pose a long-term reliability risk. [15], [49]

According to [15] water trees can eventually develop into electrical trees, but this requires certain additional conditions to be met. Electrical tree propagation along a water-tree-degraded path occurs when the water content of the tree channel decreases significantly, the ion concentration increases, and the local electric field becomes intensified. Vented water trees are particularly prone to this transition, as they can grow across the entire insulation thickness and provide a direct pathway for electrical treeing. In contrast, bow-tie water trees often have a more limited impact, as the amount of electrolyte and the possibility for gas release are low, which restricts electrical tree development.

4.3.2 Electrical tree

Electrical treeing is a tree-like or branching damage channel within dielectric, formed because of long-term electrical stress. It represents one of the most significant pre-breakdown degradation mechanisms in polymeric insulation and is a critical phenomenon, particularly for high-voltage

equipment and maintenance considerations. The presence of an electrical tree reduces the dielectric strength of the insulation material and increases the likelihood of breakdown over time. [50], [51] Electrical trees typically form in regions where the local electric field is elevated. Such regions arise, for example, at structural discontinuities in the material, in gas voids, or at electrode interfaces. The initiation of an electrical tree is often linked to charge injection from the electrode–insulation interface, with the accumulation of charges causing distortions in the electric field distribution. This, in turn, can lead to bond scission in polymer chains, the formation of microcracks, and eventually the initiation of electrical treeing. [51], [52]

Under DC stress, charge injection and subsequent transport through the insulation are key processes. Charges can become trapped in localised states within the material, forming space charges that distort the field distribution and lower the threshold field required for tree initiation. [50], [53] Since the growth rate of electrical trees is roughly proportional to frequency, one might expect treeing to be difficult under pure DC conditions. However, studies have shown that electrical trees can develop particularly under combined voltage stresses, such as DC–pulse or DC–AC composite voltages. [2], [50] The combined effects of pulse-induced charge injection and mechanical stress can accelerate polymer chain scission and microdamage formation [51]. According to [54], even when the AC component is much smaller than the DC bias, it can significantly influence tree growth by periodically injecting and extracting charges, thereby weakening the stabilizing effect of space charges. The effect of the AC ripple becomes more pronounced as its proportion increases compared to DC bias. At low relative shares of AC composed to DC, tree growth is restrained, while higher amplitudes accelerate propagation and produce electrical tree morphologies closer to those under pure AC conditions. Morphological differences in electrical trees also emerge under positive DC bias with superimposed AC, trees tend to form along a few main channels accompanied by stronger PD activity, while under negative DC bias the growth rate is slower and trees with many micro-branches dominate, associated with more dispersed PD activity. [54]

Polarity reversals or rapid changes in the applied voltage in HVDC systems increase the likelihood of electrical tree formation. These transients interact with accumulated space charges, enhancing the local electric field and initiating partial discharges that promote tree inception. The breakdown initiation voltage for treeing is lower during polarity reversal compared to unidirectional DC operation, whereas slower polarity changes reduce the probability of tree formation. Polarity reversals are further associated with more intense burst-like PD activity than steady DC, a behaviour closely correlated with accelerated tree growth and branching. [6], [55]

Temperature also plays a significant role in electrical tree formation. Elevated operating temperatures increase molecular chain mobility and free volume, allowing charges to migrate more easily through the material. As a result, charges can gain higher energies and break molecular bonds, further increasing the likelihood of tree initiation and propagation. [56]

Electrical treeing is generally considered a long-term degradation mechanism, although under certain extreme conditions, such as high pulse voltages, it can develop rapidly [50]. The growth process often proceeds through three stages, initiation, propagation, and a runaway phase, during which the tree can rapidly extend to full breakdown. While electrical treeing is not, in itself, a breakdown event, its presence is a clear indication of electrical aging of the insulation and a potential precursor to failure. [56]

4.3.3 Partial discharge

Partial discharge (PD) is a localised electrical discharge that occurs within gas-filled voids inside insulating material, at its interfaces, or in manufacturing defects where the electric field is locally intensified sufficiently to initiate the discharge [15], [55]. In voids, the field is concentrated due to the lower permittivity, and discharge occurs there before it does in the surrounding material. The inception voltage V_i required to initiate partial discharge depends on the size and shape of the void, the properties of the gas, pressure, and temperature. [57] Partial discharges cause chemical and physical changes in insulation structures. In addition, they result in erosion, heat generation, and the production of various gases. Typically, partial discharges affect the long-term service life of the insulation. [37]

The distribution of the total voltage applied to the insulation between the void, and the surrounding material can be illustrated by the equivalent DC circuit in Figure 31 a). The void is represented by capacitance C_v parallel with a spark gap and void resistance R_v. The void must be charged through the insulation in series with it, which is represented by parallel capacitor C_s and resistor R_s. The remainder of the insulation is represented by C_p in parallel with R_p. [55]

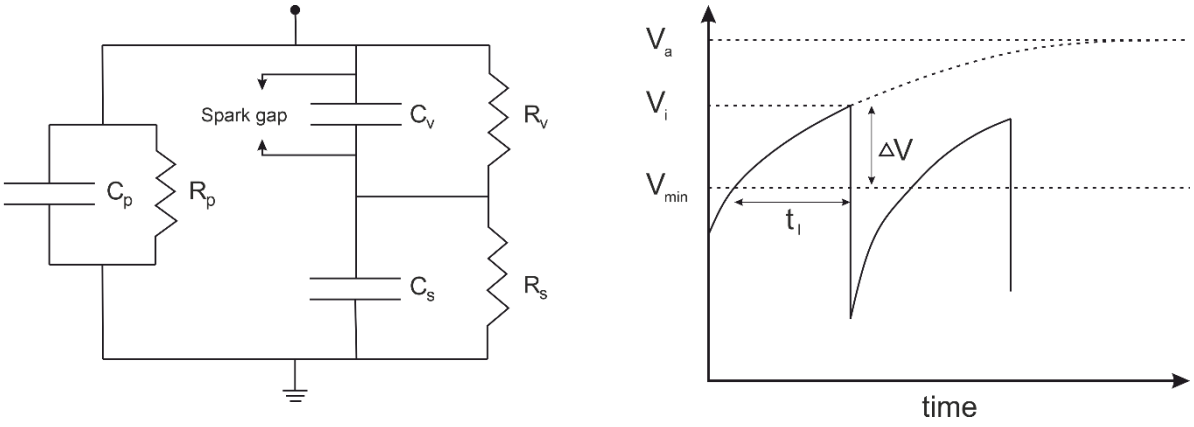

a) b)

Figure 31. *Equivalent circuit of a void a) and the corresponding voltage (DC) behaviour across the void during partial discharge activity b).*

The initiation of a partial discharge requires two conditions to be satisfied, the voltage across the cavity must exceed the minimum voltage V_{min} to start PD, and a free electron must be present at a suitable position to trigger the ionisation process. The appearance of such an initiating electron is a stochastic event, and as a result, a time delay t_l occurs between the moment the voltage surpasses V_{min} and the actual onset of the discharge. During this statistical delay, the cavity voltage continues to rise above the minimum voltage, a surplus described as ΔV. PD ignites at inception voltage that is $V_i = V_{min} + \Delta V$, as illustrated in Figure 31 b). During a partial discharge, charge is transferred across the void and accumulates on its internal surfaces. These accumulated charges create a field in the opposite direction to the external field applied to the void. As a result of the discharge, the voltage across the void decreases and the PD is extinguished. The discharge process is influenced by the overvoltage ΔV, which depends on the rate at which the applied voltage increases. Over time, the charges deposited by the discharge gradually diffuse into the surrounding insulation, allowing the voltage in the void to rise again. Once the voltage across the void exceeds the inception level, a new PD can occur. If, however, the discharge does not extinguish but instead develops into a self-sustaining ionisation process, this may lead to complete breakdown of the insulation. [15], [55]

Paschen's law can be used to describe how the breakdown voltage of a gas depends on the product of the gas pressure p and the electrode gap distance d. Figure 32 presents a schematic illustration of Paschen's law, with both axes shown on a logarithmic scale, showing that the breakdown voltage reaches its minimum at a specific $p * d$ value. This is referred to as the Paschen minimum. When $p * d$ decreases below the minimum, the breakdown voltage increases. This is because there are insufficient ionising electron collisions in the gas before an electron reaches the opposite electrode. In other words, the electric field is too weak to initiate an electron avalanche, as the gap is short and there are few gas molecules. Conversely, when $p * d$ increases above the minimum, the breakdown

voltage also rises. In this case, the gas density is so high that electrons collide with gas molecules too frequently and lose energy, thus failing to reach the kinetic energy required for ionisation. [58]

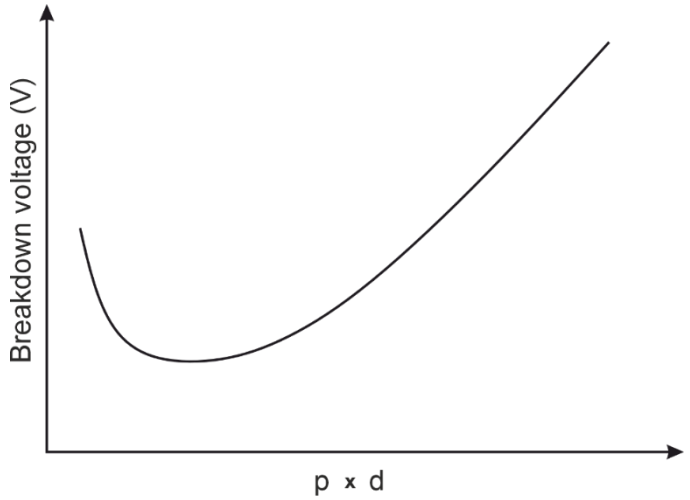

Figure 32. *Representation of Paschen curve showing the relation between the multiplication of pressure (p) and gap length (d) versus breakdown voltage (V) in logarithmic scale.*

As partial discharge progresses, the leading edge of the discharge avalanche accumulates negative charge from higher mobility electrons. Behind this front, lower mobility positive ions remain. This asymmetric distribution of charges distorts the local electric field and effectively shortens the distance over which the voltage across the void is distributed. This effect shifts the operating point of the discharge on the Paschen curve. If the original operating point lies on the left-hand side of the Paschen minimum, the shortening of the voltage distribution gap can lead to an even higher breakdown voltage, which may weaken the discharge. Conversely, if the operating point lies on the right-hand side of the minimum, a shorter gap may bring the operating point closer to the minimum, increasing the likelihood of discharge. In other words, depending on which side of the Paschen curve the operating point is located, the effect of a non-uniform field can either hinder or promote discharge development. [15]

As previously noted, the damage mechanisms of discharges are mainly physical and chemical. Ion bombardment can cause localised damage to the structure of the insulation, particularly when accompanied by a rise in temperature or pre-existing defects. The kinetic energy of individual ions is often insufficient to break bonds, but a high charge density in a small area can lead to material degradation, especially in insulation that has aged mechanically or chemically. [55], [59] In terms of chemical damage, partial discharges produce reactive oxygen species which react with and degrade polymer chains. Unlike ion bombardment, which causes localised damage, these species diffuse rapidly and damage larger areas, particularly the internal surfaces of voids. [15]

Partial discharges occur less frequently under DC than under AC. Nevertheless, transient events such as switching operations or voltage changes can temporarily increase their occurrence rate even under DC conditions [55]. Under DC loading, the electric field distribution within the insulation shifts over time, causing the highest field stress to migrate towards the outer edge. As a result, the likelihood and onset of partial discharges depend not only on the applied voltage but also on the location of void within the insulation. [60], [61]

4.4 Breakdown mechanisms

Breakdown in electrical insulation can be initiated by several different physical and electrical mechanisms, which depend both on the structure of the material and on operating conditions such as electric field strength, temperature, humidity, and the nature of the electrical load. In polymeric insulations, the degradation process is often complex and may result from the combined action of multiple mechanisms, where, for example, heat, mechanical stress, and electric-field-induced phenomena reinforce one another. Space charge can influence the changes occurring as a result of all these mechanisms. The following subsections examine the most important breakdown mechanisms individually. In the case of solid insulation, breakdown always results in the loss of insulating capability.

4.4.1 Thermal breakdown

All insulating materials possess a small electrical conductivity, which under voltage contributes to heat generation through leakage current and associated power losses. Conductivity is therefore one of the mechanisms by which temperature can rise within the insulation. *Thermal breakdown* occurs when this temperature increase becomes sufficient to degrade the insulation properties and reduce its dielectric strength below the applied voltage. If the heat generated and dissipation are in balance, the insulation remains intact. However, if conductivity increases with rising temperature, the rate of heat generation accelerates uncontrollably, leading to thermal runaway and ultimately the failure of the insulation. [15]

Thermal breakdowns can be described by two distinct phenomena, *destructive breakdown* and *thermal instability*. From a thermal perspective, three states described in Figure 33 can be distinguished for an insulating material, stable, metastable, and unstable. In the stable state, when the voltage is below a certain threshold voltage, the insulation warms up and eventually reaches a stable equilibrium state in which the heat generated by the insulation equals the heat dissipated to its surroundings. In this state, the temperature remains constant. In the metastable state, the voltage is increased above the first threshold, and although the temperature still stabilises, at higher temperatures equilibrium can no longer be achieved. In such conditions, even a small increase in voltage causes heat generation to exceed the material’s ability to dissipate heat, leading to an

uncontrolled temperature rise and thermal runaway. This critical voltage level is often defined as the maximum value below which thermal breakdown does not occur, but above which the temperature will eventually rise to the point of failure. In the unstable state, the voltage is so high that the temperature never reaches equilibrium, and heating continues until breakdown occurs. [15]

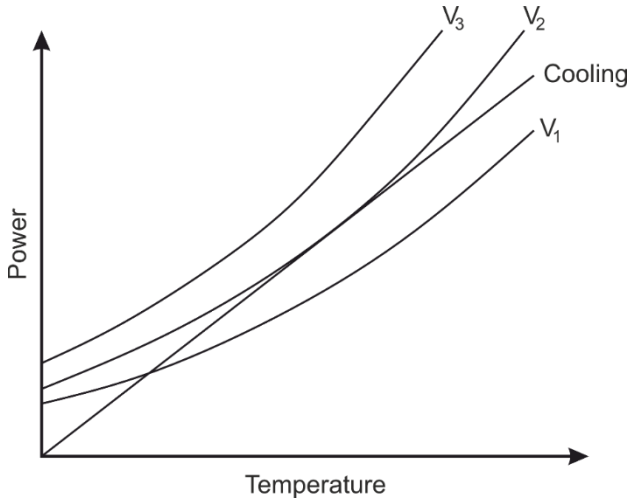

Figure 33. *Relationship between generated power and temperature for different applied voltages $V_1 < V_2 < V_3$, illustrating thermal stability between heating and cooling of the insulation.*

Unlike in steady-state thermal breakdowns, in *impulse breakdowns* the thermal capacity of the material or insulation cannot be neglected. In steady-state conditions, temperature changes are slow enough that only the balance of thermal power needs to be considered. In impulse breakdown, the temperature rise is so rapid that heat conduction can be neglected. Consequently, localised heating or hot spots may occur at material defects or inhomogeneities, where enhanced current density and electric field further accelerate the temperature increase. When comparing steady-state breakdown to impulse breakdown, breakdown under impulses occurs at higher temperatures. [15], [62]

Space charge influences the impulse breakdown behaviour of dielectric materials. Experiments on polyethylene have shown that during DC pre-stressing, homocharge accumulate near the electrode tip, which reduces the field in that region. This effect can increase the impulse breakdown field if the impulse polarity is the same as in pre-stressing and correspondingly decrease it, if the polarity is opposite. The effect also depends on the voltage rise time, as this determines the time available for charge accumulation. [63]

In general, breakdown occurs at weak points in the insulation, where local conductivity may be higher, thermal conductivity lower, or the electric field greater than in the surrounding material [15]. In thin polymer films, an increase in current has been observed before breakdown, indicating *filamentary breakdown*, a phenomenon in which the current flows through a narrow, rapidly heating

channel. In such a case, the local temperature rises sharply, forming a conductive path through the insulation. [64]

4.4.2 Electromechanical breakdown

Electromechanical breakdown occurs when the mechanical stress induced by the electric field exceeds the tolerance of the dielectric material. This phenomenon has been observed in several thermoplastics, where softening due to increased temperature reduces the material's ability to resist mechanical stress. The force arises from electrostatic interactions and can result in a reduction in the thickness of the insulation. As the insulation becomes thinner, the electric field strength increases, which may trigger another breakdown mechanism before actual electromechanical failure occurs. [15], [65]

Crack propagation in dielectric materials can be classified into *electrofracture* and *filamentary electromechanical breakdown*. In electrofracture, electrostatic forces cause the growth of a narrow, tubular crack within the insulation. This is a gradual degradation process, an ageing mechanism, where the crack grows progressively over time. In filamentary electromechanical breakdown, the phenomenon occurs at higher local electric fields and is regarded as a true breakdown mechanism, meaning a rapid and sudden failure of the insulation, rather than mere ageing. In both cases, the electric field strength at the crack tip is intensified, promoting further crack propagation within the material. [15]

In some materials, hot spots caused by Joule heating may not trigger thermal runaway, but the resulting reduction in Young's modulus can still lead to electromechanical failure. A combination of insulation thinning increased electric field at the crack tip, and elevated temperature together contribute to the weakening of the Young's modulus. This mechanism is more common in thin films, as in these the electric field is more strongly affected by even a small crack than in materials with actual insulation thicknesses. [15] The presence of space charge further increases the mechanical deformation of the material, as the field alteration caused by the charge amplifies the electromechanical stress acting on it [66]. Electromechanical stress may also act with other breakdown mechanisms, such as electrical breakdown, thereby not only accelerating the progression of damage but also reducing the overall dielectric strength [65].

4.4.3 Electrical breakdown

Electrical breakdown in solid insulating materials has been attributed to either the energy or the number of electrons increasing to such an extent that the material enters an unstable state, resulting in at least localised damage to the crystal lattice, or to breakdown through *impact ionisation or avalanche breakdown* processes. [37] Free electrons moving in an electric field can transfer energy

to the crystal lattice via electron–phonon scattering. However, there is an upper limit to the rate at which energy can be transferred to the lattice. When this limit is exceeded, an imbalance arises that can lead to breakdown. If the electric field continues to increase, electrons gain energy faster than they can transfer it to the lattice, causing their energy to rise uncontrollably. This inevitably leads to the electrical failure of the material which can be considered as true *internal breakdown.* [15]

Although electron–lattice interaction is an important mechanism for energy transfer, it is not the only one. Electrons can also collide with other electrons or with defect sites in the material, transferring energy through these interactions. When electrons collide with other free or trapped electrons, impact ionisation and avalanche breakdown can occur. Furthermore, as the temperature rises, the crystal lattice's ability to absorb energy decreases, making energy transfer to the lattice less efficient. This accelerates the rise in electron energy and reduces the breakdown field strength. [15]

In impact ionisation or avalanche breakdown, electrons with sufficient energy collide with bound or trapped electrons, releasing them. After the collision, both the original and the freed electron continue to move freely and gain further energy from the electric field, allowing the process to repeat. This initiates a chain reaction in which the number of free electrons increases rapidly and leads to breakdown. The growth in number of free electrons can be limited by factors such as recombination with positive ions, diffusion, or capture by electronegative atoms. [37] In polymers, the release of a trapped electron through collision may, in some cases, leave the trap positively charged. This results in the formation of a positive space charge behind the avalanche front edge, which weakens the local electric field and can therefore extinguish the avalanche. On the other hand, if the trap was initially neutral, its emptying does not produce this field-suppressing effect. [15]

Electrical breakdown is a complex process influenced by numerous factors, including ionisation, the accumulation of space charges within the discharge channel, changes in the molecular and crystalline structure of the insulation, and heating. Water trees, electrical trees, and partial discharges can significantly promote the occurrence of breakdown by reducing the dielectric strength of the insulation. When the local electric field strength exceeds a critical threshold, electrical discharges occur, damaging the insulation through physical and chemical processes. Eventually, a conductive channel is formed within the insulation, in which electrical conductivity increases, and full breakdown occurs. [37]

4.4.4 Free volume breakdown

As the temperature increases, the free volume in polymers grows, which explains the reduction in breakdown strength above the glass transition temperature. Conversely, it has been observed that increasing pressure improves breakdown strength because the free volume decreases. The internal free volume of a polymer provides electrons with a pathway along which they can accelerate under

the influence of the electric field. If the electrons gain sufficient kinetic energy, they can cause structural damage, such as the breaking of molecular chains. [15], [67]

The cohesive energy of the polymer also plays an important role in determining breakdown strength. Cohesive energy describes the intermolecular binding interactions, such as dispersion forces or dipole–dipole interactions and indicates how strongly the structural units of the material are bound together. The greater the cohesive energy, the more difficult it is to cause mechanical or electrical damage to the structure, and the higher the breakdown strength. This is evident in polymers whose chains are held together by both dipole–dipole interactions and van der Waals forces. [15]

The effect of free volume on breakdown behaviour appears to depend not only on the amount of free volume itself but also on field polarity and the voltage rise rate. Under negative polarity with a slow voltage rise, injected charges can accumulate and form a space-charge region near the electrode. This charge cloud partially shields the electrode, weakening the local electric field at the initiation site. As a consequence, a higher external voltage is required to re-establish the critical local field strength for breakdown, resulting in an increased breakdown voltage. In contrast, under positive polarity or with a rapid voltage rise, such a stabilizing charge distribution does not have time to form, and the breakdown voltage remains lower. In addition, reducing the free volume, for instance by adding nanoparticles, shortens the acceleration paths of electrons and further improves breakdown strength. [15], [67]

5 MEASUREMENT METHODS FOR SPACE CHARGE

5.1 Pulsed Electro Acoustic (PEA) method

The pulsed electro acoustic method is a one of the simplest and most effective techniques for measuring the dynamic spatial distribution of space charge in dielectric materials [68], [69]. It is a non-destructive method and is also suitable for remeasurement of samples. PEA measurement circuit mainly consists of a DC voltage source V_{DC} to generate a high electric field in the sample, a pulse generator $e(t)$ to generate a shock wave response from the charges, a piezoelectric transducer to convert the acoustic signal into a voltage signal and an amplifier to generate a final output signal for reading. [70] Figure 34 shows a schematic diagram of the PEA measurement circuit and its components.

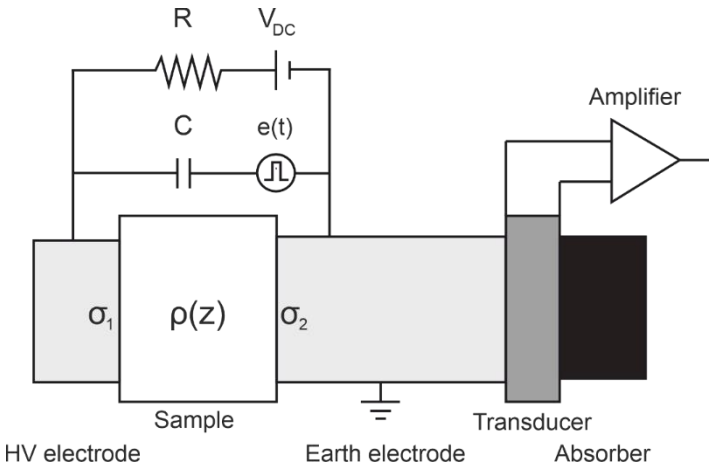

Figure 34. *Representation of the PEA measuring circuit and its main components.*

The idea of the measurements is that the sample, of thickness d, located between the electrodes, contains a spatial charge $\rho(z)$. An external electric field pulse $e_p(t)$ of duration Δt with a fast rise and fall time is applied to the sample. The pulse induces a perturbation force $\Delta F(z,t)$ on the spatial charges $\rho(z)$ in the sample. This instantaneous electric field causes a small dislocation of the charges in the material from their proper position, which generates an acoustic shock wave $\Delta p(z,t)$ that propagates from the sample through the ground electrode to the piezoelectric transducer. The sum of the acoustic waves generated by the charges is the total wave $p(t)$. This total acoustic wave arrives at the transducer, which converts it into an electrical signal $v_e(t)$, which is passed to the amplifier and through it to the measuring device. Since the charges in the material are located at different locations in the material, they arrive at different times at the transducer detecting the pressure. This delay due to the location of the charge indicates the location of the charge in the

dielectric material and the amplitude of the signal indicates the density and sign of the charge. [68], [71], [72]

The accumulation of space charge as a function of time can be studied by connecting a DC voltage V_{DC} across the sample before pulsing. Compared to the previous description, this causes additional surface charges σ_1 and σ_2, which also experience a perturbation force and generate a shock wave, as do the charges in the sample. Both bulk and surface charge components can then be observed in the PEA signal. [68], [71]

Figure 35 shows the evolution of the spatial charge distribution measured by PEA as a function of time for a material studied in this thesis (Blend-4). The measurements were performed at University of Bologna (partner in NEWGEN project). The measurement was performed by exposing the sample to DC voltage for three hours, after which the voltage was removed. The voltage was then switched off for one hour. The PEA measurement has been performed throughout the four-hour measurement protocol. The measured sample is approximately 200 µm thick which is shown between 0.05-0.25 mm in y-axis in Figure 35, the first and last 0.05 mm representing the electrodes between which the sample is located. The measurement shows how the charge in the sample evolves from left to right over time. The measurement clearly shows a positive homo charge throughout the measurement, but also a hetero charge that starts to develop at around 3000 seconds and increases up to three hours. In addition, at the beginning of the measurement, a decreasing positive homocharge is observed near the positive electrode as the measurement progresses.

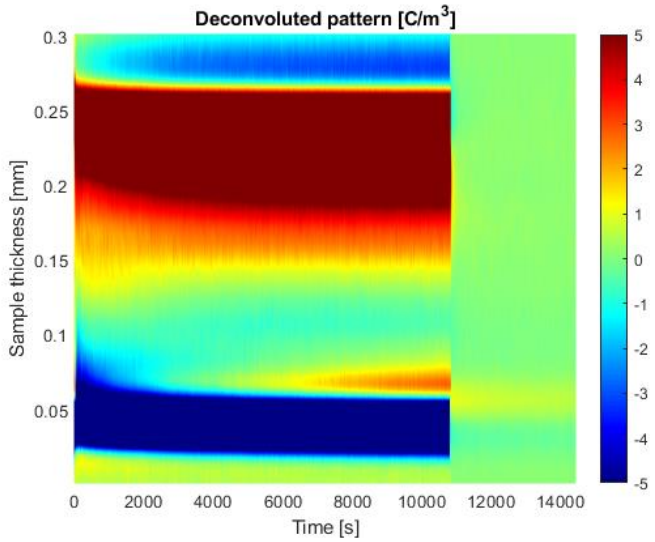

Figure 35. *PEA measurement result for 200 µm thick Blend-4 measured by NEWGEN project partner University of Bologna. Poling temperature t_p was 70 °C, and a poling field E_p of 30 V/µm was applied Voltage was kept on for three hours and voltage off for one hour. Negative space charge shown in blue and positive in red as time progresses from left to right.*

5.2 Thermally stimulated current (TSC)

Electret charge in a material can originate from several mechanisms, such as the orientation of permanent dipoles, charge trapping due to structural defects or impurities, and the presence of heterogeneous regions, such as interfaces between amorphous and crystalline phases in polymers [73]. Unlike metals and semiconductors, dielectric materials can retain charge for extended periods. This is particularly true for semicrystalline and amorphous polymers, which tend to accumulate space charge due to their high DC resistivity. [74]

When a solid dielectric material is exposed to an external electric field, charge movement occurs both on its surface and within the bulk. Free charges can move and may leave the dielectric, whereas bound charges are part of the material's structure and cannot move freely. Charges located on the surface are referred to as surface charges, while those within the material are known as space charges. [74] If the surface charge has the same polarity as the polarising electrode, it is called a homocharge. If it has the opposite polarity, it is termed a heterocharge. [22] In the presence of ion pairs in the material, an electric field may separate the ions. If the ion mobility is low, their effect is primarily limited to the material’s polarisation. However, if the ions are mobile, they will drift toward the oppositely charged electrode. The behaviour of these ions depends on the properties of the electrode. If no charge exchange occurs at the interface, surface charge accumulates. Conversely, if the electrode can neutralise the ion, excess charge may be injected into the material. External factors such as corona discharge and ionising radiation may also introduce surface charges onto the dielectric. [74]

In dielectrics, the primary source of excess charge is the injection of electrons and holes from the electrode–insulator interface. Typically, this charge accumulation remains limited due to the moderate voltages applied. However, when the electric stress on the insulation persists over long periods, a significant amount of space charge may gradually build up within the material. [74]

Trapped charges are generally released by thermal activation [74]. At room temperature, this release is slow, which would make the measurement time consuming because dipoles and charges remain nearly immobile at low temperatures Elevated temperatures are also used during poling, since they accelerate the filling of traps. When the material is heated, dipoles and charges regain their mobility, leading to shorter measurement times [73]. which ensures the trapped charges within the material form space charge, which may significantly alter the internal electric field distribution. Thermally Stimulated Current (TSC) measurements aim to investigate the charge state of a dielectric material under the influence of an electric field [28].

5.3 TSDC and TSPC measurement techniques

Measurements carried out in this thesis were performed using *the Thermally Stimulated Depolarisation Current* (*TSDC)* method. In a conventional TSDC measurement, the sample is first heated to the desired poling temperature. Once this temperature is reached, an electric field is applied to the sample for a selected period, during which charges redistribute, and dipoles align with the direction of the field. The sample is then cooled rapidly under the applied electric field, so that a significant fraction of the charges and dipole orientation is frozen in place. After removing the electric field, the sample is short-circuited at low temperature to allow any residual surface charges to dissipate. Finally, the sample is reheated at a constant rate, and the resulting depolarisation current is measured. [74], [75]

Although the TSDC process itself is relatively simple, a moderate number of parameters can be adjusted. These include the poling voltage, temperature, time, as well as the cooling temperature and rate, all of which influence the outcome of the measurements. [26] As noted, the TSC method can be performed under various voltage and temperature conditions, which enables distinguishing between two techniques: TSDC and Thermally Stimulated Polarisation Current (TSPC). To obtain a comprehensive understanding of the dielectric properties of materials, multiple complementary tests, such as represented here, should be used in combination, with systematic variation of their parameters. [74]

The following Figure 36 illustrates the principle of the TSDC measurement, showing the progress of temperature and electric field over time during the measurement.

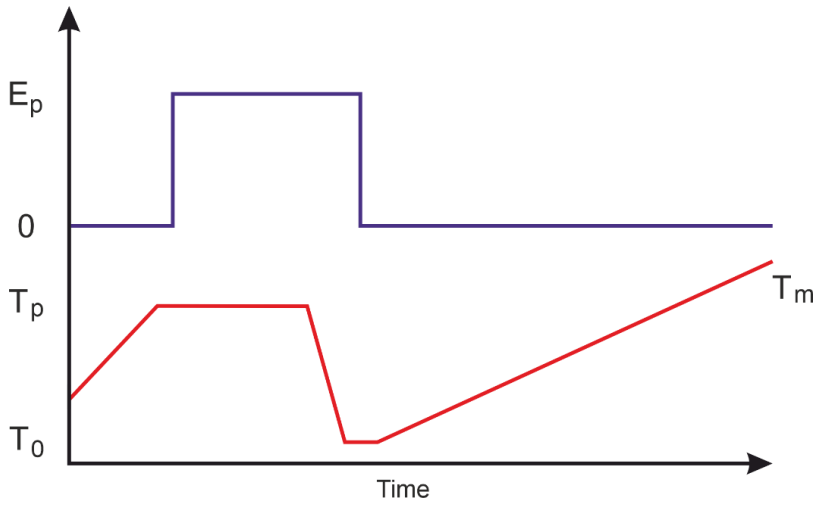

Figure 36. *Principle of the TSDC method, illustrating its phases, heating the sample, poling, rapid cooling, short-circuiting, and linear heating with depolarisation current measurement.*

The TSDC method enables the analysis of phenomena related to charge accumulation and transport in dielectric materials [76]. From the measurement results, such as peak temperature T_m and peak current density J_m, various charge-related mechanisms can be distinguished, including dipole relaxation, trapped charge release, and space charge relaxation. In addition, other parameters can be calculated from the measurement, such as activation energy E_a and defect concentration. [77]

The TSDC measurement system used in this thesis consisted of a liquid N_2 based temperature control system with an accuracy of ±0.1 °C (Novocontrol Novocool), a high voltage DC source (Keithley 2290E-5) and an electrometer (Keithley 6517B). A shielded sample cell equipped with a PT100 temperature sensor (Novocontrol BDS1200 HV sample cell) and shielded cables were used. A diode-based overload protection circuit and a 100 kΩ series resistor were utilised to protect the electrometer in case of a sample breakdown during high voltage application. All TSDC measurements reported in this thesis were performed under short-circuit (SC) conditions. The TSDC measurement procedure was as follows:

1. Sample is heated to polarisation temperature T_p (70-90°C) and held under isothermal conditions for 5 minutes.
2. DC poling field E_p (15-30 V/µm) is applied for time t_p (30-120 min).
3. Temperature is rapidly decreased to T_0 (-50°C) and maintained for 5 min (voltage on).
4. Voltage is removed; sample is short-circuited and held under isothermal conditions for 3 min.
5. Sample is heated at a linear rate of β (3.0°C/min) up to T_{max} (145 °C) while recording the depolarisation current.

Measurement circuit during different phases of the measurement in Figure 37 a) and b) and sample configuration utilised for the TSDC measurements is shown schematically in Figure 37 c). A conductive Ag-filled fluorosilicone rubber electrode, Au bulk electrode and a metal spring ring was

used on the upper side of the metallised sample film to soften the contact and to distribute the pressure applied to the sample uniformly. The bottom metallised surface of the sample was also contacted with an Au bulk electrode.

The samples used in the measurements were prepared in a cleanroom using a metallizing device (Metallointi Mattila) by evaporating 100 nm of gold on both sides of the sample. The samples were then placed short-circuited into a vacuum oven at 50 °C for at least 24 hours before testing to ensure that the initial charge level in the sample would be as low as possible. Before the actual TSDC measurement, the complex permittivity and loss factor of the sample were measured using a Novocontrol Alpha-A High Performance Frequency Analyser to verify proper alignment and reliable contact in the measurement holder. After confirmation, the actual TSDC measurement was carried out according to the protocol described above.

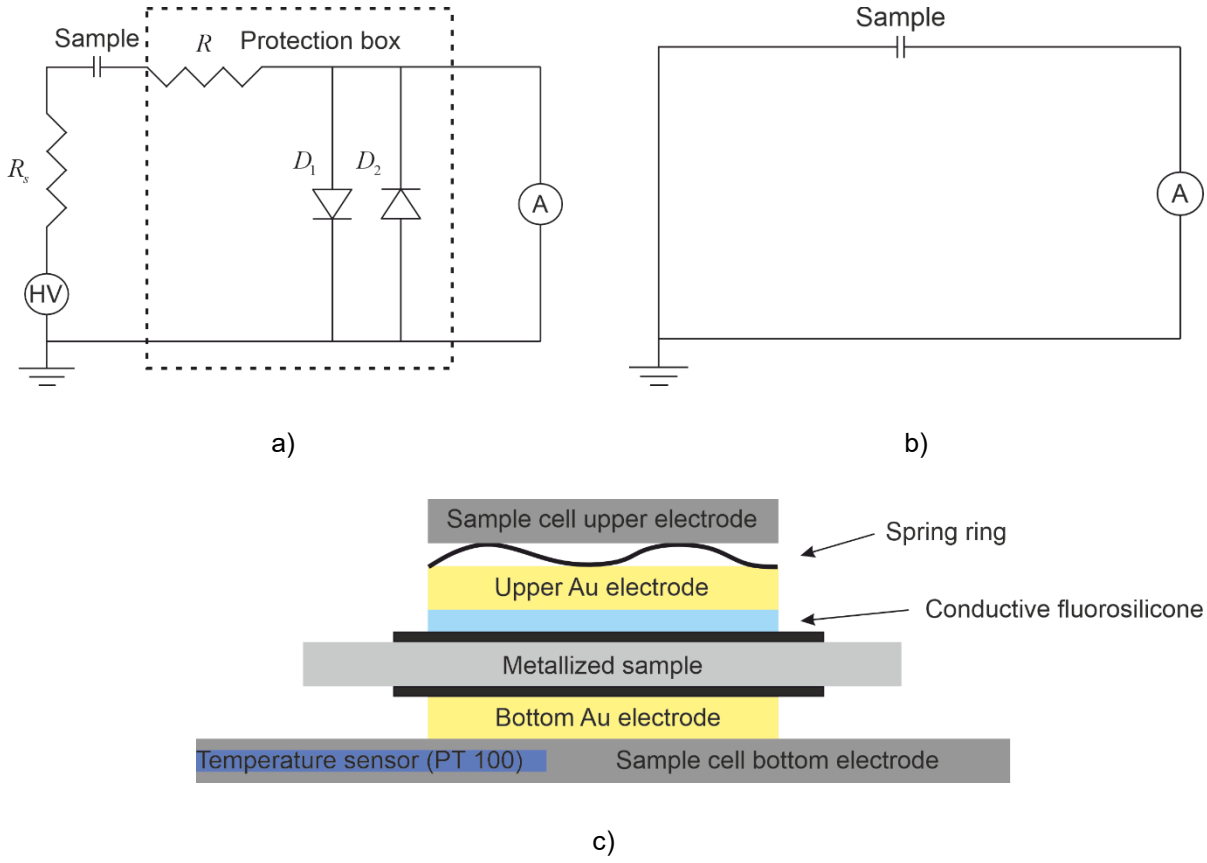

Figure 37. *Schematic diagrams of the TSDC measurement setup a) when sample is poled, b) when sample is short circuited and c) sample configuration in sample cell.*

As previously described, thermally stimulated depolarisation current (TSDC) measurements can be performed not only in the conventional short-circuit (SC) configuration but also in the open-circuit (OC) mode. In the open-circuit method, the sample is typically metallised only on one side, which is connected to the electrode, while the opposite side remains unmetallised and is separated from the counter-electrode by an air gap as represented in Figure 38 a). Alternative implementations include the use of a thin insulating spacer between the sample and one electrode, or a setup identical to

short-circuit measurements but with an additional series capacitor in the circuit as represented in Figure 38 b). Regardless of the configuration, the underlying principle remains the same, trapped charges in the dielectric are released during linear heating, resulting in a current–temperature spectrum that reflects the trapping and release processes. [78], [79]

The difference between SC and OC measurements arises from the way released charges interact with the electrodes. In the SC configuration, both surfaces of the dielectric are in direct contact with electrodes, which allows charges of opposite polarity to flow in the circuit simultaneously. These bidirectional charge flows can partially cancel each other, thereby obscuring part of the information carried by the discharge current. [80] Moreover, charges accumulated at the dielectric surface may recombine directly with the image charges on the adjacent electrode, and thus their contribution may be lost in SC method [78]. In contrast, in the OC method the unmetallised surface and air gap act as a blocking layer. The charges released in the dielectric cannot recombine immediately with electrode charges but instead induce image charges across the gap, which appear as a measurable current in the external circuit. In this way, both bulk space charges and surface charges can be detected, giving the OC method a broader sensitivity than the SC method. [80]

The main advantage of the OC method is its ability to reveal information that may be suppressed in SC measurements. OC thermograms often show a clearer coexistence of homocharge and heterocharge. These effects are easier to interpret in OC mode, since recombination losses present in SC measurements are avoided. [78], [79] The OC method, however, also has drawbacks. Bulk and surface contributions are superimposed in the external circuit and thus cannot be easily distinguished [80]. Several modifications have been proposed to improve the performance of the OC method compared air gap configuration. The use of spacers between unmetallised and electrode, series capacitor [81] and glass assisted TSDC technique [80]. These enhancements have been proposed to create more reliable blocking than just an air gap.

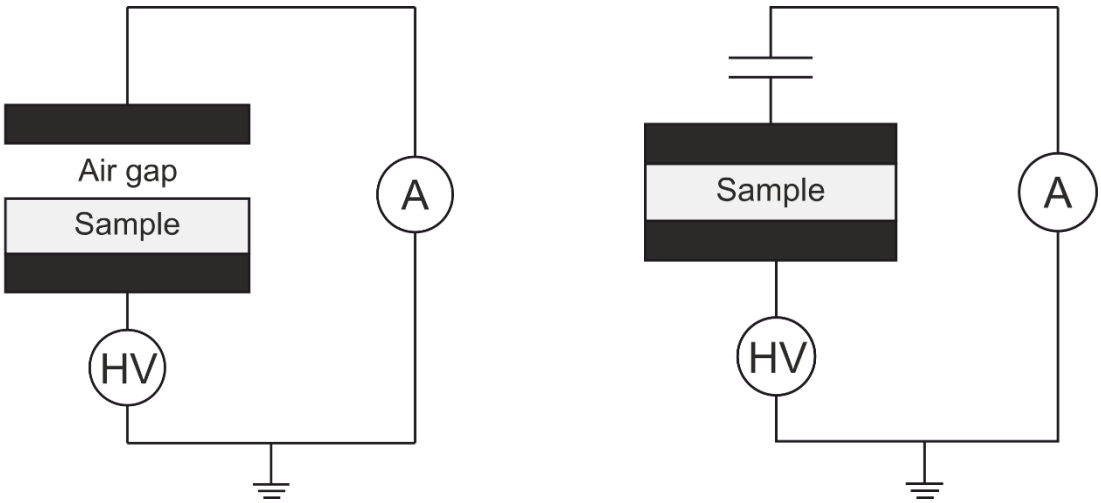

a) b)

Figure 38. *Representation of air gap (open-circuit) TSDC measurement circuit a) where spacers could be also used in air gap and alternative option where capacitor is used as an air gap in b).*

In the *TSPC* measurement, both preheating and poling of the sample are omitted compared to TSDC. The measurement begins by cooling the sample to a low temperature, applying a DC voltage, and then heating the sample at a constant linear rate while recording the resulting current. The measured current consists of conduction current, and a polarisation current arising from the progressive alignment of dipoles as their thermal relaxation times decrease with increasing temperature. If the material contains permanent or induced dipoles that can reorient within the temperature range of the measurement, their alignment with the applied field produces peaks in the TSPC spectrum. The temperature at which each peak occurs is related to the activation energy of the corresponding relaxation process, and the peak magnitude typically increases with the applied field strength. [82], [83]

At higher temperatures, the measured current often exhibits a monotonic increase that no longer originates from dipolar polarisation but from thermally activated electrical conduction. As the temperature rises, an ohmic conduction current starts to dominate the TSPC spectrum. [84] The onset temperature of this conduction driven rise depends on the material's structure, chemical composition, and potential additives. [79], [80]

6 RESULTS AND DISCUSSION

The objective of this thesis was to investigate charge transport and trapping phenomena in polymeric insulations under high electric field strengths using TSDC method. A total of six different materials were studied, and by varying measurement parameters, the aim was to identify characteristics of the samples, to compare and analyse how the ratios of polymer components and the presence of additives and its amount affect the measurement results. The measurements were designed to address three main objectives.

First, the repeatability of TSDC measurements was examined by testing five identical samples under the same measurement conditions. Second, the effect of poling time on space charge behaviour was investigated by using six samples of same material with different poling durations. Third, the influence of sample thickness on the measurement results was analysed by comparing three different sample pairs. In addition to these primary objectives, the study also provided insights into the influence of additives on space charge formation, comparison of PEA and TSDC measurement results on net charge accumulation and factors effecting glass transition behaviour.

6.1 Studied materials, their composition and components

The polypropylene blends investigated in this thesis consisted primarily of three base components mixed in different proportions. The three components were: homophasic PP random copolymer (RACO), heterophasic PP copolymer (HECO), and propylene-based elastomer (PBE). All blends contained total of 0.30 wt-% antioxidants (AO1) in a 1:1 ratio (a hindered phenolic antioxidant, Irganox® 1010, and a phosphite processing antioxidant, Irgafos® 168), and some blends also included the additive polypropylene grafted maleic anhydride (PP-g-MAH or Add) at either 1.0 or 2.5 wt-%. The compositions of the samples used in this thesis, including polypropylene ratios and additives, are presented in Table 1. Blends consisting of RACO/HECO/PBE are referred to as ternary blends, whereas blends composed of RACO/HECO are referred to as binary blends.

Table 1. *Measured samples, their polymer component ratios and additive contents.*

Material	Polymer component ratio			PP-R composition		
	RACO	HECO	PBE	Polymer [wt-%]	AO1 [wt-%]	Add [wt-%]
Blend-1	0.55	0.20	0.25	99.70	0.30	
Blend-2	0.55	0.20	0.25	98.70	0.30	1.00
Blend-3	0.55	0.20	0.25	97.20	0.30	2.50
Blend-4	0.70	0.30		99.70	0.30	
Blend-5	0.70	0.30		98.70	0.30	1.00
PP cast film*				100		

** Commercial capacitor grade*

As reported in [85], the TSDC currents of the individual PP components RACO, HECO, and PBE were measured and are represented in Figure 39 with Blend-1 studied in this thesis. RACO exhibits very low TSDC current, HECO shows peaks at +60 °C and +95 °C whereas PBE displays a broad peak ranging from +30 to +85 °C and a smaller peak at +135 °C. According to [85] relaxation peaks of the individual components are observed in the blends, and that variations in peak intensities are assumed to result from the proportions of the components in the final blend. In the spectrum of Blend-1 in Figure 39, the characteristic peaks of both HECO and PBE can be identified. Since Blend-1 is consisting of 55 % RACO, 20 % HECO, and 25 % PBE of the total polypropylene blend fraction. As expected, the current profile of Blend-1 lies in between of the individual components, reflecting the contribution of each polymer fraction to the measured TSDC current.

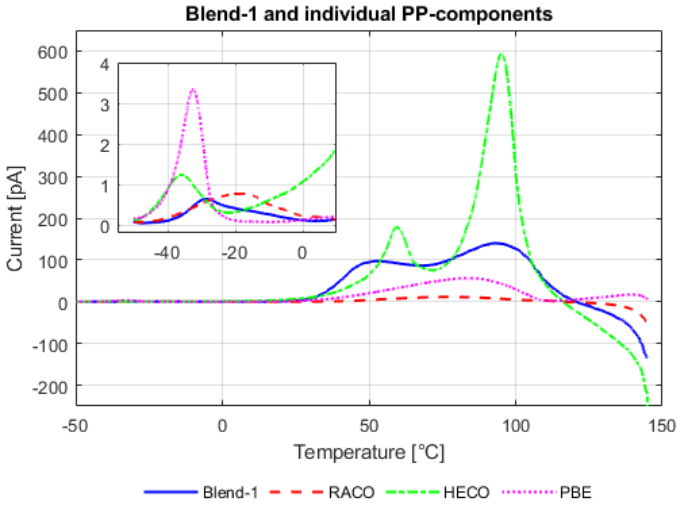

Figure 39. *Individual PP components (RACO, HECO, PBE) and their TSDC measurement results [85] and as a comparison Blend-1 shown to illustrate how the constituents contribute to the overall TSDC response. Measurements parameters used* $T_p = 90\,°C$, $t_p = 40\,min$, $T_0 = -50\,°C$, $V_p = 15\,V/\mu m$ *and* $T_{max} = 145\,°C$.

6.2 General observation in the TSDC measurements

Figure 40 a) and b) presents the TSDC measurement results of all blends investigated in this thesis, and it can be observed that they exhibit an α-relaxation peak in the temperature range of approximately -30 to 5 °C, as well as a varying number of ρ-relaxation peaks caused by deep traps, starting from around +35 °C depending on the blend and extending up to the maximum measurement temperature of +145 °C. As previously discussed in section 3.5.3, α-relaxation is caused by the increase in molecular segment mobility at the glass transition temperature T_g [10], [86]. Since polypropylene is non-polar and does not contain a significant number of permanent dipoles, the ρ-peaks observed at higher temperatures are primarily attributed to thermally activated release of trapped charges [87]. In [88], these deep traps are proposed to result from additives such as

antioxidants and chemical impurities introduced into the insulation material. Space charge can also accumulate at the interfaces between crystalline and amorphous regions in semi-crystalline polymers [73]. Not all peaks can be observed due to the melting temperature of the material.

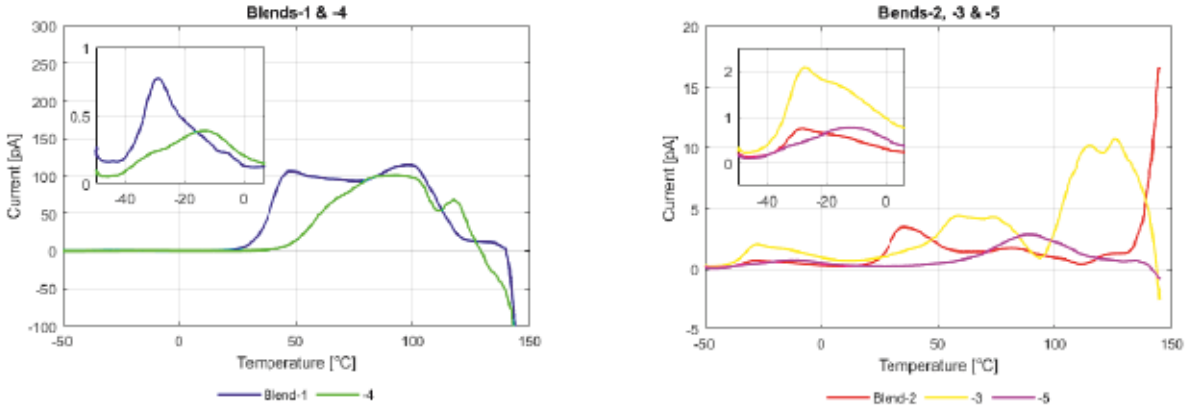

a) b)

Figure 40. *Different blends measured in this thesis and the representation of α- and ρ-relaxation peaks observed in the measurements. Blend-1 and -4 separated from -2, -3 and -5 because of their different current intensity scales.*

6.3 Repeatability

Due to the long duration of each TSDC measurement, typically only one measurement per sample is performed in the NEWGEN project to ensure the feasibility of completing the measurements within a reasonable timeframe. Therefore, it is important to assess the reliability of the measurements and how potential differences between the samples would appear in the results. To evaluate repeatability, five parallel TSDC measurements were performed using Blend-1. The measurement protocol applied to each sample was as follows: (i) sample was poled in DC-field $E_p = 15\ V/\mu m$ for 40 minutes in isothermic conditions $T_p = 90\ °C$. (ii) Sample was cooled rapidly to $T_0 = -50\ °C$ and held there for five minutes. (iii) The poling voltage was removed, and the sample was short-circuited through the electrometer used for measuring current, maintaining isothermal conditions for 3 minutes. (iv) Finally, the sample was heated at a linear rate of $\beta = 3.0\ °C/min$ up to a maximum temperature of $T_{max} = 140\ °C$ while continuously recording the depolarisation current.

The measurement results in Figure 41 demonstrate that the α-relaxation, associated with the glass transition, occurs at the same temperature and with comparable intensity in all five samples. In contrast, the ρ-peaks related to space charge effects show greater variability. Three samples (1, 3, and 4) exhibit nearly identical behaviour. In sample 2, the current between the ρ-peaks does not decrease as in the others but instead forms a broader peak spanning a wider temperature range. In sample 5, the ρ-peaks occur within the same temperature range as in the other samples, but their

peak intensity is in the higher temperature range. In addition, all samples display negative current towards the end of the measurement, before the end of the measurement is reached.

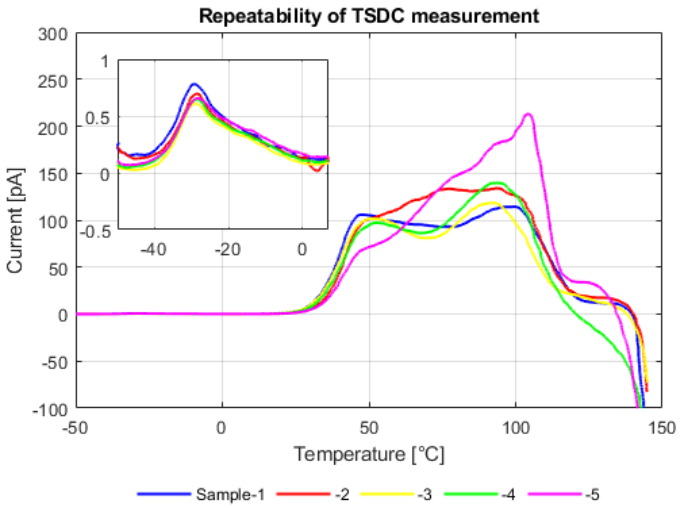

Figure 41. *Repeatability measurement for five identical samples with measurement parameters* $T_p = 90\,°C$, $t_p = 40\,min$, $T_0 = -50\,°C$, $V_p = 15\,V/\mu m$ *and* $T_{max} = 145\,°C$.

The measurements revealed that the intensity and temperature of charge release from shallow traps in the amorphous regions at the glass transition temperature were similar across all samples. This was expected, as the proportion of PP-components was the same in each sample. However, the ρ-relaxation peaks of sample 5 showed slightly different behaviour compared to other samples. In Figure 42 that shows charging currents, sample 5 also stood out due to its higher charging current, which may indicate a higher accumulation of space charge, as also observed in the TSDC measurements. Nevertheless, charging current alone cannot directly predict the behaviour of the depolarisation current in TSDC measurements, as part of the current is not recorded during the short-circuit phase. Overall, although sample 5 deviates slightly from the other samples, its ρ-peaks still occur within the same temperature range, and the anomalous current observed towards the end of the measurement also shows values similar to the other samples. Thus, the general trends remain consistent across all five samples.

All samples exhibited a negative current towards the end of the measurement. In [89], such anomalous TSDC currents are explained by the partial return of injected charges to the electrode during heating. Since dipolar processes cannot reverse the current direction, the phenomenon must be related to injected charges [90]. If the returning charge current exceeds the electrode's ability to absorb the charges, a charge barrier may form at the interface. In this case, opposite-polarity charges can still move, causing a net current away from the injecting electrode and resulting in the observed anomalous TSDC signal. [89]

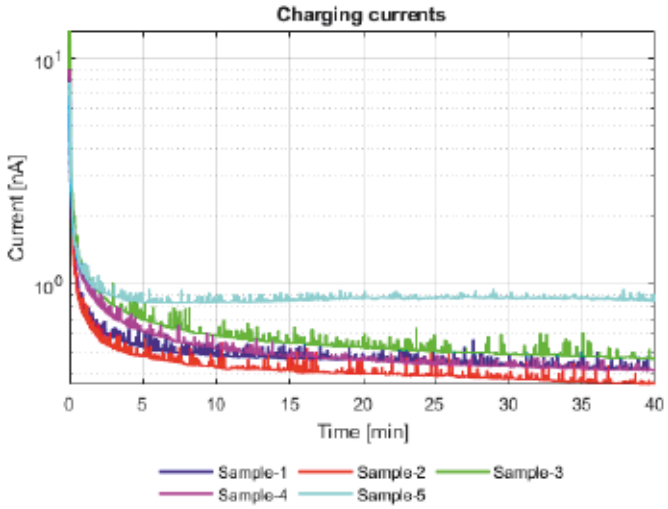

Figure 42. *Charging current measured in TSDC measurement from the moment the voltage is switched on until the temperature is changed from 90 °C to –50 °C.*

Figure 43 shows measurement results for ternary Blend-1, -2, and -3 under a DC electric field of $E = 30\ V/\mu m$ at temperature of $T = 70\ °C$, using the same measurement protocol as described earlier in this chapter. In these blends, the ratio of the PP-components is the same, while the only variable is the concentration of the additive. Blend-1 contained 0 wt-% of PP-g-MAH, Blend-2 contained 1.0 wt-%, and Blend-3 contained 2.5 wt-%.

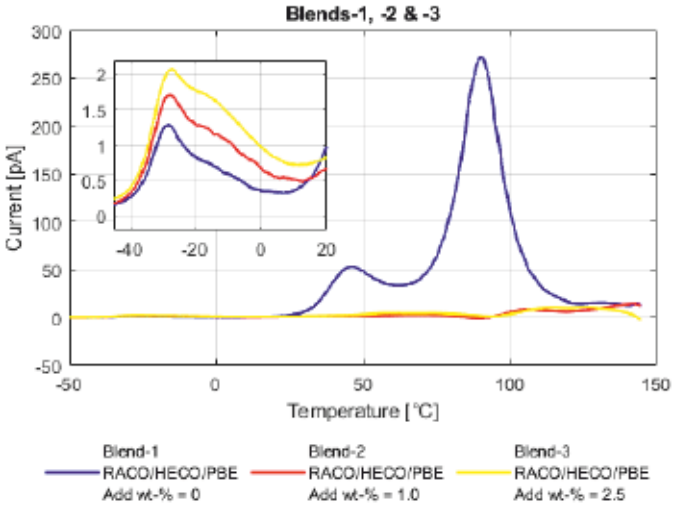

Figure 43. *TSDC measurements for Blend-1, -2 and -3. Measurement parameters* $T_p = 90\ °C, t_p = 40\ min$, $T_0 = -50\ °C$, $V_p = 15\ V/\mu m$ *and* $T_{max} = 145\ °C$.

Figure 43 shows that the addition of the additive (PP-g-MAH) in Blend-2 and -3 leads to a clear reduction in total accumulated charge, while higher additive concentrations also increase the current at the glass transition temperature. Similar behaviour is observed for Blend-4 and -5, where the only

difference is the additive content. These findings indicate that the variations seen in repeatability measurements shown in Figure 41 are minor and do not affect the overall conclusion. TSDC method provides sufficient resolution to identify the influence of additives and to support the NEWGEN project in screening suitable insulation material candidates.

6.4 Effects of poling time variation

The effect of poling time on the TSDC measurement was investigated using six identical ternary Blend-2 (RACO/HECO/PBE) 1.0 wt-% of PP-*g*-MAH samples, each subjected to a different poling duration: 30, 40, 50, 60, 90 and 120 minutes. The measurement results are shown in Figure 44. At the glass transition temperature, a current peak appears at approximately –28 °C, with nearly identical intensity across all samples irrespective of the poling time. Additionally, all samples exhibit a second peak in the temperature range of +33 to +36 °C. At this peak, the 30-, 40-, and 60-minute samples exhibit similar intensities, whereas the 50-, 90-, and 120-minute samples show slightly higher values, with the 120-minute sample being the highest. At higher temperatures, around +80 °C, +115 to +120 °C and at the end of the measurement there are additional peaks. The last peak cannot be observed completely before the measurement ends. In the temperature range of +115 to +120 °C, three samples, 30, 40, and 50 min, exhibit similar behaviour. However, with longer poling times of 60, 90, and 120 minutes, the samples display an increasing trend in current intensity in ascending order. Based on these results, it can be concluded that at around 60 minutes of poling, and for longer durations, the deeper traps are revealed more effectively than at shorter times.

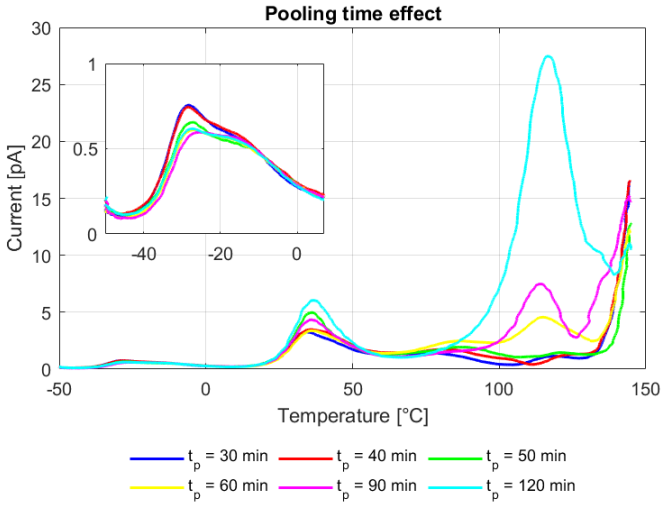

Figure 44. *The effect of variable poling time on TSDC measurement. Poling times* $t_p = 30, 40, 50, 60\ 90$ *and* 120 *minutes.*

Tzimas et al. [91] investigated the effect of DC poling time on the space charge behaviour of XLPE samples by comparing poling durations of 2 and 26 hours. The results showed that a longer poling

time led to the formation of heterocharge, while samples poled for a shorter duration of 2 hours exhibited mainly homocharge. With increased poling time, charges had more time not only to migrate deeper into the material but also to become trapped in deeper energy levels. No significant difference in total charge was observed, rather the charges had shifted into deeper traps. Similarly, Mudarra et al. [86] studied the effect of poling parameters on TSDC measurement results and found, in line with [91], that longer poling times increased the trap depth in PMMA samples. They also observed that the total accumulated charge in the sample increased as a function of poling time until it reached a saturation point. This saturation of charge accumulation was explained by the fact that the shifted charges reduce the potential barrier of traps, which facilitates the release of charges from the traps.

By examining Figure 44, it shows that in the present measurements the current also increases in the shallow trap region at around +35 °C. However, this observation is not fully conclusive, since the trend does not follow the exact order of poling times. The 30-, 40-, and 60-minute samples exhibit similar current intensities, whereas the 50-, 90-, and 120-minute samples show higher values, although not in that order. Among these, the 120-minute sample displays the highest current intensity, followed by the 50-minute and 90-minute samples.

Figure 45 presents the charge accumulated per unit volume during the TSDC measurement. Up to approximately +80 °C, the samples show very similar charge accumulation. Beyond this temperature, differences start to appear, becoming pronounced in the samples poled for 60 minutes or longer. Among these, the samples poled for 60 to 120 minutes exhibit the highest net charge, as summarised in Table 2, while the samples poled for 30-, 40-, and 50-minutes show nearly identical net charge values.

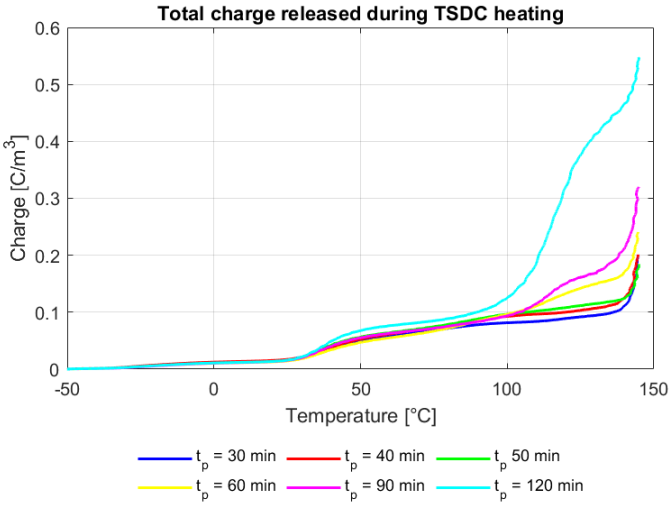

Figure 45. *Total charge accumulation of the test samples poled for 30-, 40- and 50 minutes.*

The effects of poling time observed in the measurements are largely consistent with the results presented by Tzimas et al. [91] and Mudarra et al. [86]. A longer poling time of 60 to 120 minutes was found to increase the amount of charge stored in deep traps compared to shorter poling times. The differences in net charge accumulation between the 30-, 40-, and 50-minute samples were basically non-existing. Increased net charge accumulation observed from 60-minute and above samples differ from the findings of Mudarra et al. [86], in which the total charge appeared to reach a saturation point. This discrepancy may be explained by the longer poling durations used in their study, where saturation had already occurred, whereas the shorter poling times used in this thesis and results indicates saturation threshold is not yet reached. It is worth noting from the net charge accumulation shown in Table 2 that the net charge only begins to increase once the poling time reaches 60 minutes.

Table 2. *Table 1 Influence of poling time on net charge accumulation in Blend-2*

Material	**Poling time [min]**	**Net charge [C/m^3]**
Blend-2 RACO/HECO/PBE Add [wt-%] = 1.0	30	0.20
	40	0.20
	50	0.18
	60	0.24
	90	0.32
	120	0.55

The results obtained in these measurements demonstrate that poling time has an influence on the trapping of charges. From the perspective of the NEWGEN project, this finding is relevant because it shows that the experimental conditions affect the interpretation of charge storage and transport

mechanisms. Shorter poling times provide limited additional information, as the net charge accumulation remains essentially unchanged. In contrast, longer poling times enable the activation of deeper traps and therefore give access to information that reveals a trap distribution that more realistically represents the effects arising from long-term operation.

TSDC provides valuable insight into trapping phenomena and their dependence on poling time, but it represents only one aspect of the overall dielectric characterisation. In the selection of materials for further investigation within the NEWGEN project, the decision is not made based solely on TSDC results. Other critical properties are also considered, such as breakdown strength, mechanical performance, accelerated aging tests, and charge dynamics obtained from PEA measurements. To confirm whether the observed influence of poling time is specific to Blend-2 or a more general phenomenon, similar tests should be conducted on other candidate materials. In practice, characteristic TSDC peaks of a given material can already be observed with shorter poling times. However, extending the poling time provides a more detailed picture of the filling of deeper traps and offers insight that is more representative of real service conditions.

6.5 Effect of variable sample thickness

One of the main objectives of the measurements was to analyse the effect of sample thickness on the results obtained from TSDC measurements. This was achieved by comparing 100 µm and 200 µm ternary Blend-1 samples (RACO/HECO/PBE) to each other, as well as binary Blend-4 and -5 (RACO/HECO), the latter which contains additive, with the same thickness levels. An exception to the measurement protocol described in the repeatability section was the applied poling field strength, which was set to $E_p = 20\,V/\mu m$. At the glass transition temperature, shown in Figure 46 a), both samples exhibit similar behaviour in terms of peak temperature. However, in the 100 µm thick sample, the current peaks observed in the temperature range of +45 to +110 °C are more intense than those in the thicker 200 µm sample. At the end of the measurement, a noticeable rise in current is observed in the thicker sample, whereas no such effect is seen in the thinner one.

In Figures 46 b) and c), for binary Blend-4 and -5, the current intensity at the glass transition temperature is at the same level, but the peak temperature shifts slightly higher. For both blends, the ρ-peaks caused by space charges behave similarly, their intensities are lower, and they appear at slightly higher temperatures in the thicker samples.

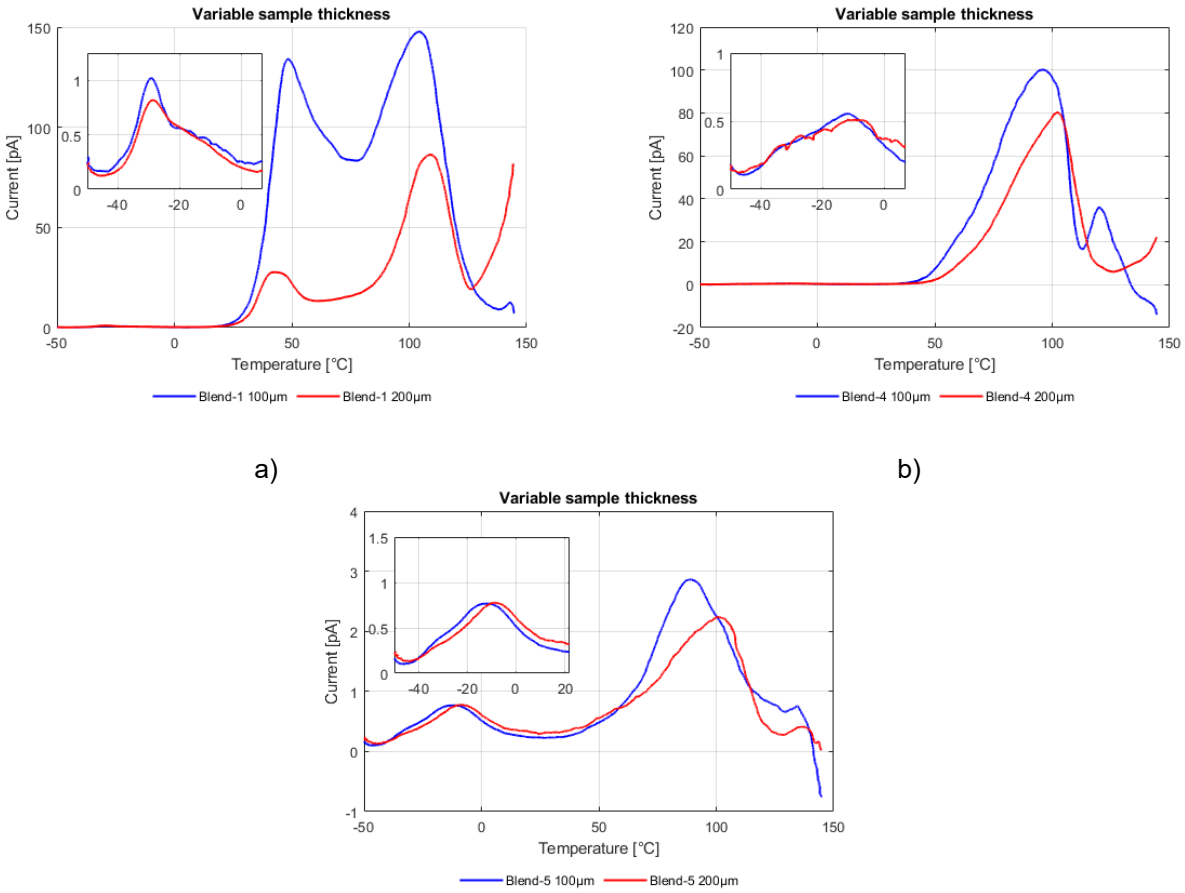

Figure 46. *TSDC measurement for ternary Blend-1 (55 % RACO, 20 % HECO, and 25 % PBE) and binary Blend-4 and -5 (70 wt-% RACO and 30 wt-% HECO of the total polypropylene blend fraction) with sample thicknesses of 100 and 200 µm compared to each other.*

The results show that for Blend-1, the sample thickness does not appear to significantly affect the depth of the traps, although the trap intensity is clearly lower in the thicker sample. The measurements for Blend-4 and -5 behave very similarly, which is expected given that the PP component ratios are the same in both, with only Blend-5 containing an additional 1.0 wt-% of the additive PP-g-MAH. In Figure 46 a), compared to b) and c), the notable difference is that no delay in the ρ-peaks is observed in a), whereas in b) and c), a delay in charge release and lower intensity are evident.

The delay in space charge release seen in Figure 46 b) and c) can potentially be explained by the transit time dependence on thickness, given by $\tau_c = d^2 / \mu V$ where d is the sample thickness, μ the mobility, and V the applied voltage. Furthermore, the observed delay in the relaxation peaks for thicker samples may be related to their slower temperature rise compared to thinner ones. As a result, the release of trapped charges occurs slightly later. Interestingly, no such delay is observed between the different thicknesses of the Blend-1 samples, which consist of 55 % RACO, 20 % HECO, and 25 % PBE in contrasts with Blend-4 and -5, which are composed of 70 % RACO and 30

% HECO. The most significant difference between the blends is the absence of the PBE component in Blend-4 and -5, which may contribute to the observed behaviour.

The thickness dependence of space charge accumulation can also be interpreted in terms of recombination distance. The thicker the sample, the more likely that mobile charges will be trapped or recombine with oppositely charged carriers before reaching the opposite electrode. Deep traps influence charge accumulation in two ways; they slow down charge transport and act as efficient recombination centres. If there are only a few deep traps or the sample is thin enough, injected charges can traverse the sample and form significant heterocharge. In contrast, in thicker samples or materials with a high density of deep traps, a large portion of the charges will recombine, reducing the heterocharge or even inverting it into homocharge. [92], [93] The results obtained from the measurements support this behaviour, where recombination is more effective in thicker samples compared to thinner ones.

6.6 Effect of additive content on charge accumulation

One of the objectives of the NEWGEN project is to develop additives that improve the space charge behaviour of PP and XLPE based HVDC cable insulation materials [4]. The following section examines the effects of the additive observed in the measurements, with particular emphasis on how it influences space charge accumulation in the insulation material.

Figure 47 a), b), c) and d) compare how the added additive affects charge accumulation during the TSDC measurements. In Figure 47 a), Blend-4 and -5 are compared, both have the same PP component ratio, but Blend-5 contains an additional 1.0 wt-% of the additive PP-g-MAH. Both samples have a thickness of 100 µm. These samples were poled at a field strength of $20\,V/\mu m$ for 40 minutes. Figure 47 b) shows the same Blend-4 and -5 with a sample thickness of 200 µm and a poling field of $15\,V/\mu m$. In Figure 47 c), Blend-1 and -2 are compared, with Blend-2 containing an additional 1.0 wt-% of the additive PP-g-MAH compared to Blend-1. Samples were also poled at $15\,V/\mu m$. Figure 47 d) compares the ternary Blend-2 and -3, which differ only in additive content, 1.0 wt-% in Blend-2 and 2.5 wt-% in Blend-3.

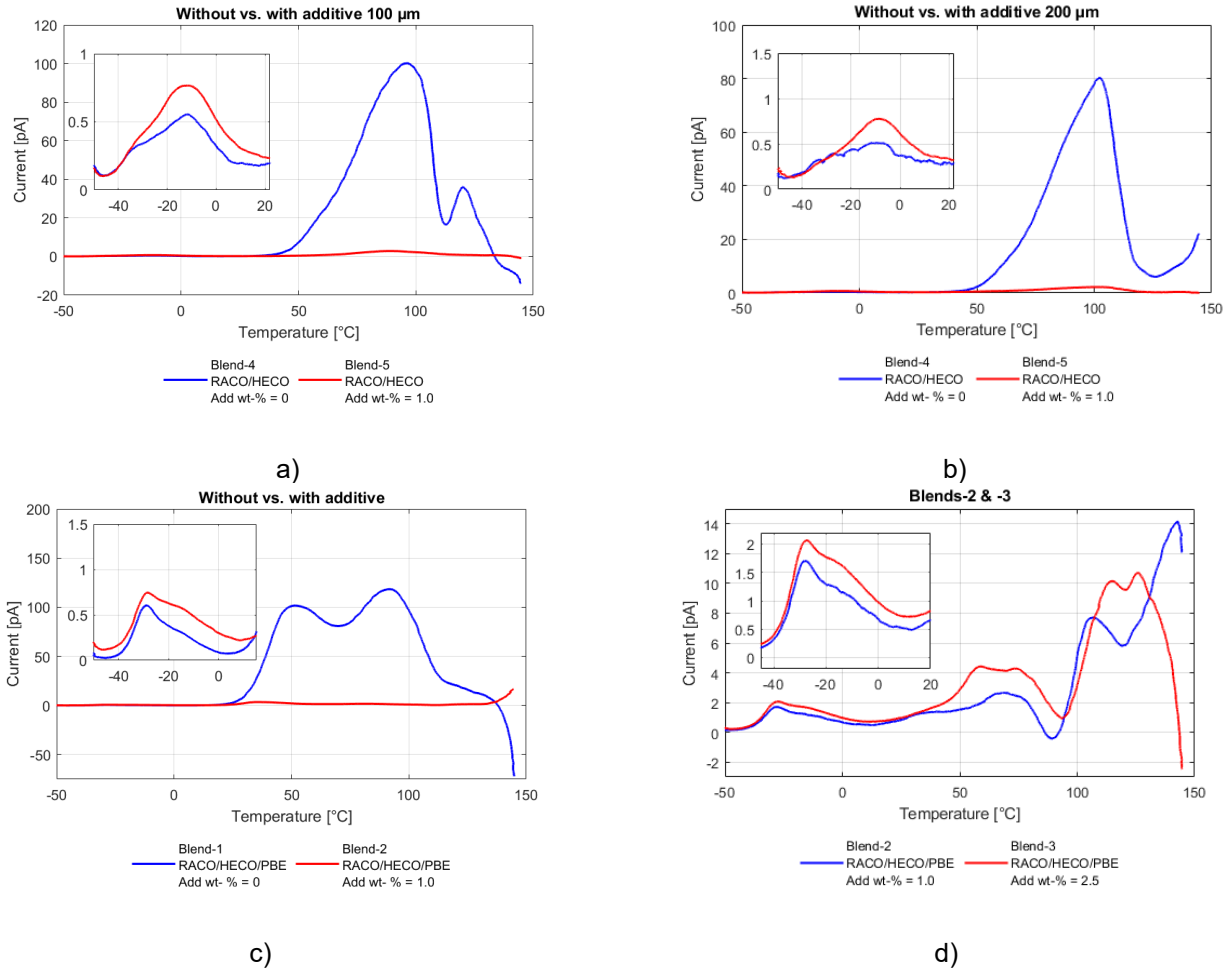

Figure 47. *Impact of additive on the TSDC currents. In a) and b) Blend-4 and -5 with thicknesses of 100 and 200 µm, c) Blend-1 and -2 and d) Blend-2 and -3 are compared.*

Two consistent trends were observed. First, as the additive content increased, the current peak at the glass transition temperature increased. Secondly, the total accumulated charge decreased markedly when 1.0 wt-% additive was introduced compared to the case without additive, regardless of the PP blend composition. Whether the blend consisted of RACO/HECO/PBE or RACO/HECO additive decreased the space charge accumulation. The reduction in space charge accumulation was also consistent across different material thicknesses and independent of the measurement parameters used. For Blend-2 and -3, the TSDC current behaviour followed the same overall trend. The most noticeable difference between Blend-2 and -3 appears toward the end of the measurement. When the net charges are compared later in Table 3, no significant differences are observed between the two samples.

6.7 Net charge comparison between TSDC and PEA measurements

The results of the TSDC measurements conducted in this thesis can be compared with the PEA measurements performed by the project partner University of Bologna in Italy. Some of the samples were measured with same poling parameters as in Bologna $Ep = 30\,kV/\mu m$ and $T_p = 70°C$,

enabling comparison of the observed trends. In addition, the field enhancement factor (FEF %), calculated for the Bologna samples, shows correlation with the net charge accumulation. The main difference in this specific comparison lies in the specimen thickness. The Bologna PEA measurements were conducted on 200 µm thick samples, whereas the TSDC measurements in this thesis were performed on 100 µm thick samples. Earlier results in this thesis already showed that thinner samples in TSDC measurements tend to exhibit higher current intensities compared to thicker samples under otherwise identical conditions.

A comparison of the net charge densities in Table 3 shows that the values obtained by TSDC are generally consistent with those measured by PEA. When comparing the binary (RACO/HECO) and ternary (RACO/HECO/PBE) blends without additive (PP-g-MAH), Blend-1 exhibits a higher net charge accumulation than Blend-4 in both measurements, although the difference is relatively small in the PEA results. Figure 48 a) – e) shows PEA measurement for Blend-1 to -5 and Figure 48 f) TSDC measurements for the same blends.

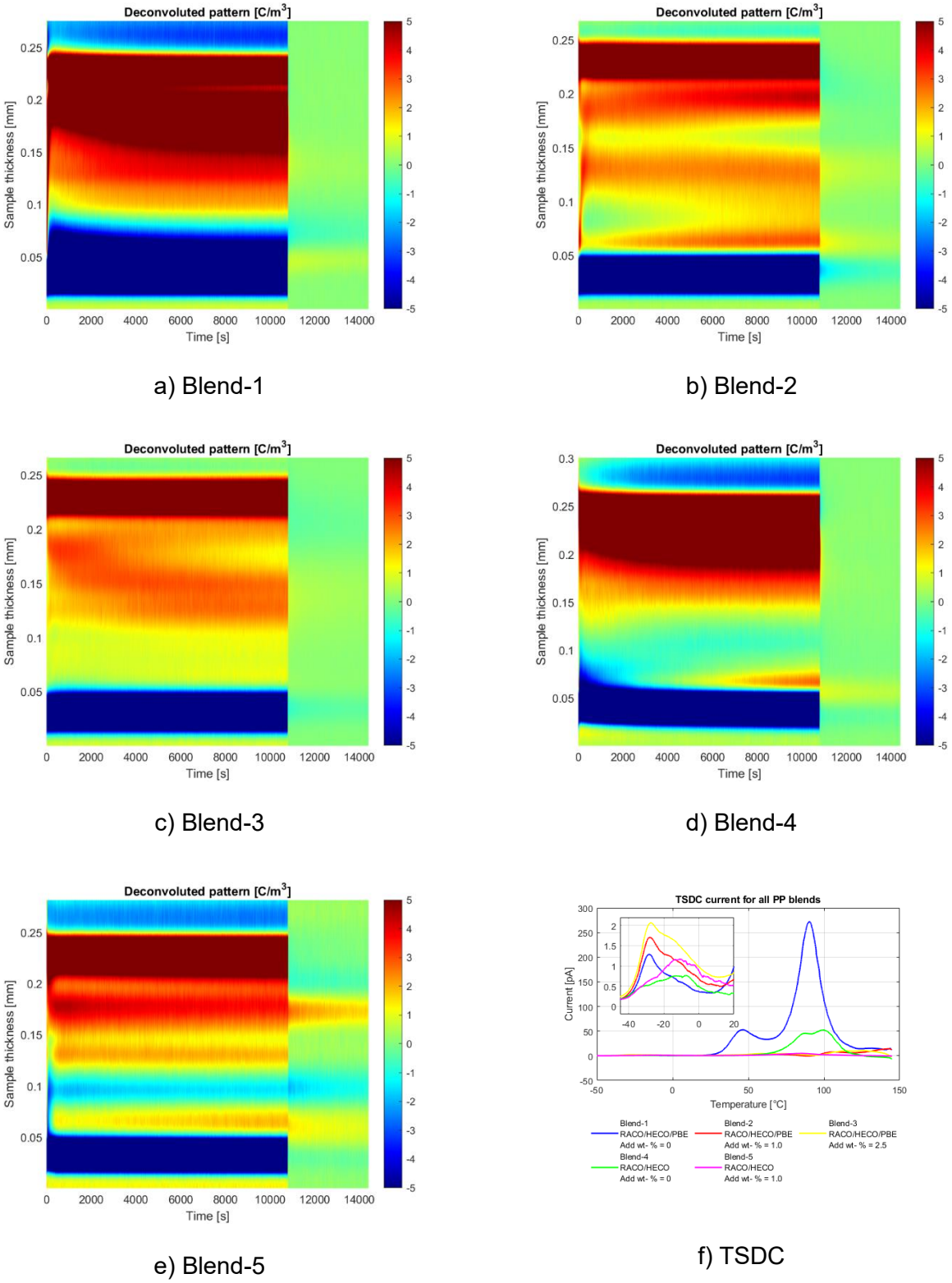

Figure 48. *Comparison of space charge distribution measured by PEA a) – e) for Blend-1 to –5 and corresponding TSDC current curves f).*

Both PEA and TSDC measurements demonstrate that the introduction of the additive PP-g-MAH reduces the net charge accumulation. In the PEA measurements, this trend is also visible between

Blend-2 and -3, which share the same PP components (RACO, HECO, PBE) but differ in additive content. The higher charge accumulation of Blend-1 and -4 is also visually observable from the results of the PEA measurements, when compared to their counterparts containing the same PP components and ratios but with the addition of the additive. Blend-2 contains 1.0 wt-% additive, while Blend-3 contains 2.5 wt-%. This kind of net charge decrease is not observed in TSDC measurements between Blend-2 and -3. Although the absolute values of net charges cannot be directly compared due to the differences between the two measurement techniques, both methods reveal similar trends.

Table 3. *Net charge accumulation of Blend-1 to -5 measured by PEA and TSDC.*

Material	PP-components	Add [wt-%]	FEF %	Net charge PEA [C/m^3]	Net charge TSDC [C/m^3]
Blend-1	RACO/HECO/PBE	0	15.80	1.62	4.03
Blend-2	RACO/HECO/PBE	1.0	6.67	0.86	0.35
Blend-3	RACO/HECO/PBE	2.5	3.00	0.46	0.32
Blend-4	RACO/HECO	0	12.67	1.58	0.79
Blend-5	RACO/HECO	1.0	5.30	0.85	0.12

TSDC measurements yielded lower net charge accumulations for Blend-2 to -5 compared to their PEA counterparts, apart from Blend-1, which showed a higher value in TSDC. Moreover, whereas the PEA results indicated a higher net charge in Blend-2 compared to Blend-3, the TSDC results suggested nearly identical net charge levels for Blend-2 and -3. Another important distinction is the difference in poling protocols, in PEA, the samples were subjected to a longer poling time (3 hours), and the charge accumulation was evaluated at that time, whereas in TSDC the samples were poled for only 40 minutes, and the depolarisation current was monitored during heating. In addition, in TSDC the current during the initial direct short-circuit phase is not captured, which further deviates the results from the methods. This deviation highlights differences in the two methods, but overall, the measurements support the same general conclusion, the incorporation of additive systematically reduces space charge accumulation in PP blends measured compared to ones that doesn't have the additive.

6.8 Glass transition temperature

The glass transition temperatures of Blend-1 to -5, as well as PP cast films, shown in Figure 49, differ from each other. The α-relaxation peak of PP cast films appears at approximately +5 °C, while for binary Blend-4 and -5 the corresponding peak is around −9 °C, and for ternary Blend-1, -2 and -3 it is nearly −30 °C. The essential distinction is that Blend-1, -2 and -3 are ternary blend, whereas Blend-4 and -5 are binary blend, without PBE. Additionally, the only difference between Blend-4 and -5 is the concentration of PP-g-MAH, Blend-4 contains none, while Blend-5 includes 1.0 wt-%. The

highest current peak values are observed for Blend-3, and the lowest for Blend-4 and the PP cast film.

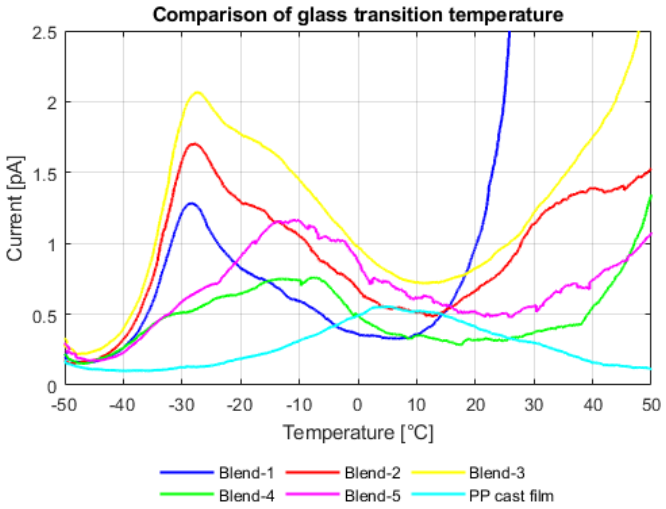

Figure 49. *Comparison of current–temperature curves spectrums for different polypropylene blends and a reference PP cast film, illustrating the glass transition region.*

When comparing the current peak intensities, a consistent trend emerges, blends with the same additive concentration but different PP component ratios show lower current peaks when the relative RACO content is higher and PBE is absent. For example, Blend-4 and -5, which are binary blends (RACO/HECO), exhibit smaller peaks compared to ternary blends with the same additive level, Blend-1 and -2. The highest peak is observed for Blend-3, where additive concentration is highest, while the lowest peaks are found in Blend-4 and the PP cast film. According to [4], adding the PBE component increases the amorphous phase of the material, while the RACO component has a high degree of crystallinity. Based on this, it is consistent that Blend-4 and -5 exhibit lower current intensity peaks compared to Blend-1 and -2. This can be attributed to the cooperative segmental molecular motion occurring in the amorphous region at the glass transition temperature. [10], [13]

When examining the glass transition temperatures of the PP based blends, it is observed that ternary blends exhibit the lowest T_g. This can be explained by the presence of the PBE component, which increases the amorphous content of the material. The observation aligns with [13], which states that the glass transition temperature depends on the structure of the polymer chain, affecting the rigidity of the molecular chains.

When comparing PP cast films with other tested materials, it is found to have the highest glass transition temperature. This observation is in agreement with the flexural modulus values reported in [94], as well as with the previously mentioned influence of chain stiffness. The study showed that blending PBE and HECO components with isotactic PP homopolymer decreased the flexural modulus values compared to pure isotactic PP, confirming the impact of increased flexibility.

6.9 Future work

The present measurements indicate that deeper traps begin to fill when the poling duration exceeds approximately 50 minutes in measurements where poling time was investigated. A natural continuation would be to examine whether similar behaviour is observed in other polypropylene blends, or whether the onset of deeper trap filling occurs at shorter or longer poling times depending on the material. This question is particularly important since the currently employed poling duration is 40 minutes, which may not be sufficient to activate deeper traps. Such comparisons would provide valuable insight into material-specific differences and help to identify blends that offer a more favourable or unfavourable trap distribution for long-term insulation performance.

Practical limitations of the measurement setup also need to be taken into account. If the filling of deep traps consistently requires significantly longer poling times than the 40 minutes currently used as an internal standard, measurement feasibility becomes restricted by the available working day. In such cases, alternative approaches such as optimised poling conditions could be explored to obtain reliable information on deep trap behaviour without excessively long test durations.

In addition to the planned investigations on poling time, it would also be valuable to complement the existing PEA measurements on the blends with open-circuit TSDC experiments. A particular focus could be placed on assessing whether the OC configuration is capable of providing comparable information on the coexistence of homocharge and heterocharge, which PEA measurements have already revealed. Since the high voltages required in these experiments prevent the use of an air gap due to the risk of breakdown, the series capacitor configuration presents a feasible alternative. By adopting such an approach, the reliability of the OC measurements could be improved, while at the same time enabling a more direct comparison with the results obtained from PEA.

7 CONCLUSIONS

The aim of this thesis was to study charge transport and trapping phenomena in polymer insulations using thermally stimulated depolarisation current measurements. Primary objectives of the measurements were to assess the repeatability of the TSDC method, to examine the influence of varying poling times, and to analyse the impact of sample thickness on the results. In addition, the measurements provided insights into the role of the additives and polypropylene blends and its effect on the glass transition temperature. These aspects were investigated by systematically varying the measurement parameters, including poling field, poling temperature, poling time, and sample thickness.

Parallel tests were carried out on five samples of a ternary blend (Blend-1) to confirm the applicability of the TSDC method. No differences were observed between the samples in the temperature at which the TSDC current appeared, nor in the current intensity within the glass transition region. Similarly, all samples exhibited deep traps at the same temperature ranges and an anomalous current towards the end of the measurement. One of the five samples displayed a slightly deviating TSDC spectrum and also showed a somewhat higher charging current. However, the variation between these measurements was small compared to the differences observed when comparing blends with and without additives. From the perspective of measurement repeatability, the results show that the resolution of the TSDC method is sufficient for the NEWGEN-project purposes of screening suitable materials for further investigation, even though the protocol still involves some manually performed steps.

In the poling time variation tests, measurements were performed on six identical samples of a Blend-2 with poling times of 30, 40, 50, 60, 90, and 120 minutes. At the glass transition temperature, all samples behaved similarly in terms of TSDC current intensity and the temperature of the α-relaxation peak. At approximately +35 °C, a β-relaxation peak was observed, where a slight increase in current intensity occurred for samples poled 50, 90 and 120 minutes. However, this increase did not follow the order of poling times. 120-minute sample had the highest current intensity, followed by the 50-minute and 90-minute samples. In the deeper traps at higher temperature around +80 °C the current intensity increased consistently with longer poling times, the 120-minute sample exhibited the highest value, the 90-minute the second highest, and the 60-minute the third highest. In the other samples, current intensities were equal. Poling time did not influence temperatures where relaxation peaks occurred.

In net charge accumulation comparison, no differences were observed among the 30-, 40-, and 50-minute samples, which all showed similar values. Net charge began to increase in the 60-, 90-, and

120-minute samples, in chronological order, with the 120-minute sample showing the highest accumulation. Based on both the TSDC spectra and the net charge results, it can be concluded that poling time has a significant effect on how much charge is trapped and at what depth within the material. To verify these findings and ensure that the chosen poling times are appropriate, it would be valuable to conduct similar tests on other blends.

When examining the effect of sample thickness, it was observed that thickness had no significant impact on the current intensity at the glass transition temperature. However, the current released from deeper traps was consistently lower in thicker samples. For the ternary blend (Blend-1), no delay in the relaxation peaks was observed between 100 μm and 200 μm samples, whereas the binary blends (Blend-4 and -5) showed a delay in both the glass transition region and the deeper trap-related peaks when the thickness increased. The lower current intensities of deeper traps in thicker samples can be explained by more effective charge recombination and differences in relaxation peak delays between binary and ternary blends are attributed to the absence of the PBE component in the binary blends.

Regardless of the measurement parameters or sample thickness, compared to samples without additive (PP-g-MAH), the ones with additive were found to exhibit higher current intensity at the glass transition temperature, though with no effect on the temperature at which the α-relaxation peak occurred. Nevertheless, all observed current intensities were relatively low. When comparing samples without additive to those containing 1.0 wt-%, the additive significantly reduced the amount of charge released from deeper traps. This trend was consistent regardless of the PP component ratios, as the α- and β-relaxation peaks followed the same behavior. Comparisons of net charge accumulation obtained from both PEA and TSDC measurements support these findings and confirm the observed influence of the additive in reducing charge accumulation. While a clear reduction was observed when 1.0 wt-% additive was introduced, increasing the concentration further to 2.5 wt-% did not result in additional reduction in the TSDC measurements. In contrast, the PEA measurements revealed a further reduction in charge accumulation when the additive concentration was increased from 1.0 wt-% to 2.5 wt-%. Determining the optimal additive concentration to maximise the benefits requires further investigation.

The intensity and occurrence of the current peak at the glass transition temperature were influenced by both the additive concentration and the composition of the PP blend. Among all tested materials, the ternary blends exhibited the lowest glass transition temperature, followed by the binary blends, while the PP cast film showed the highest. Additive concentration did not affect the glass transition temperature itself but increased the current intensity in proportion to its content. The PBE component increases the amorphous fraction of the ternary blends and reduces chain stiffness, which explains the lower glass transition temperatures and higher current intensities observed in ternary blends. In comparison, PP cast films, with their inherently rigid chain structure, show the highest glass transition

temperature, whereas blending with other PP components, as in the binary blends, lowers T_g by increasing flexibility and usability of the material**.**

Based on the observed results, it would be worthwhile to study the effect of varying poling time in other polypropylene blends in order to verify whether the behaviour of deep trap filling is consistent across materials. Such work would help determine whether material-specific differences exist in the onset of deep trap activation. In addition, future studies could focus on modifying the current measurement circuit (short-circuit) into the open-circuit configuration with a series capacitor. This approach could provide complementary insights into the coexistence of homocharge and heterocharge. Establishing whether open-circuit measurements can yield results consistent with PEA would strengthen the overall understanding of charge trapping and transport phenomena in polypropylene-based insulation systems.

REFERENCES

[1] G. Mazzanti, 'High voltage direct current transmission cables to help decarbonisation in Europe: Recent achievements and issues', *High Volt.*, vol. 7, no. 4, pp. 633–644, Aug. 2022, doi: 10.1049/hve2.12222.

[2] J. C. Fothergill, 'The coming of Age of HVDC extruded power cables', in *2014 IEEE Electrical Insulation Conference (EIC)*, Philadelphia, PA, USA: IEEE, June 2014, pp. 124–137. doi: 10.1109/EIC.2014.6869361.

[3] G. Mazzanti, 'Issues and Challenges for HVDC Extruded Cable Systems', *Energies*, vol. 14, no. 15, p. 4504, July 2021, doi: 10.3390/en14154504.

[4] G. Mazzanti *et al.*, 'The Horizon Europe NEWGEN Research Project: For a New Generation of High-Voltage DC Insulation Materials, Cables, and Systems after 24 Months since the Start of the Project', *IEEE Ind. Appl. Mag.*, pp. 2–12, 2025, doi: 10.1109/MIAS.2025.3559863.

[5] S.-W. Lee, H.-J. Kim, I.-S. Kwon, and J.-S. Lim, 'Evaluation of Electrical Performance and Life Estimation of PPs for HVDC Power Cable', *Energies*, vol. 14, no. 18, p. 5673, Sept. 2021, doi: 10.3390/en14185673.

[6] M. A. Fard, M. E. Farrag, S. McMeekin, and A. Reid, 'Electrical Treeing in Cable Insulation under Different HVDC Operational Conditions', *Energies*, vol. 11, no. 9, p. 2406, Sept. 2018, doi: 10.3390/en11092406.

[7] L. H. Sperling, *Introduction to physical polymer science*, 4th ed. New York: J. Wiley & sons, 2006.

[8] U. W. Gedde and M. S. Hedenqvist, *Fundamental Polymer Science*. in Graduate Texts in Physics. Cham: Springer International Publishing, 2019. doi: 10.1007/978-3-030-29794-7.

[9] J. Seppälä, *Polymeeriteknologian perusteet*. Otatieto, 1997. Accessed: Mar. 03, 2025. [Online]. Available: https://research.aalto.fi/fi/publications/polymeeriteknologian-perusteet

[10] A. R. Blythe, *Electrical properties of polymers*, 1. paperback ed. in Cambridge solid state sciences series. Cambridge: Cambridge Univ. Pr, 1980.

[11] R. O. Ebewele, *Polymer science and technology*. Boca Raton, Fla.: CRC Press, 2000.

[12] A. Rudin and P. Choi, *The Elements of Polymer Science and Engineering*. Academic Press, 2012.

[13] W. D. Callister, *Materials Science and Engineering*. New York: Wiley, 2019.

[14] 'Chirality and Stereoisomers', Chemistry LibreTexts. Accessed: Mar. 05, 2025. [Online]. Available: https://chem.libretexts.org/Bookshelves/Organic_Chemistry/Supplemental_Modules_(Organic_Chemistry)/Chirality/Chirality_and_Stereoisomers

[15] L. A. Dissado, J. C. Fothergill, and G. Stevens, *Electrical Degradation and Breakdown in Polymers*, 1st edn, vol. 1992.

[16] H. D. Young, *Sears and Zemansky's University physics with modern physics*. Pearson Education, 2015.

[17] J. J. O'Dwyer, *The Theory of Electrical Conduction and Breakdown in Solid Dielectrics*. Clarendon Press, 1973.

[18] F. H. Abd Nasir and K. L. Woon, 'Charge carrier trapping in organic semiconductors: Origins, impact and strategies for mitigation', *Synth. Met.*, vol. 307, p. 117661, Sept. 2024, doi: 10.1016/j.synthmet.2024.117661.

[19] P. F. Lang, 'Fermi energy, metals and the drift velocity of electrons', *Chem. Phys. Lett.*, vol. 770, p. 138447, May 2021, doi: 10.1016/j.cplett.2021.138447.

[20] R. Hoffmann, C. Janiak, and C. Kollmar, 'A chemical approach to the orbitals of organic polymers', *Macromolecules*, vol. 24, no. 13, pp. 3725–3746, June 1991, doi: 10.1021/ma00013a001.

[21] G. Teyssedre and C. Laurent, 'Charge transport modeling in insulating polymers: from molecular to macroscopic scale', *IEEE Trans. Dielectr. Electr. Insul.*, vol. 12, no. 5, pp. 857–875, Oct. 2005, doi: 10.1109/TDEI.2005.1522182.

[22] G. Mazzanti and M. Marzinotto, *Extruded Cables for High-Voltage Direct-Current Transmission*, 1st edn, vol. 2013. Newark: Wiley.

[23] P. P. Kumar and S. Yashonath, 'Ionic conduction in the solid state', J. Chem. Sci., Vol. 118, No. 1, January 2006, pp. 135–154.

[24] F.-C. Chiu, 'A Review on Conduction Mechanisms in Dielectric Films', *Adv. Mater. Sci. Eng.*, vol. 2014, pp. 1–18, 2014, doi: 10.1155/2014/578168.

[25] K.-C. Kao, *Dielectric phenomena in solids: with emphasis on physical concepts of electronic processes*. Amsterdam ; Boston: Academic Press, 2004.

[26] G. G. Raju, *Dielectrics in Electric Fields*, vol. 2003. CRC Press.

[27] J. G. Simmons, 'Poole-Frenkel Effect and Schottky Effect in Metal-Insulator-Metal Systems', *Phys. Rev.*, vol. 155, no. 3, pp. 657–660, Mar. 1967, doi: 10.1103/PhysRev.155.657.

[28] T. L. Hanley, R. P. Burford, R. J. Fleming, and K. W. Barber, 'A general review of polymeric insulation for use in HVDC cables', *IEEE Electr. Insul. Mag.*, vol. 19, no. 1, pp. 13–24, Jan. 2003, doi: 10.1109/MEI.2003.1178104.
[29] M. Salah Khalil, 'International research and development trends and problems of HVDC cables with polymeric insulation', *IEEE Electr. Insul. Mag.*, vol. 13, no. 6, pp. 35–47, Nov. 1997, doi: 10.1109/57.637152.
[30] R. J. Fleming, M. Henriksen, and J. T. Holboll, 'The influence of electrodes and conditioning on space charge accumulation in XLPE', *IEEE Trans. Dielectr. Electr. Insul.*, vol. 7, no. 4, pp. 561–571, Aug. 2000, doi: 10.1109/94.868078.
[31] R. Coelho, 'Charges in non homogeneous dielectrics', in *IEEE 1997 Annual Report Conference on Electrical Insulation and Dielectric Phenomena*, Minneapolis, MN, USA: IEEE, 1997, pp. 1–10. doi: 10.1109/CEIDP.1997.634546.
[32] J. T. Holboll, K. R. Bambery, and R. J. Fleming, 'Space charge and steady state current in LDPE samples containing a permittivity/conductivity gradient', in *2000 Annual Report Conference on Electrical Insulation and Dielectric Phenomena (Cat. No.00CH37132)*, Victoria, BC, Canada: IEEE, 2000, pp. 381–384. doi: 10.1109/CEIDP.2000.885305.
[33] M. Meunier, N. Quirke, and A. Aslanides, 'Molecular modeling of electron traps in polymer insulators: Chemical defects and impurities', *J. Chem. Phys.*, vol. 115, no. 6, pp. 2876–2881, Aug. 2001, doi: 10.1063/1.1385160.
[34] M. Meunier and N. Quirke, 'Molecular modeling of electron trapping in polymer insulators', *J. Chem. Phys.*, vol. 113, no. 1, pp. 369–376, July 2000, doi: 10.1063/1.481802.
[35] J. R. Reitz and F. J. Milford, 'Foundations of electromagnetic theory', Addison-Wesley Publishing Company, London, 1960.
[36] 'Fundamentals of Dielectrics'. Accessed: May 15, 2025. [Online]. Available: https://application.wiley-vch.de/books/sample/3527351019_c01.pdf
[37] M. Aro, M. Karttunen, K. Nousiainen, and V. Palva, *Suurjännitetekniikka*, 3rd edn, vol. 2011. Jyväskylä.
[38] J. Martinez-Vega, Ed., *Dielectric materials for electrical engineering*. London: ISTE, 2010.
[39] G. Giannoukos, M. Min, and T. Rang, 'Relative complex permittivity and its dependence on frequency', *World J. Eng.*, vol. 14, no. 6, pp. 532–537, Dec. 2017, doi: 10.1108/WJE-01-2017-0007.
[40] G. C. Montanari and P. H. F. Morshuis, 'Space charge phenomenology in polymeric insulating materials', *IEEE Trans. Dielectr. Electr. Insul.*, vol. 12, no. 4, pp. 754–767, Aug. 2005, doi: 10.1109/TDEI.2005.1511101.
[41] J. C. Fothergill, 'Ageing, Space Charge and Nanodielectrics: Ten Things We Don't Know About Dielectrics', in *2007 IEEE International Conference on Solid Dielectrics*, Winchester, UK: IEEE, July 2007, pp. 1–10. doi: 10.1109/ICSD.2007.4290739.
[42] R. Minguez, L. Barrenetxea, E. Solaberrieta, and E. Lizundia, 'A simple approach to understand the physical aging in polymers', *Eur. J. Phys.*, vol. 40, no. 1, p. 015502, Jan. 2019, doi: 10.1088/1361-6404/aaf244.
[43] J. R. White, 'Polymer ageing: physics, chemistry or engineering? Time to reflect', *Comptes Rendus Chim.*, vol. 9, no. 11–12, pp. 1396–1408, Oct. 2006, doi: 10.1016/j.crci.2006.07.008.
[44] A. O. Ibhadon, 'Physical aging in isotactic polypropylene', *J. Appl. Polym. Sci.*, vol. 62, no. 11, pp. 1843–1846, Dec. 1996, doi: 10.1002/(SICI)1097-4628(19961212)62:11%3C1843::AID-APP8%3E3.0.CO;2-Q.
[45] L. Guadagno, C. Fontanella, V. Vittoria, and P. Longo, 'Physical aging of syndiotactic polypropylene', *J. Polym. Sci. Part B Polym. Phys.*, vol. 37, no. 2, pp. 173–180, Jan. 1999, doi: 10.1002/(SICI)1099-0488(19990115)37:2%3C173::AID-POLB6%3E3.0.CO;2-W.
[46] F. Zhang, R. Yang, and D. Lu, 'Investigation of Polymer Aging Mechanisms Using Molecular Simulations: A Review', *Polymers*, vol. 15, no. 8, p. 1928, Apr. 2023, doi: 10.3390/polym15081928.
[47] J. L. Chen and J. C. Filippini, 'The morphology and behavior of the water tree', *IEEE Trans. Electr. Insul.*, vol. 28, no. 2, pp. 271–286, Apr. 1993, doi: 10.1109/14.212252.
[48] Y. Zhang, D. Liu, J. Wu, and Y. Yin, 'Investigation on space charge behavior in water tree aged crosslinked polyethylene (XLPE) cable by experiment and simulation', in *2017 International Symposium on Electrical Insulating Materials (ISEIM)*, Toyohashi: IEEE, Sept. 2017, pp. 613–616. doi: 10.23919/ISEIM.2017.8166564.
[49] Y. Z. Arief, M. Shafanizam, Z. Adzis, and M. Z. H. Makmud, 'Degradation of polymeric power cable due to water treeing under AC and DC stress', in *2012 IEEE International Conference on Power and Energy (PECon)*, Kota Kinabalu, Malaysia: IEEE, Dec. 2012, pp. 950–955. doi: 10.1109/PECon.2012.6450355.
[50] L. W. Zhu, B. X. Du, J. G. Su, T. Han, and M. G. Danikas, 'Electrical treeing initiation and breakdown phenomenon in polypropylene under DC and pulse combined voltages', *IEEE Trans. Dielectr. Electr. Insul.*, vol. 26, no. 1, pp. 202–210, Feb. 2019, doi: 10.1109/TDEI.2018.007454.

[51] J. Su, B. Du, J. Li, and Z. Li, 'Electrical tree degradation in high-voltage cable insulation: progress and challenges', *High Volt.*, vol. 5, no. 4, pp. 353–364, Aug. 2020, doi: 10.1049/hve.2020.0009.
[52] T. Tanaka and A. Greenwood, 'Effects of Charge Injection and Extraction on Tree Initiation in Polyethylene', *IEEE Trans. Power Appar. Syst.*, vol. PAS-97, no. 5, pp. 1749–1759, Sept. 1978, doi: 10.1109/TPAS.1978.354668.
[53] M. Fujii, H. Shimose, M. Fukuma, T. Takao, and M. Nagao, 'Influence of space charge under non-uniform electric field to electrical treeing in epoxy resin', in *Proceedings of 2011 International Symposium on Electrical Insulating Materials*, Kyoto: IEEE, Sept. 2011, pp. 58–61. doi: 10.1109/ISEIM.2011.6826302.
[54] M. Liu, Y. Liu, Y. Li, P. Zheng, and H. Rui, 'Growth and partial discharge characteristics of electrical tree in XLPE under AC-DC composite voltage', *IEEE Trans. Dielectr. Electr. Insul.*, vol. 24, no. 4, pp. 2282–2290, 2017, doi: 10.1109/TDEI.2017.006537.
[55] P. H. F. Morshuis and J. J. Smit, 'Partial discharges at dc voltage: their mechanism, detection and analysis', *IEEE Trans. Dielectr. Electr. Insul.*, vol. 12, no. 2, pp. 328–340, Apr. 2005, doi: 10.1109/TDEI.2005.1430401.
[56] J. V. Champion, S. J. Dodd, J. Alison, and L. Askew, 'Electrical tree growth and space charge behaviour of epoxy resin blends', in *ICSD'98. Proceedings of the 1998 IEEE 6th International Conference on Conduction and Breakdown in Solid Dielectrics (Cat. No.98CH36132)*, Vasteras, Sweden: IEEE, 1998, pp. 321–324. doi: 10.1109/ICSD.1998.709290.
[57] J. C. Devins, 'The physics of partial discharges in solid dielectrics', in *Conference on Electrical Insulation & Dielectric Phenomena - Annual Report 1984*, Claymont, DE, USA: IEEE, Oct. 1984, pp. 15–31. doi: 10.1109/EIDP.1984.7683959.
[58] E. Kuffel, W. S. Zaengl, and J. Kuffel, *High voltage engineering: fundamentals*, 2nd ed. Oxford ; Boston: Butterworth-Heinemann, 2000.
[59] P. Morshuis, A. Cavallini, D. Fabiani, G. Montanari, and C. Azcarraga, 'Stress conditions in HVDC equipment and routes to in service failure', *IEEE Trans. Dielectr. Electr. Insul.*, vol. 22, no. 1, pp. 81–91, Feb. 2015, doi: 10.1109/TDEI.2014.004815.
[60] A. Imburgia *et al.*, 'Interaction Between Electric Field Profile and Partial Discharges Simultaneously Detected in a Loaded HVDC Cable: Space Charge Analysis', in *2024 IEEE Conference on Electrical Insulation and Dielectric Phenomena (CEIDP)*, Auburn, AL, USA: IEEE, Oct. 2024, pp. 1–4. doi: 10.1109/CEIDP61745.2024.10907493.
[61] G. Rizzo, P. Romano, A. Imburgia, and G. Ala, 'Partial Discharges in HVDC Cables - The Effect of the Temperature Gradient During Load Transients', *IEEE Trans. Dielectr. Electr. Insul.*, vol. 28, no. 5, pp. 1767–1774, Oct. 2021, doi: 10.1109/TDEI.2021.009602.
[62] P. Adda, O. Lesaint, R. Hanna, N. Boussetta, and E. Vorobiev, 'Modelling of current and temperature rise during discharge initiation in water', *IEEE Trans. Dielectr. Electr. Insul.*, vol. 25, no. 5, pp. 1974–1979, Oct. 2018, doi: 10.1109/TDEI.2018.007428.
[63] M. Ieda, 'Dielectric Breakdown Process of Polymers', *IEEE Trans. Electr. Insul.*, vol. EI-15, no. 3, pp. 206–224, June 1980, doi: 10.1109/TEI.1980.298314.
[64] M. Hikita, I. Kanno, G. Sawa, and M. Ieda, 'Consideration on Filamentary Thermal Breakdown by Measuring Pre-Breakdown Current in Solid Dielectrics', *Jpn. J. Appl. Phys.*, vol. 24, no. 8R, p. 984, Aug. 1985, doi: 10.1143/jjap.24.984.
[65] J. C. Fothergill, 'Filamentary electromechanical breakdown in polymers', in *[1992] Proceedings of the 4th International Conference on Conduction and Breakdown in Solid Dielectrics*, Sestri Levante, Italy: IEEE, 1992, pp. 323–327. doi: 10.1109/ICSD.1992.224932.
[66] T. Anh, L. Berquez, L. Boudou, and J. Martinez-Vega, 'Effect of trapped space charge on mechanical deformation induced by electric field', *IEEE Trans. Dielectr. Electr. Insul.*, vol. 18, no. 5, pp. 1416–1422, Oct. 2011, doi: 10.1109/TDEI.2011.6032810.
[67] D. An, X. Zha, J. Gao, Y. Long, K. Wu, and J. Li, 'Role of free volume on breakdown of epoxy nanocomposites: measurement and manipulation', in *2022 IEEE International Conference on High Voltage Engineering and Applications (ICHVE)*, Chongqing, China: IEEE, Sept. 2022, pp. 1–4. doi: 10.1109/ICHVE53725.2022.10014459.
[68] Ying Li, M. Yasuda, and T. Takada, 'Pulsed electroacoustic method for measurement of charge accumulation in solid dielectrics', *IEEE Trans. Dielectr. Electr. Insul.*, vol. 1, no. 2, pp. 188–195, Apr. 1994, doi: 10.1109/94.300251.
[69] R. Bodega, P. H. F. Morshuis, and J. J. Smit, 'Space charge measurements on multi-dielectrics by means of the pulsed electroacoustic method', *IEEE Trans. Dielectr. Electr. Insul.*, vol. 13, no. 2, pp. 272–281, Apr. 2006, doi: 10.1109/TDEI.2006.1624272.
[70] G. Ala *et al.*, 'Review of acoustic methods for space charge measurement', in *2015 AEIT International Annual Conference (AEIT)*, Naples: IEEE, Oct. 2015, pp. 1–6. doi: 10.1109/AEIT.2015.7415270.

[71] T. Takada, Y. Tanaka, N. Adachi, and Xiaokui Qin, 'Comparison between the PEA method and the PWP method for space charge measurement in solid dielectrics', *IEEE Trans. Dielectr. Electr. Insul.*, vol. 5, no. 6, pp. 944–951, Dec. 1998, doi: 10.1109/94.740780.
[72] A. Gupta and C. C. Reddy, 'On the estimation of actual space charge using pulsed electro-acoustic system', *IEEE Trans. Dielectr. Electr. Insul.*, vol. 23, no. 5, pp. 3086–3093, Oct. 2016, doi: 10.1109/TDEI.2016.7736873.
[73] G. M. Sessler, Electrets, 2nd ed. Berlin, Springer, 1987.
[74] K.-S. Suh, J. Tanaka, and D. Damon, 'What is TSC?', *IEEE Electr. Insul. Mag.*, vol. 8, no. 6, pp. 13–20, Nov. 1992, doi: 10.1109/57.168887.
[75] F. Namouchi, W. Jilani, and H. Guermazi, 'Thermally stimulated depolarization current and dielectric spectroscopy used to study dipolar relaxations and trap level distribution in PMMA polymer', *J. Non-Cryst. Solids*, vol. 427, pp. 76–82, Nov. 2015, doi: 10.1016/j.jnoncrysol.2015.07.004.
[76] H. Song, J. P. Goud, J. Ye, W. Jung, J. Ji, and J. Ryu, 'Review of the thermally stimulated depolarization current (TSDC) technique for characterizing dielectric materials', *J. Korean Ceram. Soc.*, vol. 60, no. 5, pp. 747–759, Sept. 2023, doi: 10.1007/s43207-023-00305-5.
[77] S. Yoon, C. A. Randall, and K. Hur, 'Correlation Between Resistance Degradation and Thermally Stimulated Depolarization Current in Acceptor (Mg)-Doped $BaTiO_3$ Submicrometer Fine-Grain Ceramics', *J. Am. Ceram. Soc.*, vol. 93, no. 7, pp. 1950–1956, July 2010, doi: 10.1111/j.1551-2916.2010.03647.x.
[78] P. K. Khare, J. M. Keller, and S. C. Datt, 'Open- and short-circuit thermally stimulated currents in ethyl cellulose (EC): polymethyl methacrylate (PMMA) blend', *Bull. Mater. Sci.*, vol. 22, no. 2, pp. 109–113, Apr. 1999, doi: 10.1007/BF02745562.
[79] P. Saxena, P. Shukla, and M. S. Gaur, 'Air-gap thermally stimulated discharge currents in PVDF-PMMA double-layered samples', *J. Therm. Anal. Calorim.*, vol. 147, no. 4, pp. 2957–2968, Feb. 2022, doi: 10.1007/s10973-021-10680-y.
[80] B. Yan, J. Zhang, X. Gao, and G. Chen, 'A glass-assisting thermally stimulated discharge technique', *J. Appl. Phys.*, vol. 135, no. 12, p. 124102, Mar. 2024, doi: 10.1063/5.0196163.
[81] S. N. Fedosov, A. E. Sergeeva, and T. A. Revenyuk, 'How to increase informativity of the TSDC method', in *2005 12th International Symposium on Electrets*, Salvador, Bahia, Brazil: IEEE, 2005, pp. 273–275. doi: 10.1109/ISE.2005.1612374.
[82] S. W. S. McKeever and D. M. Hughes, 'Thermally stimulated currents in dielectrics', *J. Phys. Appl. Phys.*, vol. 8, no. 13, pp. 1520–1529, Sept. 1975, doi: 10.1088/0022-3727/8/13/014.
[83] E. Rysiakiewicz-Pasek and V. Y. Livshits, 'Application of the thermally stimulated polarization current method for measuring of the electrical conductivity of alkali aluminosilicate glasses', in *[1991 Proceedings] 7th International Symposium on Electrets (ISE 7)*, Berlin, Germany: IEEE, 1991, pp. 669–674. doi: 10.1109/ISE.1991.167292.
[84] R. Singh, B. K. Kaushik, and J. K. Quamara, 'Investigations of thermally stimulated polarization current in polyetherimide', *APPL PHYS*, vol. 46, 2008.
[85] M. Niittymäki *et al.*, 'Screening of Suitable Random Copolymer Polypropylene Blends for HVDC Cable Insulation', in *2024 IEEE 5th International Conference on Dielectrics (ICD)*, Toulouse, France: IEEE, June 2024, pp. 1–4. doi: 10.1109/ICD59037.2024.10613125.
[86] M. Mudarra, J. Belana, J. C. Ca□adas, and J. A. Diego, 'Polarization time effect on PMMA space-charge relaxation by TSDC', *J. Polym. Sci. Part B Polym. Phys.*, vol. 36, no. 11, pp. 1971–1980, Aug. 1998, doi: 10.1002/(SICI)1099-0488(199808)36:11%3C1971::AID-POLB18%3E3.0.CO;2-4.
[87] I. Rytöluoto, M. Niittymäki, and K. Lahti, 'Practical Notes on the Measurement and Interpretation of Thermally Stimulated Discharge Currents in Biaxially Oriented Polypropylene', *Proc. Nord. Insul. Symp.*, no. 26, pp. 64–69, Aug. 2019, doi: 10.5324/nordis.v0i26.3280.
[88] T. Umemura, T. Suzuki, and T. Kashiwazaki, 'Impurity Effect of the Dielectric Properties of Isotactic Polypropylene', *IEEE Trans. Electr. Insul.*, vol. EI-17, no. 4, pp. 300–305, Aug. 1982, doi: 10.1109/TEI.1982.298498.
[89] P. Khare and S. K. Jain, 'Anomalous thermally stimulated currents and space charge in poly(vinyl pyrrolidone)', *Polym. Int.*, vol. 49, no. 3, pp. 265–268, Mar. 2000, doi: 10.1002/(SICI)1097-0126(200003)49:3%3C265::AID-PI357%3E3.0.CO;2-5.
[90] H. J. Wintle, 'Reversals in Electrical Current and Other Anomalies in Insulating Polymers', *IEEE Trans. Electr. Insul.*, vol. EI-21, no. 5, pp. 747–762, Oct. 1986, doi: 10.1109/TEI.1986.348923.
[91] A. Tzimas, S. M. Rowland, L. A. Dissado, M. Fu, and U. H. Nilsson, 'The effect of dc poling duration on space charge relaxation in virgin XLPE cable peelings', *J. Phys. Appl. Phys.*, vol. 43, no. 21, p. 215401, June 2010, doi: 10.1088/0022-3727/43/21/215401.
[92] K. Kadowaki, S. Mitsunari, H. Yoshioka, S. Nishimoto, and I. Kitani, 'Influence of thickness on field distortion due to space charge migration in LDPE sheet', in *2008 International Symposium on Electrical*

Insulating Materials (ISEIM 2008), Yokkaichi: IEEE, Sept. 2008, pp. 127–130. doi: 10.1109/ISEIM.2008.4664513.

[93] Zepeng Lv, Xia Wang, Kai Wu, Xi Chen, Yonghong Cheng, and L. A. Dissado, 'Dependence of charge accumulation on sample thickness in Nano-SiO_2 doped IDPE', *IEEE Trans. Dielectr. Electr. Insul.*, vol. 20, no. 1, pp. 337–345, Feb. 2013, doi: 10.1109/TDEI.2013.6451375.

[94] B. Diban *et al.*, 'Characterization of Isotactic-Polypropylene-Based Compounds for HVDC Cable Insulation', in *2024 IEEE 5th International Conference on Dielectrics (ICD)*, Toulouse, France: IEEE, June 2024, pp. 1–4. doi: 10.1109/ICD59037.2024.10613139.